PLANNING AND DELIVERY COMPARISON OF SIX LINAC-BASED STEREOTACTIC RADIOSURGERY TECHNIQUES

Varun Singh Thakur

Department of Medical Physics
McGill University, Montreal
March 2012

A thesis submitted to McGill University in partial fulfillment of the requirements of the degree of Master of Science in Medical Physics

Abstract

This work presents planning and delivery comparison of linac-based SRS treatment techniques currently available for single lesion cranial SRS. In total, two dedicated SRS systems (Novalis Tx, Cyberknife) and a HI-ART TomoTherapy system with six different delivery techniques are evaluated. Four delivery techniques are evaluated on a Novalis Tx system: circular cones, dynamic conformal arcs (DCA), static non-coplanar intensity modulated radiotherapy (NCP-IMRT), and volumetric modulated arc therapy (RapidArc) techniques are compared with intensity modulation based helical Tomotherapy on the HI-ART Tomotherapy system and with non-isocentric, multiple overlapping based robotic radiosurgery using the CyberKnife system. Thirteen patients are retrospectively selected for the study. The target volumes of each patient are transferred to a CT scan of a Lucy phantom (Standard Imaging Inc., Middleton, WI, USA) designed for end-to-end SRS QA. In order to evaluate the plans, several indices scoring the conformality, homogeneity and gradients in the plan are calculated and compared for each of the plans. Finally, to check the clinical deliverability of the plans and the delivery accuracy of different systems, a few targets are delivered on each system. A comparison between planned dose on treatment planning system and dose delivered on Gafchromic EBT film (ISP, Wayne, New Jersey, USA) is carried out by comparing dose beam profiles, isodose lines and by calculating gamma index.

Abrégé

Cette étude présente la planification et la comparaison de livraison de doses de les techniques de traitement par accélérateur linéaire (linac) à base de radiochirurgie stéréotactique (RCS) actuellement disponibles pour la RCS des lésions crâniennes uniques. Au total, deux systèmes RCS (Novalis Tx, Cyberknife) et un système HI-ART TomoTherapy avec six techniques différentes de livraison de doses sont évalués. Trois techniques de livraison de doses d'un système Novalis Tx sont évalués: arcs dynamiques conformationnelles, radiothérapie avec modulation d'intensité statique non-coplanaire et les techniques de thérapie volumétrique par arc modulé (RapidArc) sont comparées avec la tomothérapie hélicoïdale par modulation d'intensité sur le système HI-ART TomoTherapy et la radiochirurgie robotique non-isocentrique à multiples chevauchements du système CyberKnife. Treize patients sont rétrospectivement sélectionnés pour l'étude. Les volumes cibles de chaque patient sont transférés sur un scan tomodensitométrique d'un fantôme Lucy (Standard Imaging Inc, Madison, WI, Etats-Unis) conçu pour l'assurance qualité des systèmes RCS. Afin d'évaluer les plans de traitements, plusieurs métriques de notation de conformalité telles que l'homogénéité et les gradients du plan de traitement sont calculées et comparées pour chacun des plans. Enfin, dans le but de vérifier la faisabilité de livraison clinique des plans de traitements et la précision de livraison des différents systèmes, quelques cibles sont délivrées sur chaque système. Une comparaison entre la dose prévue sur le système de planification du traitement et la dose délivrée sur un film de type GAFCHROMIC EBT (ISP, Wayne,

New Jersey, USA) est effectuée par comparaison des profils de faisceaux de dose, des lignes de doses de même intensité (isodose) et en calculant l'indice gamma.

Acknowledgements

I have many people to express my gratitude for making this project possible. First, I would like to thank my supervisor William Parker, co-supervisors Russell Ruo and Emilie Soisson for their continuous support, guidance and encouragement. Especially I would like to thank Russell for mentoring me throughout the year including many weekends and late hours, without his guidance this thesis work would never be possible. I also like to thank Dr. Jan Seuntjens for providing me the financial support throughout the year.

There are a few peoples to whom I would like to extend a special thank you. I would like to thank Robert Doucet (CHUM) for helping me with the CyberKnife. I also like to thank Hugo Bouchard and Frederic Girard (CHUM) for helping me in film dosimetry.

I would like to thank staff and student of the Medical Physics Unit for their friendship, help and discussion over the last two years. In particular, I would like to thank Martin Vallieres for generously translating my abstract to French and Greg Twork for helping me with Tomotherapy unit.

I would like to extend my thanks to Standard Imaging Incorporation (Middleton, WI) for providing us adopter to interface used with Lucy phantom for each of the SRS delivery technique used in this study.

From my personal life, I would like to thank my parents, brother, sister in law and my niece for their continuous love and faith in me.

Table of Contents

List of Figures

List of Tables

Chapter 1. Introduction to Stereotactic Radiosurgery

1.1 INTRODUCTION

In stereotactic radiosurgery (SRS), a high dose (>10 Gy) of ionizing radiation is delivered to a small stereotactically localized target (< 4 cm) in a single fraction. Historically, this technique was used only for intracranial lesions and functional disorders such as acoustic neuroma, trigeminal neuralgia, arteriovenous malformation, brain metastasis and other primary brain tumors. Recently the technique has been adapted for extra-cranial targets in the lung and liver. The word stereotactic is combination of two words, the Greek word "stereo" means "three dimensional" and the Latin word "tact" means "touch", the word stereotactic stands for three dimensional arrangements to touch and the word radiosurgery means using radiation as a surgical tool.

The goal of stereotactic radiosurgery is to deliver a large obliterative dose to the tumor with high accuracy and conformality to minimize the dose to the surrounding healthy tissues. To meet this goal, several basic requirements for stereotactic radiosurgery must be met including: accurate localization, mechanical precision, accurate and optimal dose distribution and patient safety. Different organizations have set forth their SRS recommendations such as the American Association of Physicists in Medicine AAPM(1) and Radiation Therapy Oncology Group RTOG(2). Recommendations by the AAPM Task Group 42 for a clinically acceptable SRS plan are: 1) Dose delivery in

positional accuracy shall be within ±1 mm and 2) Absolute dose delivery should be less than of ±5% of the prescribed dose(1).

The different terms associated with cranial radiosurgery are stereotactic radiosurgery (SRS) and stereotactic radiotherapy (SRT). Similar to SRS, SRT is also generally used for cranial tumors but a relatively lower dose (typically ~ 2 Gy/fraction) is delivered in multiple fractions.

1.2 HISTORY OF STEREOTACTIC RADIOSURGERY

The history of stereotactic radiosurgery can be traced back to the discovery of X-rays by Wilhem Konrad Rontgen in 1895 and the discovery of radioactivity by Becquerel in 1896. The credit for the invention of radiosurgery goes to Swedish neurosurgeon Lars Leksell. Leksell's interest to develop a non invasive technique to treat intracranial lesions led to the development of stereotactic radiosurgery(3). In 1951 Leksell used the 200 kVp stationary X-ray beam for the first radiosurgery treatment but due to the low penetrating power of 200 kVp X-rays this technique wasn't efficient for tumors lying deep in the brain.

During the 1960s, Liden and Larsson at Uppsala University used proton beams generated from a cyclotron to treat brain lesions, they called this technique "stralkniven" (ray knives)(4). During the same time another group of Woodruff and colleges(5) at the University of California at Berkeley developed a similar technique, but it eventually became clear that the use of a large proton accelerating unit was complicated and costly(6).

In 1968, Leksell(7) was the first to develop the Gamma Knife which used 179 focused Cobalt-60 sources, this unit was installed in Sophiahemmet Hospital in

Stockhom, Sweden, and was used to treat arteriovenous malformations (AVMs) and acoustic neuromas(8). In 1974 the unit was replaced with the second Gamma Knife unit that could produce a more spherically shaped dose distribution. Irregularly shaped tumors required multiple isocenters or "shots" in order to conform the dose distribution to the target shape. Although, the Gamma Knife has been developed over the last five decades, in 2007 a recent model Leksell Gamma Knife Perfexion^{TM} (Elekta, Stockholm, Sweden) was introduced containing 192 Cobalt-60 sources that are further divided into 8 groups. These groups can be individually positioned to three different field sizes (4 mm, 8 mm, and 16 mm). The Perfexion^{TM} model includes automated features for improved workflow, efficiency and safety. In addition it extends the use of the Gamma Knife to stereotactic radiotherapy by offering the possibility to treat with relocatable head frames.

In the 1960's, several companies began manufacturing linear accelerators (linacs) for radiotherapy. With the advancement in microwave technology, linacs were able to deliver beams of different energies. Due to their lower cost and greater availability(9) linacs became the most commonly used machine in radiation therapy. In 1984 it was shown by Heifetz(10) that linacs could also deliver high doses to small targets and spare normal tissue like the Gamma Knife. In addition linacs used for conventional radiotherapy could be easily modified for use in radiosurgery. This made linear accelerators more cost effective than buying a new Gamma Knife unit specifically dedicated to radiosurgery only. In the following 10 years linear accelerators were widely accepted both for radiotherapy as well as radiosurgery.

To reduce the dose to normal tissues in 1984 Betti and Derechinsky(11) developed a multiple non-coplanar converging arc technique. Different techniques, with different

combinations of gantry and table angles were proposed in the following years. In 1986 Podgorsak et al.(12) developed a dynamic stereotactic radiosurgery technique using a 10 MV linac. In this technique, both table and gantry moved simultaneously during the treatment. All the techniques up to this point were based on fixed collimators of different diameters attached to the gantry head.

More recently, the multileaf collimator (MLC) was developed where tungsten leaves could be used to shape the field. The use of MLC improves the dose distribution for irregularly shaped tumors. The ability of multileaf collimators to move during the radiosurgery procedure opens up the possibility for the clinical use of modern techniques such as dynamic conformal arc (DCA), intensity-modulated stereotactic radiosurgery (IMRS)(13) and most recently volumetric modulated arc therapy (VMAT)(14). Corvus (Nomos Corporation, Sewickley, PA)(15) introduced in 1995 was one of the earlier planning systems used to produce plans using intensity modulated beams.

In 1993 a helical delivery based approach “Tomotherapy" was introduced by Mackie et al.(16). A linear accelerator is mounted on a ring gantry like a CT scanner. The patient is moved through the ring gantry and an intensity modulated beam is delivered using binary multileaf collimators. The same linear accelerator used for imaging the patient could also be further used for treatment planning or for patient positioning. Recently, Soisson et al.(17) have developed a technique for performing SRS on a Tomotherapy unit with treatment plans comparable to those of conventional linac based arc plans done with circulator collimators for spherical lesions.

A relatively new and innovative linac based system, the CyberKnife was developed by Adler(18) and colleagues in Stanford, California. In the CyberKnife a 6

MV Linac is mounted on six axis industrial robotic arm. The robotic arms gives the freedom to deliver many non-coplanar beams isocentrically or non-isocentrically. This system incorporates a real time imaging system used to track the patient position during the treatment. Due to the real time tracking system the CyberKnife is able to deliver a frameless stereotactic radiosurgery treatment. Several publications in the following years elaborate the accuracy and clinical capability of the CyberKnife(19-21).

1.3 CLINICAL INDICATIONS FOR SRS

Radiosurgery is used to treat four different types of disorders: functional disorders, benign tumors, malignant tumors and vascular lesions(22).

1.3.1 FUNCTIONAL DISORDERS

Stereotactic radiosurgery is used to treat functional disorders that may result in acute pain or other complications. Functional disorders treated with SRS are trigeminal neuralgia, epilepsy, parkinsons disease and chronic pain.

1.3.2 BENIGN TUMORS

Benign tumors are well circumscribed tumors having relatively low growth rate and do not spread to surrounding healthy tissues. Stereotactic radiosurgery is used to treat benign tumors such as acoustic neuroma, intracranial meningiomas, vestibular schwannomas and pituitary adenomas.

1.3.3 MALIGNANT TUMORS

Malignant tumors grow at faster rate and also spread or “metastasize” to other parts of the body including the brain. Surgical removal of primary or metastatic tumors in

the brain may not be possible and this makes radiosurgery a suitable therapeutic alternative. These tumors are more dangerous to the patient and are relatively difficult to control.

Small malignant tumors treated with stereotactic radiosurgery or radiotherapy are brain metastasis, gliomas, anaplastic astrocytoma, primary CNS lymphoma and medulloblastoma.

1.3.4 VASCULAR LESIONS

The most common vascular lesion treated with stereotactic radiosurgery is arteriovenous malformations (AVM). Under normal conditions arteries carry the oxygen rich blood from the heart to different parts of the body and the veins bring back the deoxygenated blood back to the heart for re-oxygenation. AVMs are clusters of blood vessels formed in the brain, as a result of these clusters, blood is directly transferred from the arteries to the veins bypassing brain tissue. Due to the high pressure of blood transferred directly from the arteries to veins these clusters are prone to bleed. Bleeding can cause pain, hemorrhage or even death.

1.4 TECHNICAL CONSIDERATION FOR SRS

In radiosurgery a very high dose of radiation is used to kill the tumor cells. This high dose is also destructive for the surrounding normal tissues. To spare the normal tissues it is crucial to shoot the target with maximum possible positional accuracy. This condition is even more important in SRS because small margins are used to delineate the tumor (to spare more normal tissue). The technical considerations during SRS treatment are discussed in the following sections.

1.4.1 IMMOBILIZATION AND LOCALIZATION

To maintain the accuracy and precision desired in SRS two basic conditions are: 1) Immobilization of the patient during the treatment and 2) Exact determination of tumor position. These conditions could be achieved in two different ways with a fixed frame (conventional technique) or image-based frameless technique.

When using frames a trained physician screws the stereotactic frame on the patient's head. Use of a frame solves two purposes: first because it is screwed to the patient head the chance of head movement with respect to frame is minimized (immobilization), second it sets up an external frame of reference with respect to which co-ordinates of internal structures of brain could be defined (localization). To determine the co-ordinates of internal structures a localization box with N-shaped fiducial rods is attached to the head frame before the patient undergoes imaging. Stereotactic frames are very precise and reliable for intracranial tumors but they are inconvenient to the patient and are not very practical if treatment is distributed over few days as in SRT. As a result of recent improvements in image guidance systems a relatively new approach called frameless SRS is used in many clinics.

In frameless SRS, a non invasive mask is used to immobilize the patient. Patient motion within the mask can result into the uncertainty of less than 1 mm. In room imaging techniques are used to localize the patient. To place the tumor at the machine's isocenter, images of the patient are taken and compared with digitally reconstructed radiographs (DRRs) from the planning system. The DRRs are reference images with the patient in the planned position. Frameless SRS is less painful to the patients and is able to produce comparable accuracy to the conventional technique with frames(23-25).

1.4.2 IMAGING FOR SRS PLANNING

Diagnostic imaging modalities used in stereotactic radiosurgery are (a) Computed Tomography (CT), (b) Magnetic Resonance Imaging (MRI) and (c) Digital Subtraction Angiography (DSA).

CT can provide high resolution images of a patient by selecting different slice thicknesses. To determine the co-ordinates of a tumor, a localization box with CT fiducial rods is used. CT image acquisition depends upon the fact that different structures have different attenuation coefficients for an incident low energy X-ray beam. In addition to the image of internal anatomy, a CT scan can also provide the information about the electron density of different tissues imaged. This information could be further used to apply the heterogeneity corrections during dose calculations(26).

Because of the fact that CT image acquisition depends upon the different attenuation coefficients of different materials, a CT scan can provide good contrast between bony anatomy and normal brain tissue but provides less contrast between normal tissue and the tumor (because they both have nearly the same attenuation).

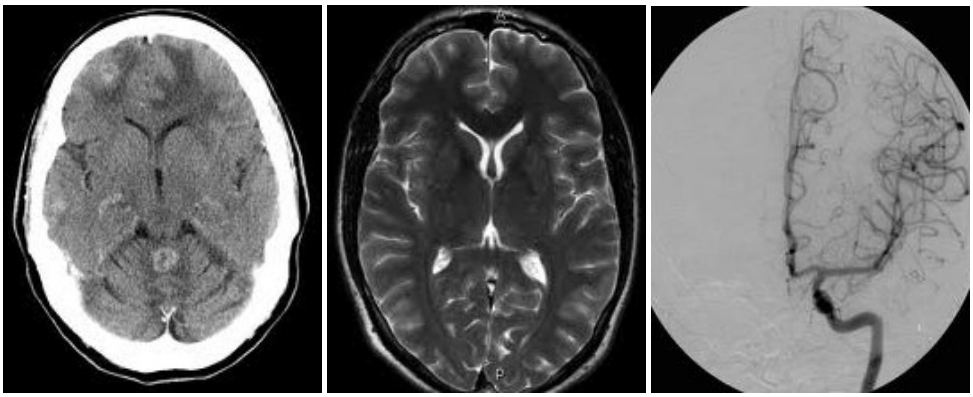

(a) (b) (c)

Figure 1.1 CT (a), MRI (b) and DSA (c) image of patient with various brain lesions.

MRI uses the nuclear spin property of a large number of hydrogen atoms present in the human body to produce an image. MRI typically shows greater contrast between tumor and surrounding normal tissues than CT images. The MRI technique suffers a few technical complications such as relatively long (~ 30 minutes) image acquisition time and it does not provide any information about the electron density(27). Patient motion during the long imaging time can produce artifacts in the image.

As a result of the advancement in computer technology, it is possible to superimpose geometrically CT and MRI images using mathematical registration techniques to utilize the information of both image modalities. This process is typically called "fusion" or "registration". Once the images are registered, different viewing tools allow the planner to view the images superimposed on top of each other.

DSA is used to acquire enhanced images of blood vessels; it is mainly used to diagnose AVMs. In DSA a radio opaque contrast medium having a selective absorption for X-rays is used to highlight the blood vessels. In DSA, a patient undergoes the imaging twice, first without the contrast agent (background image) and then with the contrast agent injected into the body (contrast image). To produce the DSA image of blood vessels, image without the contrast agent is subtracted from the image with contrast agent. The resultant image shows only the blood vessels. To determine the co-ordinates of the tumor a stereotactic head frame is used.

1.4.3 DELIVERY MODALITIES

There are three types of ionizing radiations/particles used in SRS treatment: Gamma rays, Megavoltage X-rays and charged particles. The work of this thesis concentrates on all the Linac based techniques that use megavoltage X-rays for the SRS

treatment. The following is a brief description of the modalities used for stereotactic radiosurgery in this work, a more detailed discussion of these modalities is given in Chapter 2.

Novalis Tx: The Novalis Tx system (Varian Inc., Palo Alto, CA, USA) uses megavoltage X-rays generated from a linear accelerator. The Novalis Tx has many added features as compared to a conventional Linac including a high definition multileaf collimator, 6D robotic couch and 0.5 mm isocenter. It is a dedicated SRS delivery system but may also be used for conventional radiation therapy.

Tomotherapy: The Tomotherapy Unit (TomoTherapy Inc., Madison, WI, USA) also uses a Linac based technique. A 6 MV Linac rotates with constant velocity on a circular ring and the patient is translated continuously through the bore. Tomotherapy can used for SRS and for conventional radiotherapy. A binary 64-leaf multileaf collimator is used for beam intensity modulation.

CyberKnife: The CyberKnife system (Accuray Inc., Sunnyvale, CA, USA) is relatively new Linac based technique. A 6 MV Linac is mounted on 6 axis robotic arm. Different collimators (cones) are used to shape the beams. The CyberKnife is capable of using the imaging techniques to track the tumor motion during the treatment and compensate it by re-adjusting linac positions.

1.4.4 TREATMENT PLANNING

The basic requirement of SRS planning is to deliver the maximum dose to the tumor while minimizing the dose to the surrounding healthy tissues. During the 1950s Lars Leksell proposed a basic idea to achieve the above requirement(3, 27-29). The idea was to place the tumor at the center of cross-section of large number of radiation beams.

Because the beams are coming from different directions they deliver maximum dose to the cross-section/tumor and less dose to the surrounding healthy tissues. The following outlines several steps that are involved in SRS treatment planning:

Localization and imaging: The first step of SRS treatment is to determine the co-ordinates of the tumor with respect to an external frame of reference. As the patient comes into the clinic a stereotactic head frame is screwed on the patient skull by an expert physician. A localization box is used to determine the co-ordinates of the tumor with respect to the frame of reference set by the head frame. Then the patient undergoes the imaging (CT/MRI/DSA) process.

Image import and Contouring: Once the imaging is complete, data is transferred to a treatment planning station (TPS). In the TPS all the CT image slices are localized, meaning the fiducials of the localizer box are found to determine the co-ordinate system used for planning. In order to take advantage of other image modalities such as MRI, image fusion is performed. The next step is contouring where a physician contours the target and other organ at risks (OAR) structures on the image slices.

Prescription and Planning: Once the target and OARs are drawn, a radiosurgery plan may be developed. Generally the dose prescribed for solitary brain metastases is essentially determined by target size and typically is 24 Gy, 18 Gy, and 15 Gy for lesions of diameter <20 mm, 21-30 mm, 31-41 mm as recommended by the RTOG(30). Linac based techniques using circular collimators produce spherical dose distributions. For irregularly shaped tumors a multiple isocenter technique must be used where spherical distributions are added or packed together to cover the target. The result of sphere packing is a high maximum dose due to overlapping of spherical distributions. As a

result, in such cases generally the prescription isodose line is 50% of the maximum dose. Linacs equipped with MLCs are able to treat irregular targets with a single isocenter and generally have the dose prescribed around 80% of the maximum dose.

Once the dose is prescribed by the physician, a treatment plan may be developed. Treatments can be planned in two different ways: forward planning or inverse planning. In forward planning, the planner determines what the parameters must be (such as beam arrangement, beam size, and beam weights). The planner then goes through an iterative process of adjusting the initially defined parameters to improve the dose distribution. The success of forward planning largely depends upon the planning experience of the user. In inverse planning, treatment goals are defined a priori by the planner and an optimization algorithm calculates the different parameters (such as beam intensity modulation and field size) required to meet as closely as possible the initially defined planning goals. These days most of the planning systems are equipped with inverse planning algorithms.

1.4.5 PLAN EVALUATION TOOLS

Once the plans are ready there are many ways to compare them with each other or with the published literature. The most common method for plan evaluation is the visual inspection of isodose lines and dose volume histograms (DVH). Isodose lines are plotted as percentage of prescription dose or maximum dose, whereas DVHs are a condensed graphical representation of the dose distribution(31).

Although visual inspection of isodose lines and DVHs can provide some basic information about the plan, different quantitative indices have been used to determine numerical values for scoring the conformality or homogeneity of a plan. These numerical

values are very useful to compare the different characteristics of a given plan against other plans.

Commonly used quantitative indices in SRS planning are: the ratio of prescription isodose volume to target volume (PITV), Paddick's conformity index(32), maximum dose to prescription dose ratio (MDPD), Paddick's gradient index(33), and the Wagner Conformity/Gradient index(34). These parameters are discussed in more detail in Chapter 3.

1.4.6 PATIENT POSITIONING AND PLAN DELIVERY

Once the suitable treatment plan is selected and approved the next step is to treat the patient. Patient positioning is a crucial step in the success of a SRS treatment. As explained in section 1.4.1 the desired positional accuracy in SRS treatment can be achieved in two different ways: 1) Using stereotactic frames or 2) Frameless SRS.

In a conventional SRS treatment, a stereotactic frame is used for patient positioning. The co-ordinates of patients internal anatomy determined during the imaging are used for the patient positioning. The co-ordinates of the tumor are used to match its position with the machine's isocenter. The patient is fixed to the treatment table and printouts from the TPS indicating the location of the isocenter are taken. The printouts are fixed to the frame/localizer and the patient is positioned according to the isocenter location on the printouts.

In frameless SRS treatments, on board imaging techniques (stereoscopic in-room x-ray images, planar orthogonal images, and cone-beam CT) are used for the patient positioning. Once the patient is on the treatment couch with mask immobilization, images of the patient are taken with on board imaging techniques and compared with

previously generated images from a TPS. Computer algorithms automatically superimpose the images and calculate any shift required in patient position.

1.5 THESIS OBJECTIVES AND MOTIVATION

Stereotactic radiosurgery has been in use clinically for over 40 years and in that time several studies have been done comparing various planning techniques and delivery modalities(35-49). Planning comparisons may be done on the basis of the physical dose using indices such as the PITV, conformality index, MDPD and gradient index as mentioned in Chapter 3. Others groups(35-36) have also compared plans on the basis of radiobiological parameters such as the tumor control probability (TCP), normal tissue complication probability (NTCP), or biological effective dose (BED).

The primary goal of this study is to investigate delivery accuracy of six stereotactic radiosurgery systems. In this study, three modern "state-of-the-art" SRS systems: Novalis Tx, CyberKnife and a HI-ART Tomotherapy are evaluated. Four delivery techniques were evaluated on a Novalis Tx system: cones, dynamic conformal arcs (DCA), static non-coplanar intensity modulated radiotherapy (NCP-IMRT), and volumetric modulated arc therapy (RapidArc), these techniques were compared with intensity modulation based helical Tomotherapy on the HI-ART Tomotherapy system and with non-isocentric, multiple overlapping based robotic radiosurgery using the CyberKnife system.

This thesis work is divided into two sections. The first section describes the planning study comparison between all the techniques used in our study. The second section discusses the comparison between calculated and measured dose distributions for

two spherical targets (6 mm and 10 mm) and three irregular targets used in the planning study.

1.5.1 PLANNING COMPARISON STUDY

The planning study is divided into two sections: 1) Planning for very small spherical targets of different diameters and 2) For thirteen irregularly shaped tumors retrospectively selected from pool of brain lesion patients previously treated on our Novalis Tx. Treatment plans were generated for all the targets using each technique under same set of prescription dose and constraints. These plans were compared against each other using different quantitative indices (conformality, gradient and homogeneity) as explained in Chapter 3.

1.5.2 DELIVERY COMPARISON STUDY

To verify the clinical deliverability of the treatment plans, a few plans were selected to deliver on all the modalities. To verify the comparison between planned and delivered dose a comparison between dose delivered to the film and the corresponding dose plane from the TPS was performed. To quantify the comparison between two dose distributions a gamma map was calculated, a further comparison between dose profiles and isodose line was also performed.

In addition different issues associated with each modality such as: phantom positioning, delivery time, monitoring units used and accuracy using onboard imaging systems are discussed.

1.6 THESIS ORGANIZATION

Chapter 2 reviews the three delivery modalities (Novalis Tx, CyberKnife and Tomotherapy) and the treatment planning systems used for SRS planning. Chapter 3 gives an overview of the material and methods including planning specifications, phantom overview and film analysis used in this study. Chapters 4 and 5 discusses in detail the result, discussion and conclusion of this work.

1.7 REFERENCES

1. Schell MC BF, Larson DA, Leavitt, DD, Lutz WR, Podgorsak EB, Wu A. . Stereotactic Radiosurgery. . *The American Institute of Physics* 1995.
2. Shaw E, Kline R, Gillin M*, et al.* Radiation Therapy Oncology Group: radiosurgery quality assurance guidelines. *Int J Radiat Oncol Biol Phys* 1993;27:1231-1239.
3. Leksell L. The stereotaxic method and radiosurgery of the brain. *Acta Chir Scand* 1951;102:316-319.
4. Levy RP, Schulte RW, Slater JD*, et al.* Stereotactic radiosurgery--the role of charged particles. *Acta Oncol* 1999;38:165-169.
5. Woodruff KH, Lyman JT, Lawrence JH*, et al.* Delayed sequelae of pituitary irradiation. *Hum Pathol* 1984;15:48-54.
6. Larsson B, Liden K, Sarby B. Irradiation of small structures through the intact skull. *Acta Radiol Ther Phys Biol* 1974;13:512-534.
7. Leksell L. Cerebral radiosurgery. I. Gammathalanotomy in two cases of intractable pain. *Acta Chir Scand* 1968;134:585-595.
8. Steiner L, Leksell L, Greitz T*, et al.* Stereotaxic radiosurgery for cerebral arteriovenous malformations. Report of a case. *Acta Chir Scand* 1972;138:459-464.
9. Podgorsak EB, Pike GB, Olivier A*, et al.* Radiosurgery with high energy photon beams: a comparison among techniques. *Int J Radiat Oncol Biol Phys* 1989;16:857-865.
10. Heifetz MD, Wexler M, Thompson R. Single-beam radiotherapy knife. A practical theoretical model. *Journal of neurosurgery* 1984;60:814-818.
11. Betti O DV. Hyperselective encephalic irradiation with a linear accelerator. . *Acta Neurochir* 1984.
12. Podgorsak EB, Olivier A, Pla M*, et al.* Dynamic stereotactic radiosurgery. *Int J Radiat Oncol Biol Phys* 1988;14:115-126.
13. Webb S. Optimizing the planning of intensity-modulated radiotherapy. *Physics in medicine and biology* 1994;39:2229-2246.
14. Otto K. Volumetric modulated arc therapy: IMRT in a single gantry arc. *Medical physics* 2008;35:310-317.
15. Carol MP. PeacockTM: A System for Planning and Rotational Delivery of Intensity-Modulated Fields. *International Journal of Imaging Systems and Technology* 1995;6, 56-61.

16. Mackie TR, Holmes T, Swerdloff S*, et al.* Tomotherapy: a new concept for the delivery of dynamic conformal radiotherapy. *Medical Physics* 1993;20:1709-1719.
17. Soisson ET, Hoban PW, Kammeyer T*, et al.* A technique for stereotactic radiosurgery treatment planning with helical tomotherapy. *Medical dosimetry : official journal of the American Association of Medical Dosimetrists* 2011;36:46-56.
18. Adler JR, Jr., Chang SD, Murphy MJ*, et al.* The Cyberknife: a frameless robotic system for radiosurgery. *Stereotact Funct Neurosurg* 1997;69:124-128.
19. Chang SD, Murphy M, Geis P*, et al.* Clinical experience with image-guided robotic radiosurgery (the Cyberknife) in the treatment of brain and spinal cord tumors. *Neurol Med Chir (Tokyo)* 1998;38:780-783.
20. Ishihara H, Saito K, Nishizaki T*, et al.* CyberKnife radiosurgery for vestibular schwannoma. *Minim Invasive Neurosurg* 2004;47:290-293.
21. Mehta VK, Lee QT, Chang SD*, et al.* Image guided stereotactic radiosurgery for lesions in proximity to the anterior visual pathways: a preliminary report. *Technol Cancer Res Treat* 2002;1:173-180.
22. Khan FM. The Physics of Radiation Therapy. *Lippincott Williams & Wilkins* 2009.
23. Takakura T, Mizowaki T, Nakata M*, et al.* The geometric accuracy of frameless stereotactic radiosurgery using a 6D robotic couch system. *Physics in medicine and biology* 2010;55:1-10.
24. Chang SD, Main W, Martin DP*, et al.* An analysis of the accuracy of the CyberKnife: a robotic frameless stereotactic radiosurgical system. *Neurosurgery* 2003;52:140-146; discussion 146-147.
25. Breneman JC, Steinmetz R, Smith A*, et al.* Frameless image-guided intracranial stereotactic radiosurgery: clinical outcomes for brain metastases. *Int J Radiat Oncol Biol Phys* 2009;74:702-706.
26. Battista JJ, Rider WD, Van Dyk J. Computed tomography for radiotherapy planning. *Int J Radiat Oncol Biol Phys* 1980;6:99-107.
27. Lawrence S. Chin WFR. Principles and practice of stereotactic radiosurgery: New York : Springer,; c2008.
28. Leksell L. Stereotactic radiosurgery. *J Neurol Neurosurg Psychiatry* 1983;46:797-803.
29. Leksell L. The stereotaxic method and radiosurgery of the brain. *Acta chirurgica Scandinavica* 1951;102:316-319.
30. Shaw E, Scott C, Souhami L*, et al.* Single dose radiosurgical treatment of recurrent previously irradiated primary brain tumors and brain metastases: final report of RTOG protocol 90-05. *Int J Radiat Oncol Biol Phys* 2000;47:291-298.
31. Drzymala RE, Mohan R, Brewster L*, et al.* Dose-volume histograms. *Int J Radiat Oncol Biol Phys* 1991;21:71-78.
32. Paddick I. A simple scoring ratio to index the conformity of radiosurgical treatment plans. Technical note. *J Neurosurg* 2000;93 Suppl 3:219-222.
33. Paddick I, Lippitz B. A simple dose gradient measurement tool to complement the conformity index. *J Neurosurg* 2006;105 Suppl:194-201.
34. Wagner TH, Bova FJ, Friedman WA*, et al.* A simple and reliable index for scoring rival stereotactic radiosurgery plans. *Int J Radiat Oncol Biol Phys* 2003;57:1141-1149.
35. Oliveira SC. Comparison of three linac-based stereotactic radiosurgery techniques. *Medical Physics Unit McGill University, Montreal June 2003*.
36. Charpentier PE. Dosimetric evaluation of four techniques used in stereotactic radiosurgery. *Department of Medical Physics McGill University, Montreal December 2007*.
37. Baumert BG, Norton IA, Davis JB. Intensity-modulated stereotactic radiotherapy vs. stereotactic conformal radiotherapy for the treatment of meningioma located

predominantly in the skull base. *International journal of radiation oncology, biology, physics* 2003;57:580-592.
38. Soisson ET, Mehta MP, Tome WA. A comparison of helical tomotherapy to circular collimator-based linear-accelerator radiosurgery for the treatment of brain metastases. *American journal of clinical oncology* 2011;34:388-394.
39. Yu C, Jozsef G, Apuzzo ML*, et al.* Dosimetric comparison of CyberKnife with other radiosurgical modalities for an ellipsoidal target. *Neurosurgery* 2003;53:1155-1162; discussion 1162-1153.
40. Schoonbeek A, Monshouwer R, Hanssens P*, et al.* Intracranial radiosurgery in the Netherlands. A planning comparison of available systems with regard to physical aspects and workload. *Technology in cancer research & treatment* 2010;9:279-290.
41. Cardinale RM, Benedict SH, Wu Q*, et al.* A comparison of three stereotactic radiotherapy techniques; ARCS vs. noncoplanar fixed fields vs. intensity modulation. *International journal of radiation oncology, biology, physics* 1998;42:431-436.
42. Hamilton RJ, Kuchnir FT, Sweeney P*, et al.* Comparison of static conformal field with multiple noncoplanar arc techniques for stereotactic radiosurgery or stereotactic radiotherapy. *International journal of radiation oncology, biology, physics* 1995;33:1221-1228.
43. Khoo VS, Oldham M, Adams EJ*, et al.* Comparison of intensity-modulated tomotherapy with stereotactically guided conformal radiotherapy for brain tumors. *International journal of radiation oncology, biology, physics* 1999;45:415-425.
44. Podgorsak EB, Pike GB, Olivier A*, et al.* Radiosurgery with high energy photon beams: a comparison among techniques. *International journal of radiation oncology, biology, physics* 1989;16:857-865.
45. Solberg TD, Boedeker KL, Fogg R*, et al.* Dynamic arc radiosurgery field shaping: a comparison with static field conformal and noncoplanar circular arcs. *International journal of radiation oncology, biology, physics* 2001;49:1481-1491.
46. Verhey LJ, Smith V, Serago CF. Comparison of radiosurgery treatment modalities based on physical dose distributions. *International journal of radiation oncology, biology, physics* 1998;40:497-505.
47. Woo SY, Grant WH, 3rd, Bellezza D*, et al.* A comparison of intensity modulated conformal therapy with a conventional external beam stereotactic radiosurgery system for the treatment of single and multiple intracranial lesions. *International journal of radiation oncology, biology, physics* 1996;35:593-597.
48. Yu C, Luxton G, Jozsef G*, et al.* Dosimetric comparison of three photon radiosurgery techniques for an elongated ellipsoid target. *International journal of radiation oncology, biology, physics* 1999;45:817-826.
49. Clark BG, Robar JL, Nichol AM. Analysis of treatment parameters for conformal shaped field stereotactic irradiation: comparison with non-coplanar arcs. *Physics in medicine and biology* 2001;46:3089-3103.

Chapter 2. SRS Delivery Modalities and Treatment Planning Techniques

In this chapter, a description of the three linac based SRS delivery systems (Novalis Tx, CyberKnife, and Tomotherapy) used in this study is given. Each system has unique features that make them suitable for SRS treatments. The second part of this chapter describes the different treatment planning techniques associated with each delivery system.

2.1 DELIVERY MODALITIES

2.1.1 NOVALIS Tx

The Novalis Tx (Varian Inc., Palo Alto, CA, USA) is designed for both image guided radiosurgery and conventional radiotherapy. The unit comes with three photon energy modes: 6 MV photons, 18 MV photons and a special high dose rate (1000MU/min) 6 MV SRS photon beam. Different components of Novalis Tx such as gantry head and couch are designed to meet the high mechanical accuracy required for SRS treatment. The Novalis Tx is equipped with a high definition multileaf collimator (HD 120 MLC). The HD MLC contains 120 leaves including 64 central leaves of 2.5 mm width and 56 peripheral leaves of 5 mm width. Whereas a conventional linac typically has a minimum leaf width resolution of 5 mm, the smaller leaf width of the HD

MLC allows for greater conformality to irregularly shaped tumors. In addition it also comes with cones of varying diameter (4 mm to 15 mm) for treating spherical targets.

Image-guidance is used to achieve the desired localization accuracy. The Novalis Tx is equipped with a stereoscopic kV X-ray imaging system (ExacTrac X-ray 6 degree of freedom) (BrainLAB, Feldkirchen, Germany)(1) and kV X-ray on board imaging (OBI) system capable of acquiring cone beam computed tomography (CBCT) and planar 2D kV X-ray images. The ExacTrac X-ray 6D image guided radiotherapy system consists of an infrared (IR) based optical positioning system and kV X-ray imaging system. The IR system contains two cameras used to track the spherical infrared markers affixed to an array that attaches to the patient immobilization mask. The position of IR reflecting markers can be determined to an accuracy of less than 0.3mm(2). The stereoscopic kV X-ray imaging system contains two floor mounted X-ray tubes and two flat panel detectors mounted in the ceiling. For the patient positioning, initial setup is performed by using the IR system, once the patient is aligned according to external IR markers further corrections are applied on the basis of the patient's internal anatomy. Two X-ray images are taken by using the kV X-ray imaging system, these two images are further compared with the digitally reconstructed radiographs (DRR) reconstructed from the CT scan of the patient.

Figure 2.1 Novalis Tx (Courtesy of Varian and BrainLAB).

The comparison can be done manually or by using image fusion algorithms available on the ExacTrac system, two options available for comparison are 3D fusion or 6D fusion. 3D fusion calculates offsets in three translational directions whereas 6D fusion calculates offsets in three translational directions as well as in three rotational directions.

In addition to ExacTrac, the Novalis Tx also has an integrated on-board imaging (OBI) system capable of acquiring Cone Beam CT (CBCT) and planar 2D x-ray images. The OBI system consists of an additional kV x-ray source and detector that are attached to the sides of the gantry. CBCT is advantageous because it provides a 3D volumetric image for matching with the planning CT. Most often the CBCT and 2D x-ray images may be used as a second verification of the position determined by the ExacTrac system. The Novalis Tx is also equipped with a flat panel detector for MV portal imaging with the treatment beam.

Finally, the Novalis Tx also features a 6D robotic couch that can move in three translational as well as three rotational directions that includes pitch, roll and yaw. The capability of three rotational motions in addition to translational motions improves the overall patient positioning capability of the system. The robotic couch is capable of repositioning the patient using the deviations detected from the imaging systems to a sub millimeter level of accuracy.

2.1.2 TOMOTHERAPY

Tomotherapy (TomoTherapy Inc., Madison, WI, USA) a 6 MV Linear accelerator is rotating with constant velocity on a circular ring and delivers an intensity modulated beam using a binary multileaf collimator(3). The linear accelerator can also be used to take MVCT images of the patient that are used for the patient setup by correlating the patient's internal structure with the machine's co-ordinates. For SRS patient positioning a frame is used for patient immobilization and an MVCT image of the patient is taken just before the treatment and compared with the planning CT to calculate any required shift.

The Tomotherapy unit has primary jaws that can be opened to three different widths (1.0, 2.5 and 5.0 cm) and a binary MLC that can produce a maximum field width of 40 cm to generate the maximum field size of 5 cm x 40 cm. The binary MLC contains 64 leaves of tungsten with 6.25 mm leaf width projected at isocenter. The smallest field size at isocenter is 6.25 mm x 10 mm produced by one leaf open and field width of 1 cm. The beam is modulated by opening or closing the MLC leaves and does not have a flattening filter to flatten the beam profile.

Figure 2.2 TomoTherapy® Hi·Art® treatment system (Courtesy of the TomoTherapy).

For MVCT imaging, the operator can chose the “Fine”, “Normal” or “Coarse” setting that corresponds to slice width of 2 mm, 4 mm and 6 mm respectively. It has been shown that MVCT image guidance can be used for stereotactic localization(4, 5); in addition, MVCT images can be used for the dose calculations in treatment planning(6). Contrast enhanced MRI images can be fused with the MVCT images using different algorithms. Use of MVCT for planning has the advantage of using the same image both for planning and for localization.

In contrast to conventional linac based techniques, the Tomotherapy does not require the target to be placed at the machine's isocenter. For cases where multiple tumors are present, such as brain metastasis, the Tomotherapy could be treatment of choice because all the targets are treated at the same time so the patient does not need repositioning for each target as required in conventional linac based SRS treatments.

2.1.3 CYBERKNIFE

The CyberKnife (Accuray Inc., Sunnyvale, CA, USA) is a relatively new linac based radiotherapy system dedicated to stereotactic radiosurgery. A 6 MV Linac is mounted on robotic arm that can move with six degrees-of-freedom. The CyberKnife can produce non-isocentric dose delivery and is not restricted to intracranial tumors only(7). The CyberKnife is able to produce a dose rates between 300 and 1000 cGy/minute and can shape the beam using different collimators (5 mm to 60 mm).

The CyberKnife also uses a stereoscopic x-ray system for image guidance and target tracking. Two low energy kV X-ray tubes are attached to the ceiling and two flat panel amorphous silicon detectors are embedded in the floor on both sides of patient. These detectors can continuously take images and compare them with previously generated digitally reconstructed radiographs (DRRs) both for the initial patient setup as well as to track the patient setup during the treatment. If there is any change in patient position during the treatment than that information is detected and transferred to the robotic arm attached to the Linac. The robotic arm then compensates for patient positioning changes by adjusting the linac position. In addition, an independent respiratory tracking system may be used for tracking target motion due to patient respiration. The CyberKnife can use up to 1600 beams coming from different directions and they may be focused on different parts of the tumor using a non-isocentric beam arrangement.

Figure 2.3 CyberKnife® Robotic Radiosurgery System (Courtesy of Accuray).

Because the maximum dose is not delivered to isocenter but distributed over the tumor volume, the advantage of using non-isocentric beam arrangement over the conventional isocentric beam arrangement is that it can produce a more conformal and homogeneous plan especially for large tumors with large dose gradients. The combined total system accuracy of CyberKnife is reported to be sub-millimeter(8).

2.2 TREATMENT PLANNING SYSTEMS AND TECHNIQUES

In the present work all the linac based techniques currently available at the time were studied and compared. In total three different systems, the Novalis Tx, CyberKnife and the Tomotherapy with six different planning techniques were evaluated. The study included four techniques that may be delivered on the Novalis Tx: cones, dynamic conformal arc (DCA), non-coplanar intensity modulated radiotherapy (NCP-IMRT) and

volumetric arc therapy (RapidArc). Finally, two other delivery techniques were compared: robotic radiosurgery using the CyberKnife system and the helical Tomotherapy on the HI-ART TomoTherapy system.

2.2.1 iPlanTPS

In this study the iPlan v4.1 (BrainLAB, Feldkirchen, Germany) treatment planning system was used for dynamic conformal arc (DCA) and non coplanar intensity modulated radiotherapy (NCP-IMRT) planning techniques. The different steps followed to plan a stereotactic radiosurgery case on iPlan for both of these techniques are: (i) Acquisition of patient's diagnostic images, (ii) CT localization, (iii) Image fusion of MR and CT, (iv) Structure definition, (v) Selecting the isocenter and beam arrangements, and (iv) Dose calculations.

2.2.1.1 CALCULATION ALGORITHM

iPlan uses the pencil beam convolution (PBC) algorithm for dose calculations in DCA and NCP-IMRT techniques. In the PBC dose algorithm, the incident beam is divided into many small pencil beams. The BrainLAB pencil beam dose algorithm is based on a published model by Mohan et al.(9, 10).

The following is the dose calculation equation for the pencil beam algorithm in iPlan(11):

$$D(x,y,d) = MU.NLout.S_t(c_{mlc},c_{jaw}).TMR(l_{rad},c_{d,equ}).(\frac{SSD_{cal}+d_{cal}}{SSD+d})^2.IDD(x_{SID,}y_{SID},l_{rad}) \quad (2.1)$$

Where

MU is monitor units applied to the linac.

$NLout$ is nominal linac output, giving the ratio between absolute dose, measured in a water phantom for an open field (calibration field size) at a calibration depth d_{cal}, divided by the amount of MU applied.

c_{jaw} is size of equivalent squared jaw field.

c_{mlc} is size of equivalent squared MLC field.

l_{rad} is radiological path length of the beam from the tissue surface to the observation point, corrected for tissue density inhomogeneities.

SSD is source-surface distance of central beam.

SID is source-isocenter distance.

d is depth of observation point in tissue.

d_{cal} is the depth of point where $NLout$ and scatter factor where measured.

$S_t(c_{mlc}, c_{jaw})$ is total scatter factor, describing the relative output factor for a square MLC and jaw field.

$TMR(c_{d,coll}, l_{rad})$ is the tissue maximum ratio for the square field equivalent to the MLC and jaw settings in depth l_{rad}

c_d is $c.\frac{SSD+d}{SSD}$

$IDD(x_{SID,}y_{SID}, l_{rad})$ is idealized dose distribution in depth l_{rad} with

x_{SID} is $x.\frac{SID}{SSD+d}$ and y analogue.

and $IDD(x_{SID,}y_{SID}, l_{rad})$ is idealized dose distribution (IDD).

IDD for a collimator with an arbitrary shape is the two dimensional convolution of polyenergetic pencil beam kernel with the photon fluence. It is defined as

$$IDD(x, y, d) = \iint \phi(x', y', d).p(x' - x, y' - y, d).dx'.dy' \tag{2.2}$$

The photon fluence in an isocentric plane perpendicular to the central beam at a depth d is given by

$$\phi(x, y, d) = \phi_0(x, y).\, RSF(r, d) \tag{2.3}$$

Where ϕ_0(x,y) is the fluence matrix in isocenter plane and $RSF(r, d)$ is the radial factor giving the photon fluence at a distance $r = \sqrt{x^2 + y^2}$ from the central beam at a depth d in the phantom.

2.2.1.2 DYNAMIC CONFORMAL ARC (DCA)

In DCA, an arc consists of the gantry rotating around the patient while the couch angle is a fixed. During gantry motion, the positions of MLC's leaves are continuously changing to match the target shape as viewed in the beams eye view (BEV). A typical DCA plan will consist of 4 or more arcs. The advantages of using multiple non-coplanar arcs is the dose outside the tumor boundaries is spread over a larger volume resulting in more normal tissue sparing at high dose levels but a larger volume of normal tissue receiving a low dose.

In SRS planning with DCAs, the planner places the isocenter at the center of the target and adds suitable arc arrangements. The planner can chose any practical

combination of gantry rotation and couch angles. For each arc, the iPlan software is able to optimize the collimator angle to best match the leaf positioning with the target shape over the whole arc range.

DCA planning allows the user to view the BEV at increments of 10^{o} along each arc. These BEVs allow the user to readjust the position of individual leaves to get the best target conformality. To account for beam penumbra a margin of 1 mm could be used around the target for MLC leaf positioning.

Other parameters the planner may change to optimize the plan are: the gantry start and stop angles for each arc, the number of arcs and the weighting of each arc. Once the plan satisfies the requirements set by the oncologist, the plan is ready for further verification and approval.

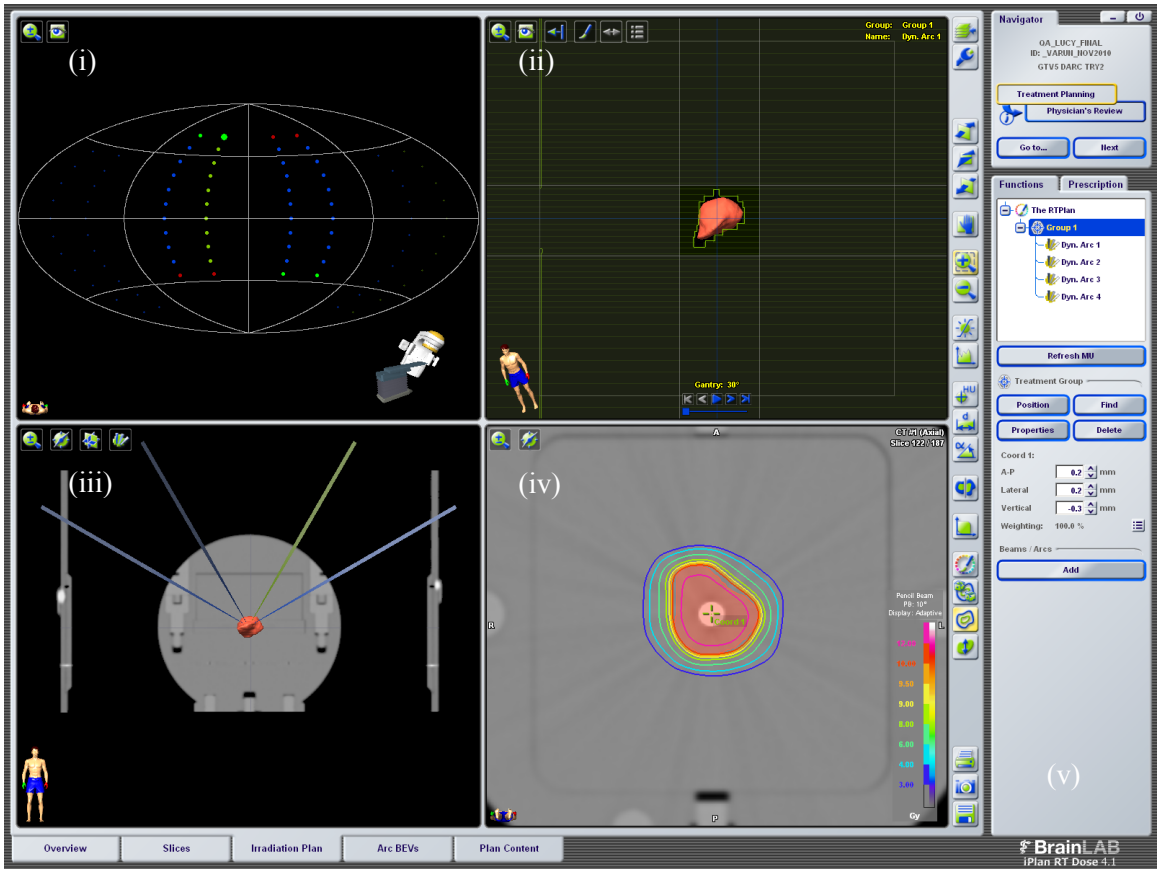

Figure 2.4 A screen capture of image from iPlan treatment planning system, which displays information provided by the system concerning the treatment plan, such as: (i) Arc arrangement (top left window) (ii) BEV (top right window), (iii) 3D view of plan (bottom left window) (iv) Axial plane with isodose distribution (bottom right window), and (v) Planned isocenter coordinates (far right panel).

Figure 2.4 shows a screenshot from the iPlan treatment planning system, which displays information provided by the system concerning the treatment plan, such as: arc arrangement, BEV, axial plane with isodose lines superimposed, 3D view of plan and miscellaneous information such as the co-ordinates of the isocenter.

2.2.1.3 NON COPLANAR INTENSITY MODULATED RADIATION THERAPY (NCP-IMRT)

Non-coplanar beam arrangement use different combinations of couch and gantry angels. Because there is no overlapping of beams coming from opposite directions, non coplanar beam arrangements improve the dose fall off outside the tumor boundaries and reduce the volume of low isodose lines. Intensity modulated radiation therapy (IMRT) uses many beams coming from different directions to achieve a highly conformal plan. In IMRT, the intensity of the beam is modulated resulting in a non uniform deposition of dose in the target(12), a combination of many such beams can result in highly conformal distribution. The idea of modulating the intensity of the beam is very useful when the tumor lies adjacent to an organ at risk or even when tumor is wrapped around critical structures.

In NCP-IMRT, multiple static beams are used, each single beam produces a non uniform dose distribution but the combination of all the non uniform beams can result in a uniform and conformal total dose distribution in the target. For SRS, a non-uniform yet conformal dose distribution may also be achievable depending on the requirements of a particular case.

IMRT often uses inverse planning approach; after the planner has added several non-coplanar beams, the planner defines the prescription dose, dose-volume or dose volume histogram (DVH) constraints for the target and critical structures, and weighting or priority for each structure. An optimization algorithm is then used to calculate the optimized fluence for each beam to fulfill these constraints. The iPlan optimization algorithm uses a Maximum Likelihood Estimator with dynamically changing penalization

or “Dynamically Penalized Likelihood algorithm”(11). iPlan comes with an interactive feature; it can generate four alternative plans with different weightings for sparing organs at risk. The IMRT uses sliding window technique to deliver the fluence as shown in figure 2.5 MLC leaves slide over the target from one side to other.

Figure 2.5 shows a screenshot from the iPlan treatment planning system, it displays four random positions of MLC leaves as they swept over the target during the delivery of one IMRT beam.

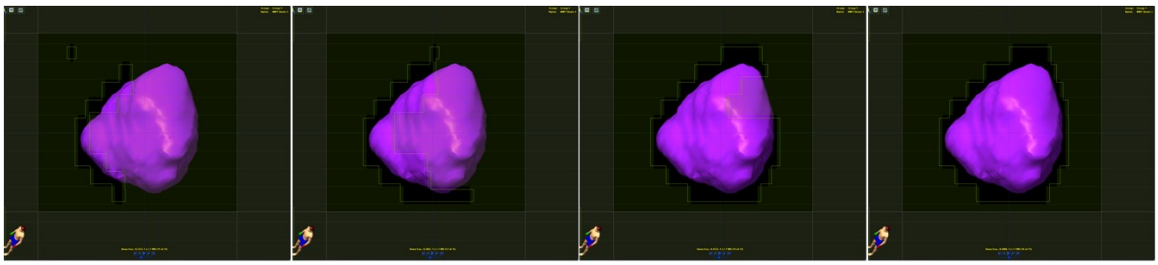

Figure 2.5 Screenshots from iPlan planning system displays four random positions of MLC leaves as they swept over the target.

2.2.2 ECLIPSE TPS

In this study the Eclipse TPS (v8.6, Varian Medical Systems) treatment planning system was used for the RapidArc planning technique.

2.2.2.1 CALCULATION ALGORITHM

The Eclipse TPS uses the Analytical Anisotropic Algorithm (AAA)(13, 14) which is a 3D pencil beam convolution superposition algorithm. The broad clinical beam is divided into small beamlets and the dose calculation uses separate convolution models for the primary photon, scattered photon and electron contamination components. The final dose distribution is obtained by the superposition of each dose component. For the homogeneous case, the dose is found as follows.

The following equation(15) is used to calculate the energy distribution from an arbitrary beamlet β:

$$E_{Ph,\beta}(\tilde{x},\tilde{y},\tilde{z}) = \phi_\beta \times I_\beta(z,\rho) \times \iint\limits_{(u,v)\varepsilon Area(\beta)} K_\beta\,(u-x, v-y, z, \rho)\,du\,dv \tag{2.4}$$

Where:

ϕ_β is photon fluence.

$I_\beta(z,\rho)$ is energy deposition density function.

$K_\beta(u-x, v-y, z, \rho)$ is photon scatter kernel.

The following equation is used to determine the energy distribution from an arbitrary beamlet β due to electron contamination:

$$E_{cont,\beta}(\tilde{x},\tilde{y},\tilde{z}) = \phi_{cont,\beta} \times I_{cont,\beta}(z,) \times \iint\limits_{(u,v)\varepsilon Area(\beta)} K_{cont,\beta}\,(u-x, v-y, z, \rho)\,du\,dv \tag{2.5}$$

Where:

$\phi_{cont,\beta}$ is electron fluence.

$I_{cont,\beta}(z,\rho)$ is energy deposition density function.

$K_{cont,\beta}(u-x,v-y,z,\rho)$ is scatter kernel for contaminating electrons.

The absorbed energy at an arbitrary calculation point is obtained by superposition of the contribution from photons and from electrons (for the homogeneous case):

$$E(\tilde{x},\tilde{y},\tilde{z}) = \sum_{\beta} E_{Ph1,\beta}(\tilde{x},\tilde{y},\tilde{z}) + E_{Ph2,\beta}(\tilde{x},\tilde{y},\tilde{z}) + E_{cont,\beta}(\tilde{x},\tilde{y},\tilde{z}) \quad (2.6)$$

Where:

$E_{Ph1,\beta}(\tilde{x},\tilde{y},\tilde{z})$ is dose contribution from primary photons.

$E_{Ph2,\beta}(\tilde{x},\tilde{y},\tilde{z})$ is dose contribution from scattered photons.

$E_{cont,\beta}(\tilde{x},\tilde{y},\tilde{z})$ is dose contribution from contaminating electrons.

2.2.2.2 VOLUMETRIC MODULATED ARC THERAPY (RapidArc)

Volumetric modulated arc therapy(16) was proposed by Otto in 2007, VMAT uses an optimization technique to sample the MLC apertures for different gantry angles as the gantry rotates around the patient. In the beginning as proposed by Otto a single gantry arc of 360^{o} was proposed but recent studies(17, 18) have shown that use of more than one arc results in a more conformal and more homogeneous dose delivery.

RapidArc is a type of IMRT where the planner must define the prescription, DVH constraints and priorities for each target or structure in the optimization. Also, the planner must define for each arc the table position and the start and stop positions for the arc. In contrast to IMRT where each beam is at a static gantry position, in RapidArc the gantry is rotating around the patient at a fixed couch angle and the radiation beam is on during the full arc delivery. The individual multileaf collimator leaves move dynamically to form various apertures as the gantry moves. In comparison to IMRT, RapidArc reduces the total number of MUs as well as the total time required to deliver the plan.

Figure 2.6 shows a screenshot from the Eclipse treatment planning system, it displays four random positions of MLC leaves during the delivery of one RapidArc. Unlike in NCP-IMRT where the sliding window technique is used, in RapidArc the MLC leaves form many small apertures to modulate the beam.

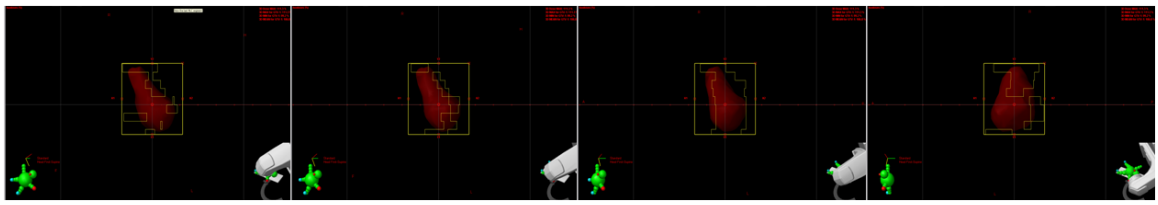

Figure 2.6 Screenshot from Eclipse TPS shows the instantaneous position of MLC leaves during the delivery of one RapidArc.

2.2.3 TOMOTHERAPY TPS

The Tomotherapy TPS (v3.1.4.23, Tomotherapy) is used to plan patients to be treated on the Tomotherapy.

2.2.3.1 CALAULATION ALGORITHM

The Tomotherapy uses a convolution superposition algorithm for dose calculations(19-23). To calculate the dose from a mono-energetic beam, the following equation is used:

$$D(r, hv) = \int T(r', hv) A(r - r', hv) dr' \tag{2.7}$$

Where:

$A(r - r', hv)$ is the convolution kernel for photon with energy hv.

$T(r', hv)$ is the total energy released per unit of mass.

For poly-energetic beam, the dose in a homogeneous phantom is calculated by using equation:

$$D(r, MV) = \int \frac{\mu}{\rho}(hv) \int \frac{d\Psi(r', hv)}{dhv} A(r - r', hv) dr' dhv \tag{2.8}$$

Where:

$\int \frac{\mu}{\rho}(hv) \frac{d\Psi(r,'hv)}{dhv} dhv$ is the total energy released per unit of mass for poly-energetic beam.

$A(r - r', hv)$ is the convolution kernel.

2.2.3.2 HI-ART HELICAL TOMOTHERAPY

For the Tomotherapy system, the TomoTherapy Hi-ART TPS (v3.1.4.23, Tomotherapy) was used for treatment planning.

In the Tomotherapy planning, the first step is to calculate the initial un-modulated distribution called a beamlet calculation. For the planning calculations, TPS divides the 360º full gantry rotation into 51 static projections. Each projection has 64 beamlets (64 MLC leaves) so a single gantry rotation has a total 3264 beamlets. Several planning parameters must be assigned at this stage such as the field width, pitch, overlap priority and calculation grid size. The initial planning constraints for the targets and OARs also entered at this point.

The couch travels continuously in the superior direction and the gantry rotates around the couch at a constant rate. The planning system determines the speed of gantry rotation for every plan; possible speeds of gantry rotation are from 4 rotations per minute to 1 rotation per minute.

At this step modulation factor, maximum and minimum dose penalty for target and DVH coverage are defined. During optimization, the uniform intensity assigned to beamlets earlier is re-optimized on the basis of newly assigned constrains. Every iteration uses dose calculations of previous iteration for re-optimization. In the Tomotherapy, an iterative least square minimization approach is used to optimize the plan. The Tomotherapy planning system uses an objective function that favors homogeneous dose distribution in the target(24). However for spherically shaped targets a planning technique(25) was used to force the system to produce non-homogeneous dose distributions normally required in SRS.

2.2.4 MULTIPLAN TPS

All of the CyberKnife plans are done with the Multiplan TPS (v3.5, Accuray).

2.2.4.1 CALCULATION ALGORITHM

The CyberKnife uses a ray tracing dose calculation algorithm to calculate the dose deposited to a target voxel by each beam(26). The following equation is used to calculate the dose per MU to each target voxel:

$$D_{beam}(v, C_{beam}) = \frac{D'(v, C_{beam})}{D'(v(d=15, SAD=800), C_{beam})} . \{D_{beam}(v(d = 15, SAD = 800), C_{beam})\} \quad (2.9)$$

Where:

Depth d=15 mm and SAD=800 mm is the point where output is defined.

$D'(v, C_{beam})$ is the average dose per history at a voxel of interest.

$D'(v(d = 15\ mm, SAD = 800\ mm), C_{beam})$ is the average dose per history at output specification point of the collimator.

$D_{beam}(v(d = 15\ mm, SAD = 800\ mm), C_{beam})$ is dose per MU at output specification point for the collimator.

2.2.4.2 INVERSE PLANNED CONE TECHNIQUE

The advantage of the CyberKnife's design is its capability of continuous image guidance during the treatment delivery. Due to this image tracking system, the use of a skeletal fixation system is unnecessary for the CyberKnife treatment. Different sets of cones are used to produce a beam of desired diameter and the planner can choose one or

more cones from the set of 12 available cones. These collimators can be changed manually or automatically as the treatment requires. In the current version of the CyberKnife, cones are replaced with variable aperture collimator called an “Iris” which is capable of producing 12 field diameters ranging from 5 to 60 mm at SAD of 800 mm. The Iris variable aperture consists of two banks (upper bank and lower bank) of 6 tungsten plates each and each bank produces a beam of hexagonal aperture. Two banks are offset by 30° resulting into a beam of dodecahedral aperture. The use of a variable aperture collimator reduces the time required to change the cone(27).

For planning, once the prescription dose is assigned planner can chose total number of beams and number of collimators for each plan. A linear optimization algorithm determines the beam geometry and beam weight required to deliver the prescribed dose. Use of large number of beams and more than one cone can improve the plan conformality and gradient but it increase the total treatment delivery time. To further improve the dose gradient the planner has option to use ring structures around the target as avoiding structures.

The Multiplan System has two planning options available(27), isocentric planning and conformal planning. Isocentric planning can be further done in two ways: forward planning where evenly weighted beams are isocentrically placed at the target or inverse planning where non-evenly weighted beams are isocentrically placed at the target. In conformal planning, beams are placed at randomly selected points on the surface of a target and the optimization algorithm calculates the weight of each beam.

For the plan optimization, Multiplan comes with two optimization approaches: simplex optimization and iterative optimization. The advantage of using the iterative

algorithm over the simplex algorithm is that the iterative algorithm always gives a solution and disperses the beams across the multiple robotic nodes. On the other hand a disadvantage of these plans is the increased time required to deliver the treatment(26).

2.3 REFRENCES

1. Jin JY, Yin FF, Tenn SE, *et al.* Use of the BrainLAB ExacTrac X-Ray 6D system in image-guided radiotherapy. *Med Dosim* 2008;33:124-134.
2. Wang LT, Solberg TD, Medin PM, *et al.* Infrared patient positioning for stereotactic radiosurgery of extracranial tumors. *Comput Biol Med* 2001;31:101-111.
3. Mackie TR, Holmes T, Swerdloff S, *et al.* Tomotherapy: a new concept for the delivery of dynamic conformal radiotherapy. *Medical Physics* 1993;20:1709-1719.
4. Forrest LJ, Mackie TR, Ruchala K, *et al.* The utility of megavoltage computed tomography images from a helical tomotherapy system for setup verification purposes. *International journal of radiation oncology, biology, physics* 2004;60:1639-1644.
5. Welsh JS, Bradley K, Ruchala KJ, *et al.* Megavoltage computed tomography imaging: a potential tool to guide and improve the delivery of thoracic radiation therapy. *Clinical lung cancer* 2004;5:303-306.
6. Meeks SL, Harmon JF, Jr., Langen KM, *et al.* Performance characterization of megavoltage computed tomography imaging on a helical tomotherapy unit. *Medical physics* 2005;32:2673-2681.
7. Adler JR, Jr., Chang SD, Murphy MJ, *et al.* The Cyberknife: a frameless robotic system for radiosurgery. *Stereotact Funct Neurosurg* 1997;69:124-128.
8. Chang SD, Main W, Martin DP, *et al.* An analysis of the accuracy of the CyberKnife: a robotic frameless stereotactic radiosurgical system. *Neurosurgery* 2003;52:140-146; discussion 146-147.
9. Mohan R, Chui C, Lidofsky L. Energy and angular distributions of photons from medical linear accelerators. *Med Phys* 1985;12:592-597.
10. Mohan R, Chui C, Lidofsky L. Differential pencil beam dose computation model for photons. *Med Phys* 1986;13:64-73.
11. BarinLAB G. Technical Reference Guide, Revision 1.0, BrainLAB Physics. 2008.
12. Webb S. The physical basis of IMRT and inverse planning. *Br J Radiol* 2003;76:678-689.
13. Ulmer W HD. A Triple Gaussian Pencil Beam Model for Photon Beam Treatment Planning. *2. Med. Phys*;5 (1995) 25-30.
14. Ulmer W HD. Corrected Tables of the Area Integral I(z) for the Triple Gaussian Pencil Beam Model. *Z. Med. Phys.*;7 (1997) 192-193.
15. Janne Sievinen WU, Wolfgang Kaissl. AAA Photon Dose Calculation Model in Eclipse™.
16. Ottoa K. Volumetric modulated arc therapy: IMRT in a single gantry arc. *Med. Phys. 35 ,,1…, January 2008* 2007.
17. Verbakel WF, Cuijpers JP, Hoffmans D, *et al.* Volumetric intensity-modulated arc therapy vs. conventional IMRT in head-and-neck cancer: a comparative planning and dosimetric study. *Int J Radiat Oncol Biol Phys* 2009;74:252-259.

18. Clivio A, Fogliata A, Franzetti-Pellanda A*, et al.* Volumetric-modulated arc radiotherapy for carcinomas of the anal canal: A treatment planning comparison with fixed field IMRT. *Radiother Oncol* 2009;92:118-124.
19. Mackie TR, Scrimger JW, Battista JJ. A convolution method of calculating dose for 15-MV x rays. *Med Phys* 1985;12:188-196.
20. Mackie TR, Bielajew AF, Rogers DW*, et al.* Generation of photon energy deposition kernels using the EGS Monte Carlo code. *Phys Med Biol* 1988;33:1-20.
21. Papanikolaou N, Mackie TR, Meger-Wells C*, et al.* Investigation of the convolution method for polyenergetic spectra. *Med Phys* 1993;20:1327-1336.
22. Mackie TR, P. J. Reckwerdt, J. Purdy, W. Grant III, J. Palta, B. Butler and C. Perez. Madison, WI,. The convolution algorithm in IMRT. 3-D Conformal and Intensity Modulated Radiation Therapy. *Advanced Medical Publishing Inc.: 179-90.* 2001.
23. Mackie TRaRPJOGH, and Shepard D M. Convolution/superposition photon dose algorithm. *General Practice of Radiation Oncology Physics in the 21st Century A. S. a. D. Mellenberg. College Park, MD, American Association of Physicists in Medicine: 39-56.* 2000.
24. TomoTherapy Planning Guide *Inc. Madison, WI* 2007.
25. Soisson ET, Hoban PW, Kammeyer T*, et al.* A technique for stereotactic radiosurgery treatment planning with helical tomotherapy. *Medical dosimetry : official journal of the American Association of Medical Dosimetrists* 2011;36:46-56.
26. Accuray. Physics Essentials Guide, 2007.
27. CyberKnife A. Equipment specification, 2009.

Chapter 3. Materials and Methods

A brief discussion about the phantom, targets, and dose prescription is provided in the first part of the chapter. The second part of the chapter contains discussion about phantom positioning, film dosimetry, and film analysis for the delivery study.

3.1 PLANNING STUDY

3.1.1 TARGET SELECTION

Two types of target volumes were used for the study: 1) Spherical targets and 2) Irregular patient tumors.

3.1.1.1 SPHERICAL TARGETS

A selection of spherical targets was used to compare the ability of each planning modality for treating very small target volumes. Using drawing tools available on eclipse TPS two spherical targets of diameters 6 mm and 10 mm were created.

3.1.1.2 IRREGULAR TARGETS

A selection of irregular tumor volumes of various shapes and sizes were used to compare the effectiveness of each planning modality studied. Target details are shown in Table 3.1. Thirteen patients with brain lesions that were treated in the Montreal General Hospital (MGH) were retrospectively selected for this study. Patient selection was based on target volume size that ranged between 0.23 - 20.76 cm^3 with a mean volume of 4.7 ± 5.3 cm^3.

N#	Target Volume (cm^3)
1	1.6
2	1.9
3	8.8
4	2.9
5	2.5
6	20.8
7	3.2
8	3.3
9	4.0
10	2.1
11	0.2
12	5.4
13	4.7

Table 3.1 Volumes of the thirteen targets used in this study.

3.1.2 PHANTOM

The Lucy phantom (Standard Imaging Inc., Middleton, WI, USA) Figure 3.1 was used for planning and delivery verification in this study. It is a spherical acrylic phantom, designed for end to end quality assurance tests for stereotactic radiosurgery. The Lucy phantom comes with adaptors to interface to each of the SRS delivery systems used in the study and can be used for accurate SRS treatment delivery verification. The phantom is divided into two hemispheres so that a film cassette may be inserted in between the hemispheres. In this study a 3 inch Gafchromic EBT 2 film (ISP, Wayne, New Jersey, USA) is inserted into the film cassette for 2D measurement verification. The cassette is inserted into the hemisphere so that the position of the film is at the center of the phantom. The film plane in addition could be rotated so that the film is aligned with the coronal or sagittal plane. Five sharp markers in the cassette are used to produce five impressions on the film that are further used for film registration purposes.

Figure 3.1 Lucy® 3D QA phantom (Standard Imaging Inc, Middleton, WI).

For planning and delivery verification, the phantom was CT scanned and all target volumes were reproduced directly on the CT scan. The phantom was scanned with slice thickness of 1 mm and a field of view of 35 cm. This scan was used for planning with the DCA, NCP-IMRT, RapidArc and the CyberKnife techniques. For the Tomotherapy planning, the CT must include the couch to account for the attenuation of the treatment couch. The phantom was scanned a second time for the Tomotherapy planning using a FOV of 51.2 cm to include the couch in the FOV. Target volumes were then copied from the first scan onto the second scan after both CTs were registered.

3.1.3 DOSE PRESCRIPTION AND PLANNING CRITERIA

For the planning comparison, it is important to maintain the same set of prescription and planning criteria for all the modalities. In this work, a set of hard constraints and soft constraints were used. For each plan hard constraints must be met but soft constraints are only used a guideline. As mentioned in Chapter 1, normally the prescription dose is based on the size of the target. However, for this study a prescription dose of 10 Gy was chosen for all the targets. The reason for this was that the second part of the project was to compare measured distributions on film in the Lucy phantom. A typical radiosurgery dose would be too large for the dynamic range of the film used here.

The plans were normalized so the following hard constraints were met: i) 99% of target volume should receive the prescription dose of 10 Gy or more ($D_{99\%} \geq 10$ Gy), ii) 99.9% of target volume should receive 9.8 Gy or more ($D_{99.9\%} \geq 9.8$ Gy), and iii) the PITV < 2 (see section 3.3.2.1 for the definition of PITV). In addition to emphasize dose fall off, a soft constraint of $D_{max} \approx 13.5$ Gy was chosen. The D_{max} was determined from typical values achievable by a standard DCA technique used at the MGH and is typical of conventional Linac-based SRS plans with a high dose gradient.

3.1.4 SRS TREATMENT PLANNING

3.1.4.1 CONES

The Novalis Tx comes with wide rage of cones (diameters 4, 6, 7.5, 10, 12.5 and 15 mm) suitable to treat spherical tumors such as brain mets and other spherical shaped tumors. In this study 6mm and 10mm diameter cones were used for the spherical targets. For planning four arcs of 100° each were used for four different couch angles.

3.1.4.2 DYNAMIC CONFORMAL ARCS (DCA)

Similar to cones, for DCA planning a template of four arcs each of 100° arc length were used for four different table angles of 30^o, 60^o, 300^o and 330^o. A leaf margin of 1 mm was added to the target during the planning. The individual arcs were optimized by use of collimator rotation and manual positioning of MLC leaves. For this study, all the arcs were equally weighted.

3.1.4.3 NON-COPLANAR IMRT (NCP-IMRT)

For the NCP-IMRT technique, a pseudo-arc template mirroring the DCA technique was used. It uses 4 static beams at each table angle of 30°, 60°, 300° and 330°

for a total of 16 beams. A leaf margin of 1 mm was used and collimator angles were optimized before optimization. As mentioned previously, the iPlan TPS gives 4 solutions after optimization. In this study, we chose to use the "PTV only" option for all plans as this option tends to favor more homogeneous dose distributions in the PTV. As a consequence, to achieve sharp dose fall off outside the tumor boundaries a ring structure of 10 mm width with a margin of 1 mm from the PTV edge was created around the PTV. This ring structure was used as an organ at risk and low dose constraints were applied to the ring to force a dose gradient outside the PTV.

3.1.4.4 VOLUMETRIC MODULATED ARC THERAPY (RapidArc)

To maintain the consistency of the comparison between different planning techniques, the same four arcs and four table angles (30^o, 60^o, 300^o and 330^o) used for DCA planning were used for RapidArc planning. The same ring structure used for NCP-IMRT planning was also used for RapidArc optimization to force a sharper dose fall off.

3.1.4.5 TOMOTHERAPY

For the HI-ART TomoTherapy (TomoTherapy Inc., Madison, WI, USA) system, in order to produce a plan emphasizing high dose gradient, a previously published technique(1) was adopted for spherical targets. This technique suggests using additional nonanatomic planning structures to achieve sharp dose fall off. According to this technique a small volume is added at the center of the tumor. During planning, a maximum dose is prescribed to this small voxel so that there shouldn't be any hot spot near the tumor boundaries. In addition this technique also suggests using a peripheral ring around the tumor to achieve sharp dose fall off. In case of irregularly shaped targets, a standard clinical planning approach was followed. The plans were done with the

smallest field width (1.05 cm), a pitch of 0.215 and modulation factor from the range of 1.5 to 2.5.

3.1.4.6 CYBERKNIFE

The CyberKnife (Accuray Inc., Sunnyvale, CA, USA) planning was done with fixed collimators, for all plans a single collimator was used. Additionally beam reduction was applied to limit the total number of beams to fewer than 150 in order to produce a clinically acceptable delivery time. Annular rings or shells were also used in the CyberKnife planning to force a larger dose gradient outside the target.

3.1.5 PLAN COMPARISON

To calculate the different indices required for the planning comparison, all the plan dose matrices were transferred back to the Eclipse planning system. For DCA, IMRT, RapidArc and the CyberKnife a image voxel size of 0.7 mm x 0.7 mm x 1 mm (FOV= 35 cm, Image resolution 512 x 512, Slice width = 1 mm) was used, whereas for the Tomotherapy, to include the couch into the scan a larger FOV was used as result a image voxel size of 1 mm x 1 mm x 1 mm (FOV = 51.2 cm, Image resolution 512 x 512, Slice width = 1 mm) was used.

3.2 SRS PLAN EVALUATION TOOLS

Comparison between different plans requires detailed analysis of different aspects of the plan such as conformality, homogeneity and dose fall off. The choice of a suitable plan for a patient generally depends upon the patient specific information such as: target position and its surrounding OAR. For example, if the patient is treated for trigeminal neuralgia where the average tumor size is very small (~4 mm) and the average dose is as

high as >70 Gy, dose homogeneity is not of primary concern instead the primary concern is a sharp dose gradient to avoid giving a high dose to the neighboring brain stem.

In other cases such as acoustic neuroma, the target is also overlying the brainstem but the tumor size is relatively large (~3 cm) and the prescription dose (12-16 Gy SRS or 50 Gy SRT) is near the tolerance of the brainstem OAR. In this case, homogeneity of dose may be preferred to avoid overdosing the brainstem OAR. In the following sections different quantitative tools used for planning comparison study are discussed in detail.

3.2.1 VISUAL INSPECTION AND DOSE VOLUME HISTOGRAM ANALYSIS

All plans were reviewed visually and quantitatively with a dose volume histogram(2) (DVH) and using various dose indices. The isodoses are calculated on the CT scan to allow for inspection of the spatial dose distribution with respect to the target and OAR structures. A DVH gives information about the amount of volume a structure receives at different dose levels and can be used to calculate several indices used to evaluate a plan but it does not give any information about the spatial distribution of dose.

3.2.2 PHYSICAL DOSE INDICES

To facilitate the comparison between different treatment planning techniques and to obtain the quantitative indices for comparison, the following planning comparison tools were used.

3.2.2.1 RTOG PITV

In the Radiation Therapy Oncology Group (RTOG)(3) radiosurgery guidelines, the conformity index (PITV) is defined as the ratio of the prescription isodose volume to tumor volume.

$$PITV = \frac{Prescription\ Isodose\ Volume\ (PI)}{Target\ Volume\ (TV)} \quad (3.1)$$

In ideal situations when the volume of prescription isodose is exactly equal to target volume or in other words zero volume of normal tissue is exposed to the prescription dose, the PITV has perfect score of 1. Any deviation from a perfect score results into higher or lower value of PITV. A higher value (>1) means the irradiation volume includes target volume and normal tissue whereas lower value (<1) implies under treatment of the tumor.

According to the RTOG guidelines(3), a score between 1 and 2 is clinically accepted, a score between 2 and 2.5 or 0.9 and 1 is considered a minor violation, and a score more than 2.5 or less than 0.9 is considered a major violation.

3.2.2.2 PADDICK CONFORMITY INDEX

The RTOG conformity index suffers from a major drawback, there is an assumption made that the prescription isodose line is at the same location as the target volume and both are of the same shape. In extreme cases it is possible that the PITV ratio is equal to 1 while two volumes do not overlap each other and are different in shape. In Figure 3.2, for all the cases shown, the PITV ratio gives the perfect score of 1, but in actuality the plans are very different in conformality and tumor coverage.

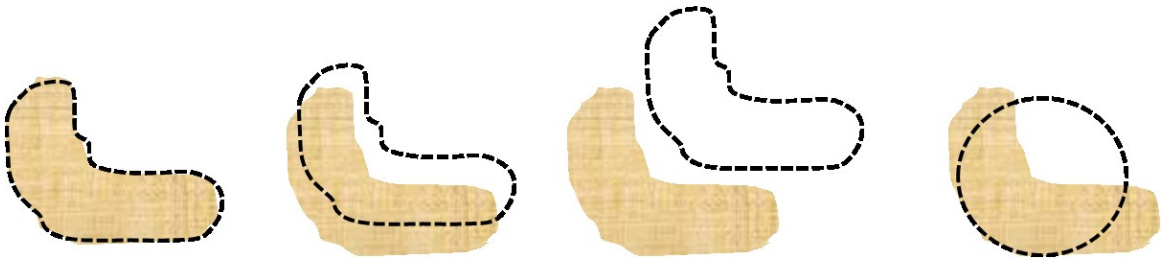

Figure 3.2 Illustration of limitation of RTOG PITV where each case shown has the same PITV of 1 but varying amounts of PTV coverage. Brown shaded area is the target and the black dashed line is the prescription isodose line.

To overcome this problem, the spatial overlap between target and prescription isodose line also needs to be taken into account. A relatively new conformity index first proposed by van't Reit et al.(4) and then later by Paddick(5) was used in this study.

$$CI_{Paddick} = \frac{TV_{RI}^2}{TV * V_{RI}} \quad (3.2)$$

Here TV_{RI} is the target volume covered by the reference isodose, TV is the target volume, and V_{RI} is the volume of the reference isodose. $CI_{Paddick}$ has an expected range of 0.5 to 1, where 1 is the perfect score. To compare the results with other work both conventional conformity index (PITV) and $CI_{Paddick}$ were calculated for this study.

3.2.2.3 PADDICK GRADIENT INDEX

A gradient index measures the sharpness in dose fall off outside the tumor boundaries and can be used for the comparison of rival plans having equal conformity index. Paddick's gradient index as used in this study is the ratio of the volume of tissue

receiving at least 50% of the prescription dose ($V_{50\%RI}$) to the volume of tissue receiving at least the prescription dose V_{RI}.

$$GI_{Paddick} = \frac{V_{50\%\,RI}}{V_{RI}} \quad (3.3)$$

A plan with a higher dose fall off would then have a lower gradient index value. The value of the GI index is always greater than one and the closer the ratio to one, the sharper the dose fall off is.

3.2.2.4 COMBINED CONFORMITY AND GRADIENT INDEX

To incorporate both conformality and dose gradient into one single index a conformity-gradient index (CGI)(6) was used. CGI is the average of the conformity index CGI_c and the gradient index CGI_g. In this definition, the conformity index is simply the reciprocal of the PITV scaled to 100. The gradient index, CGI_g, is based on the difference between the effective radius ($R_{Eff,Rx}$) of the prescription isodose volume (V_{Rx}) and the effective radius ($R_{Eff,50\%Rx}$) of the volume of 50% of the prescription isodose ($V_{50\%}$). The effective radii are calculated assuming the volumes are equivalent to a sphere. The gradient index in this formulation was based on Linac radiosurgery experience and it was assumed the ideal distance between the two radii is 3 mm (6). Therefore a perfect score of 100 for the gradient index CGI_g occurs when this distance is 3 mm. The combined conformity and gradient index is defined as:

$$CGI = \frac{(CGI_c + CGI_g)}{2} \quad (3.4)$$

$$CGI_c = 100 * \frac{Target\ Volume}{Prescription\ isodose\ volume} \quad (3.5)$$

$$CGI_g = 100 - \{100.\left[(R_{Eff,50\%R_x} - R_{Eff,R_x}\right) - 0.3\ cm) \quad (3.6)$$

$$R_{Eff,x\%} = \sqrt[3]{\frac{3V_{x\%}}{4\pi}} \quad (3.7)$$

The expected range of CGI is from 50 to 100 where 100 is the perfect score.

3.2.2.5 HOMOGENEITY INDEX

Homogeneity is the measure of uniformity of a dose distribution in the target. A simple homogeneity index was used in this study defined as:

$$HI(MDPD) = \frac{Maximum\ Dose(MD)}{Prescription\ Dose(PD)} \quad (3.8)$$

According to the recommendations of RTOG protocol(7) for any plan this ratio shall be less than or equal to 2. A ratio greater than 2 but less than 2.5 is considered as minor deviation but a ratio greater than 2.5 is considered as major deviation of protocol.

3.2.2.6 TARGET SYMETRY

To account for the irregularity in shape of different targets a symmetry index (SI) is calculated.

$$SI = \frac{\sqrt[2]{(x-r)^2} + \sqrt[2]{(y-r)^2} + \sqrt[2]{(z-r)^2}}{3r} \quad (3.9)$$

Where x, y and z are the distance from center of the target to its boundary at the central axial slice along the lateral, vertical and superior-inferior direction respectively. The effective radius, *r*, is the radius of a sphere with volume equivalent to the target

volume. A perfectly spherical target has SI of zero otherwise higher values of SI implies a larger asymmetry.

3.2.3 RELATION OF PHYSICAL DOSE INDICES

To develop a clinically acceptable treatment plan, it is very important to maintain a balance between different indices. It is well known that improvement in one index could worsen the other(8); this effect is more specific to the techniques where no intensity modulation is used. For example, an increase in maximum allowed dose to the target could improve the dose gradient of the plan but on the other hand it worsens the homogeneity of dose distribution. The issue is further elaborated with following example.

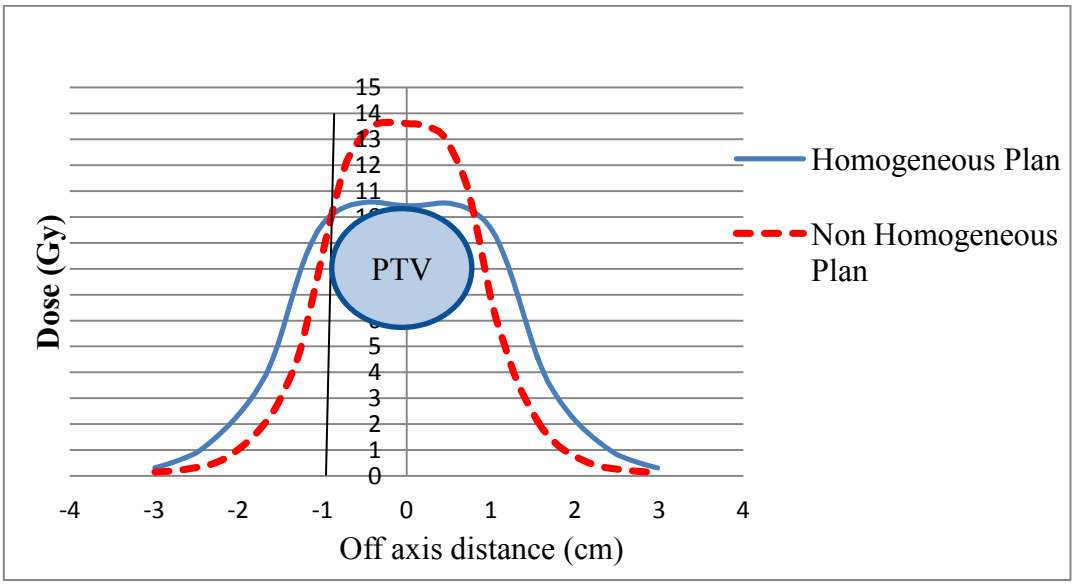

Figure 3.3 Example illustrating the co- relation between homogeneity and gradient.

In Figure 3.3, two dose profiles corresponding to two different plans are shown. Both of the plans were made to meet the same prescription coverage of the target, but the plan corresponding to the dotted (red) profile has higher value of maximum allowed dose as compared to the plan shown with the solid (blue) profile. As a result the first plan

(dotted) is poor in terms of homogeneity but better in terms of dose gradient and in contrast the second plan (solid) is good in terms of homogeneity but poor in terms of dose gradient.

3.3 DELIVERY STUDY

The second part of this work was to perform a treatment delivery study. The main objective of the delivery study was to compare the calculated and measured dose against each other and to verify the differences seen in planning between the various delivery techniques studied.

3.3.1 TARGETS

The aim of verifying the dose distributions for the different targets was to determine: i) The accuracy of dose delivery in comparison to the planned dose and ii) The delivery modality (Novalis Tx, Tomotherapy, CyberKnife) that is most suitable depending upon the target shape. The figure 3.4 shows the phantom positioning for each of the techniques used.

(a)

(b)

(c)

Figure 3.4 Phantom positioning for Tomotherapy (a), Novalis Tx (b) and CyberKnife (c) systems.

3.3.2 DOSE DISTRIBUTION ANALYSIS

For the comparison, plans were delivered to radiochromic EBT 2 (ISP, Wayne, New Jersey) film inserted into the film cassette placed in the Lucy phantom. Film is placed in the phantom so that the film plane passes through the center of the phantom. For the delivery verifications, the film was aligned to the central axial plane of the phantom. To check the accuracy of the delivery, a comparison between film measurements and treatment planning system calculated dose was performed. Dose delivered to the film was compared against the corresponding calculation slice exported from the treatment planning system. To quantify the comparison, beam profiles and gamma map analysis were compared. The different steps used during phantom positioning and film dosimetry are explained in the following sections.

3.3.3 PHANTOM POSITIONING

Different frames were used for fixation and immobilization of the phantom on the treatment couch: The BrainLAB stereotactic frame was used for the Novalis Tx, the Radionics GTC relocateable head frame was used for the Tomotherapy and no frame was required for the CyberKnife. The CyberKnife does not require a frame as the couch does not move during the treatment. The room lasers and imaging techniques available on each delivery modality were used for localization of the phantom. For the initial setup, the phantom was placed on the treatment couch and aligned by using the room lasers. Afterwards, the phantom was imaged using on board imaging techniques such as MVCT for the Tomotherapy, CBCT and ExacTrac for the Novalis Tx, and stereoscopic X-ray imaging on the CyberKnife. On board images were compared with treatment planning images by using platform specific image fusion algorithms and any required shift was

applied. Different studies have shown the MVCT imaging system on the Tomotherapy Unit(9-12), the ExacTrac system(13, 14) and OBI system(13, 15) on the Novalis Tx, and the imaging system on the CyberKnife(16, 17) to have the accuracy suitable for SRS localization.

3.3.4 EBT 2 FILM DOSIMETRY

Compared to traditional radiotherapy, dosimetry of small fields used in SRS treatment is not straight forward. Small fields pose a different challenges for the use of standard air filled ionization chambers, including the absence of charge particle equilibrium, volume averaging effect and positioning issues. Radiochromic film provides high spatial accuracy and near water equivalence nature making them a suitable dosimeter to measure beam profiles and even absolute dose for small fields and IMRT. In this study Gafchromic EBT 2 (ISP, Wayne, New Jersey) was used as a dosimeter for measurements. For calibration a piece of film is cut into 20 pieces, each of size 5 x 5 cm^2. To preserve the orientation of the films for scanning each piece was marked, and 17 film pieces were exposed at 6 cm depth on the Novalis Tx with a 10 x 10 cm^2 beam. Doses of 0 to 9 Gy was given to the film pieces. Although the prescription dose used for planning was 10 Gy, the delivery MUs were scaled down to half in order to stay in the useful dynamic dose range of the film (~8 Gy).

3.3.5 FILM ANALYSIS

To analyze the films, FILM QA (ISP, Wayne, New Jersey, USA) was used. For film scanning an EPSON 1680 scanner (EPSON, Long Beach, CA,USA) was used with scanner settings of 150 dpi and 48 bit RGB mode. Once the film is irradiated, a waiting

period of 48 h(18) was observed before further scanning. The same postirradiation time was used for both calibration and measurement films.

3.3.6 DOSE COMPARISON TOOLS (GAMMA INDEX)

For the comparison between measured dose on the film and calculated dose from the TPS, dose slice is exported to FILM QA software. To elaborate the comparison between measured and planned dose: beam profile, gamma index and isodose lines were calculated and compared. The gamma index was calculated for a different values of dose difference and distance to agreement. Dose difference (DD) is percentage difference between pixel in reference image (TPS) to the corresponding pixel in measured image (film). The distance to agreement (DTA) is the measure of the distance between the pixel in reference image to the pixel in measured image having the same dose.

3.4 REFERENCES

1. Soisson ET, Hoban PW, Kammeyer T, *et al.* A technique for stereotactic radiosurgery treatment planning with helical tomotherapy. *Medical dosimetry : official journal of the American Association of Medical Dosimetrists* 2011;36:46-56.
2. Drzymala RE, Mohan R, Brewster L, *et al.* Dose-volume histograms. *Int J Radiat Oncol Biol Phys* 1991;21:71-78.
3. Shaw E, Kline R, Gillin M, *et al.* Radiation Therapy Oncology Group: radiosurgery quality assurance guidelines. *International journal of radiation oncology, biology, physics* 1993;27:1231-1239.
4. van't Riet A, Mak AC, Moerland MA, *et al.* A conformation number to quantify the degree of conformality in brachytherapy and external beam irradiation: application to the prostate. *Int J Radiat Oncol Biol Phys* 1997;37:731-736.
5. Paddick I. A simple scoring ratio to index the conformity of radiosurgical treatment plans. Technical note. *J Neurosurg* 2000;93 Suppl 3:219-222.
6. Wagner TH, Bova FJ, Friedman WA, *et al.* A simple and reliable index for scoring rival stereotactic radiosurgery plans. *Int J Radiat Oncol Biol Phys* 2003;57:1141-1149.
7. Shaw E, Kline R, Gillin M, *et al.* Radiation Therapy Oncology Group: radiosurgery quality assurance guidelines. *Int J Radiat Oncol Biol Phys* 1993;27:1231-1239.
8. Hong LX, Garg M, Lasala P, *et al.* Experience of micromultileaf collimator linear accelerator based single fraction stereotactic radiosurgery: tumor dose inhomogeneity, conformity, and dose fall off. *Medical physics* 2011;38:1239-1247.

9. Forrest LJ, Mackie TR, Ruchala K*, et al.* The utility of megavoltage computed tomography images from a helical tomotherapy system for setup verification purposes. *International journal of radiation oncology, biology, physics* 2004;60:1639-1644.
10. Welsh JS, Bradley K, Ruchala KJ*, et al.* Megavoltage computed tomography imaging: a potential tool to guide and improve the delivery of thoracic radiation therapy. *Clinical lung cancer* 2004;5:303-306.
11. Boswell S, Tome W, Jeraj R*, et al.* Automatic registration of megavoltage to kilovoltage CT images in helical tomotherapy: an evaluation of the setup verification process for the special case of a rigid head phantom. *Medical physics* 2006;33:4395-4404.
12. Woodford C, Yartsev S, Van Dyk J. Optimization of megavoltage CT scan registration settings for thoracic cases on helical tomotherapy. *Physics in medicine and biology* 2007;52:N345-354.
13. Kim J, Jin JY, Walls N*, et al.* Image-guided localization accuracy of stereoscopic planar and volumetric imaging methods for stereotactic radiation surgery and stereotactic body radiation therapy: a phantom study. *International journal of radiation oncology, biology, physics* 2011;79:1588-1596.
14. Gevaert T, Verellen D, Tournel K*, et al.* Setup Accuracy of the Novalis ExacTrac 6DOF System for Frameless Radiosurgery. *International journal of radiation oncology, biology, physics* 2011.
15. Ma J, Chang Z, Wang Z*, et al.* ExacTrac X-ray 6 degree-of-freedom image-guidance for intracranial non-invasive stereotactic radiotherapy: comparison with kilo-voltage cone-beam CT. *Radiotherapy and oncology : journal of the European Society for Therapeutic Radiology and Oncology* 2009;93:602-608.
16. Chang SD, Main W, Martin DP*, et al.* An analysis of the accuracy of the CyberKnife: a robotic frameless stereotactic radiosurgical system. *Neurosurgery* 2003;52:140-146; discussion 146-147.
17. Tsai JT, Lin JW, Chiu WT*, et al.* Assessment of image-guided CyberKnife radiosurgery for metastatic spine tumors. *Journal of neuro-oncology* 2009;94:119-127.
18. Cheung T, Butson MJ, Yu PK. Post-irradiation colouration of Gafchromic EBT radiochromic film. *Phys Med Biol* 2005;50:N281-285.

Chapter 4. Results and Discussion

4.1 RESULTS

This chapter is divided into two sections; the first section contains the planning comparison between the Novalis Tx (Varian Inc., Palo Alto, CA, USA) based techniques (DCA, NCP-IMRT, RapidArc), the Tomotherapy (TomoTherapy Inc., Madison, WI, USA) and the CyberKnife (Accuray Inc., Sunnyvale, CA, USA). The planning comparison was done for spherical and irregular shaped targets. The second section shows the results of the delivery study for two spherical and three irregular targets planned. In addition, the clinical deliverability of plans and accuracy of different delivery techniques are evaluated.

4.2 PLANNING STUDY

4.2.1 SPHERICAL TARGETS

Table 4.1 summarizes the planning comparison results between all the techniques for two spheres of diameter 6 mm and 10 mm. These targets were planned under the same set of prescription goals defined in section 3.2.3.

Typically, for small spherically shaped targets such as solitary brain mets or the trigeminal nerve a large dose must be delivered in a single fraction. To avoid irradiating the surrounding normal tissues with a high dose, a sharp dose fall off is an important

priority. In such cases dose homogeneity is compromised to achieve a sharper dose fall off.

Traditionally in clinics with linac based SRS programs, small spherical targets are treated with collimators (cones) attached to the linac and an arc based planning approach. For point sources, the geometric penumbra is inversely proportional to the source to diaphragm distance. With cone attachments and an extended source to diaphragm distance, the geometric penumbra is reduced which helps increase the dose fall off. In contrast with conventional MLCs built into the head of the linac, the geometric penumbra of MLC is larger and with a minimum leaf width of 5 mm it is difficult to conform the field shape to a small spherical target. For the Novalis Tx, a high definition multileaf collimator (HD 120 MLC) having 2.5 mm minimum leaf width helps improve the ability to conform the field to a spherical target but still suffers from a larger geometric penumbra due to decreased source to diaphragm distance.

	Perfect score	Novalis Cones	DCA	NCP-IMRT	RapidArc	CyberKnife	Tomotherapy
Diameter 6mm							
PITV	1	1.46	1.44	1.11	2.1	1.33	2.19
Paddick's CI	1	0.7 2	0.62	0.76	0.26	0.82	0.46
Paddick's GI	<	2.79	5.92	10.4	10.75	5.25	17.38
CGI	100	94.11	86.90	92.97	54.79	91.21	61.04
MDPD	1	1.71	1.4	1.13	1.11	1.54	1.12
Diameter 10mm							
PITV	1	1.39	1.34	1.16	1.66	1.14	1.35
Paddick's CI	1	0.68	0.74	0.84	0.60	0.87	0.73
Paddick's GI	<	2.64	4.09	5.45	7.75	3.74	9.74
CGI	100	88.49	86.05	88.45	66.59	94.67	72.06
MDPD	1	1.66	1.38	1.1	1.08	1.75	1.19

Table 4.1 Summary of results for planning comparison of spherical targets. The circled data indicates the best result for a particular criteria.

The axial and coronal distribution for spherical targets of 6 mm diameter for each technique is shown in Figure 4.1.

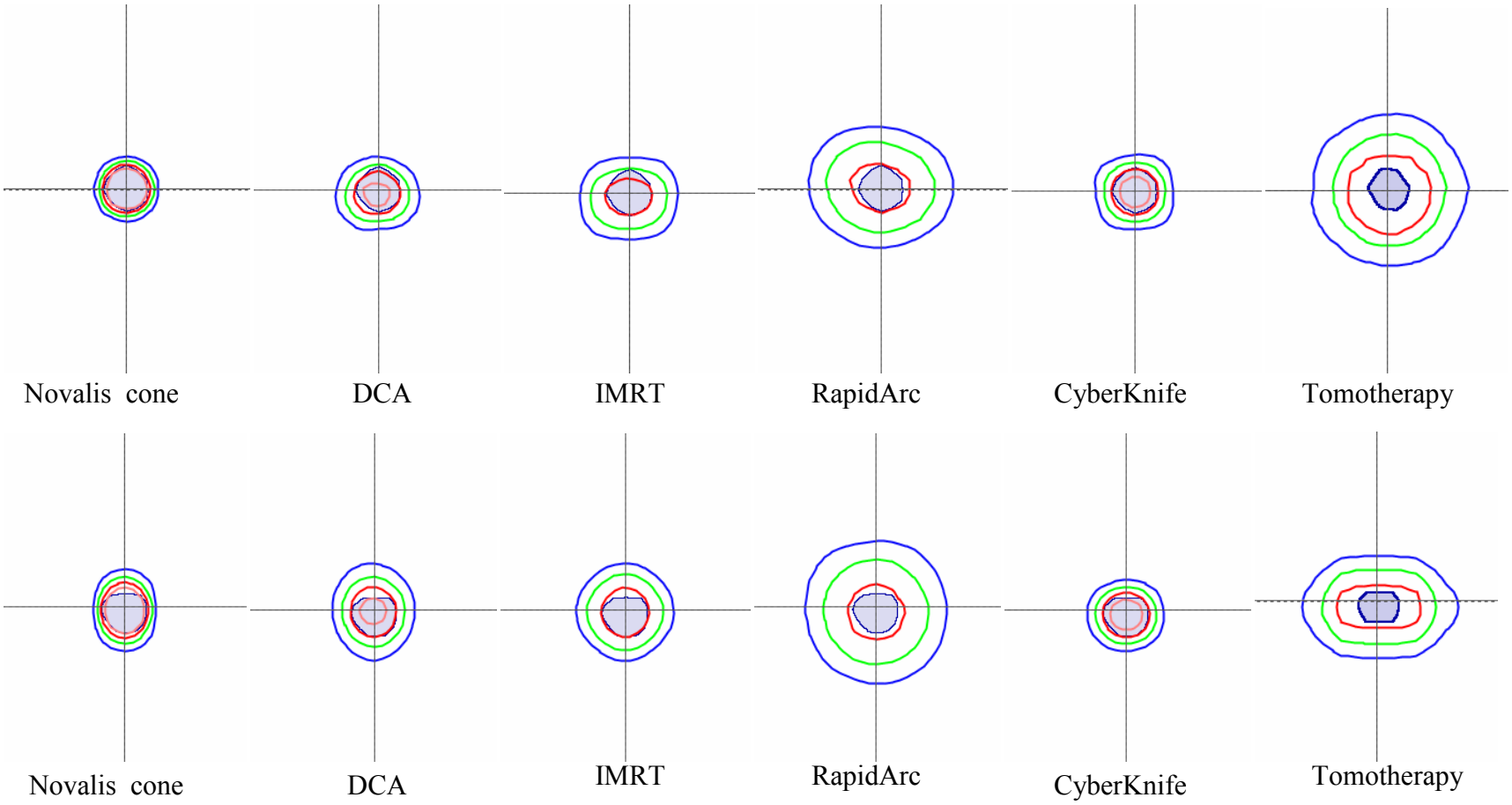

Figure 4.1 Axial (top) and coronal plane (bottom) dose distribution of 6 mm diameter spherical target for the Novalis cone, DCA, NCP-IMRT, RapidArc, CyberKnife and Tomotherapy respectively (Isodose lines: pink - 12.5 Gy, red - 10 Gy, green – 7.5 Gy, blue - 5 Gy).

The axial and coronal distribution for spherical targets of 10 mm diameter for each technique is shown in Figure 4.2.

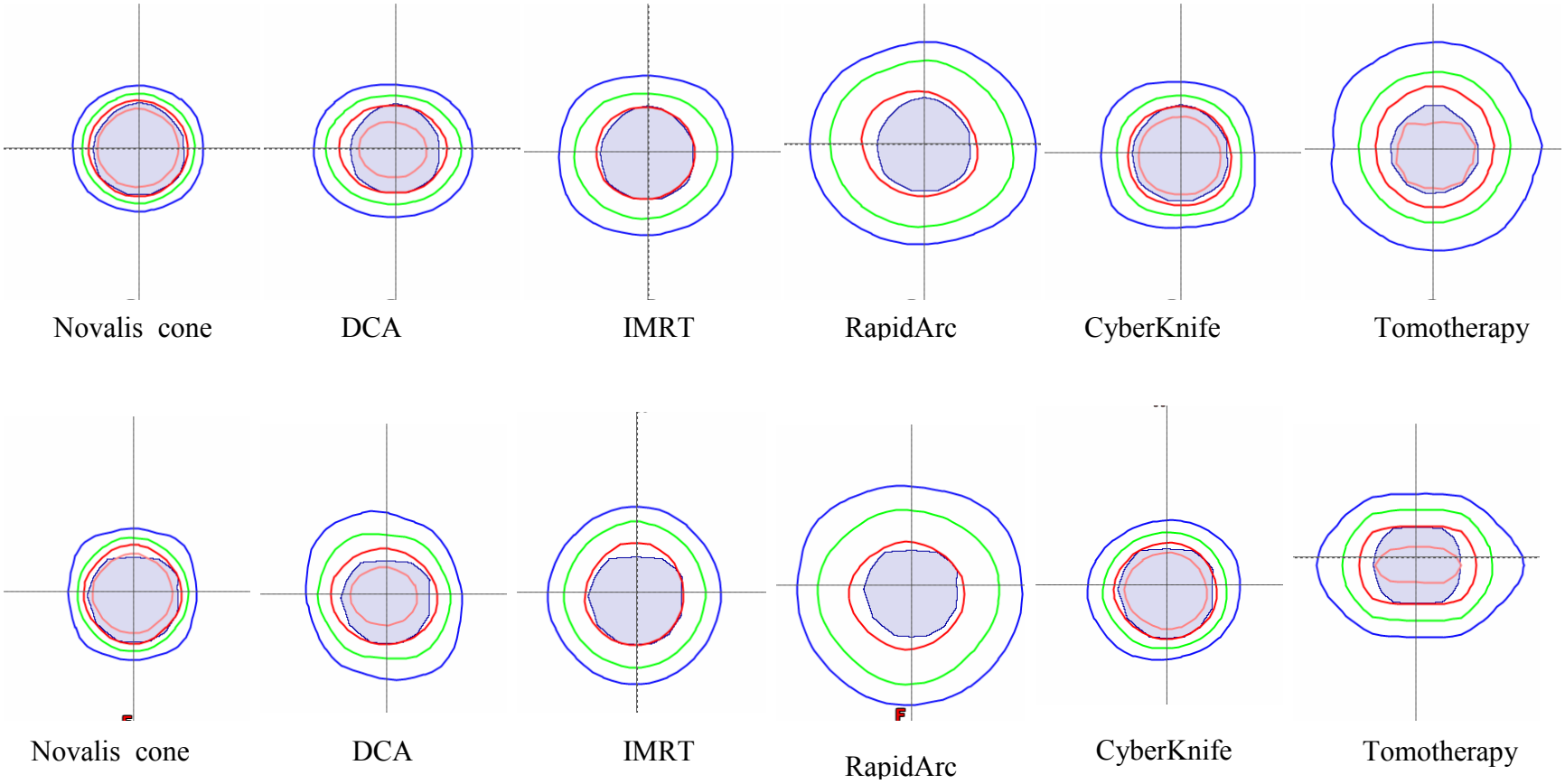

Figure 4.2 Axial (top) and coronal plane (bottom) dose distribution of 10 mm diameter spherical target for the Novalis cone, DCA, NCP-IMRT, RapidArc, CyberKnife and Tomotherapy respectively (Isodose lines: pink - 12.5 Gy, red - 10 Gy, green – 7.5 Gy, blue - 5 Gy).

From Table 4.1 it appears that dose homogeneity was directly related to the dose gradient (or inversely related to the Paddick's gradient index). This general relationship was expected for spherical targets as mentioned in section 3.3.3. Also as expected, the cone based techniques (Novalis and CyberKnife) resulted in the highest dose gradients. Among the MLC based techniques, DCA produced the next sharpest dose fall off followed by NCP-IMRT, RapidArc and the Tomotherapy. Here, it is important to mention that for the small spherical target of diameter 6 mm, the method different planning systems interpolate dose to each voxel could have significant effect on the plan quality. Based on these results, the standard cone based approach with arcs clearly shows advantages in terms of dose gradient for small spherical targets.

One limitation observed in this part of the planning study particularly with the Novalis cones comes from our prescription condition of 99.9% of the target volume receiving 9.8 Gy or more ($D_{99.9\%} \geq 9.8$ Gy). Typically plans were initially optimized to meet the constraint of 99% of the target volume receiving 10 Gy ($D_{99\%}$= 10 Gy) but the minimum dose ($D_{99.9\%}$) was not met. In order to meet the minimum dose constraint the plans were renormalized to cover the small volume of target that was not covered by 9.8 Gy. The result of renormalizing the plans was that the DVH shifts degrading the plan quality with an increase in the PITV and maximum dose to the target. Meanwhile a minimal change in the dose gradient is observed. In the clinic, the planner does not normally try to meet the minimum dose criteria ($D_{99.9\%}$) in order to spare normal tissue receiving doses above the prescription dose. Therefore the cone based plans may have been acceptable and would not have required renormalization, which would have improved the dosimetric characteristics of these plans.

It was observed that the IMRT MLC based techniques resulted in a larger Paddick's gradient index or shallower dose fall off. For the NCP-IMRT technique, the iPlan TPS gives 4 solutions with increasing amounts of priority placed on OAR sparing. In our study, we chose to use consistently the "PTV only" option that favors a homogeneous dose distribution in the PTV. Many of the planning systems did not have a "SRS" planning module so alternative optimization strategies based on large field treatments were used. For the RapidArc and Tomotherapy planning, the optimization algorithm must be forced to have a larger dose gradient. In RapidArc planning, we used an annulus ring around the PTV to drive the optimization towards a steeper dose gradient. In the Tomotherapy planning, we used a previously published technique (1) to force a steeper dose gradient. In this technique we use an annulus ring and a voxel in the center of the PTV to which a higher dose is prescribed. For all these IMRT techniques the dose fall off might be improved by changing the optimization criteria.

The CyberKnife is a cone based technique that is also inversely planned. The robotic arm has a nominal source-to-axis distance of 80 cm which allows the linac to be closer to the patient surface than a typical linac with 100 cm source-to-axis distance. This helps to reduce the geometric penumbra and increase dose fall off. The robotic arm also allows for many beam entry points that are non-coplanar which should also help to increase dose fall off. During this study it was observed that the CyberKnife had shown better dose gradient and conformality as compared to all the MLC based techniques. When comparing to the Novalis cones technique, the CyberKnife plans were quite comparable. However, it was observed that for the 6 mm diameter target, the plan with the Novalis cones (GI 2.79) had a better gradient than the CyberKnife plan (GI 5.25). For

the 10 mm diameter target, again the Novalis cones plan (GI 2.64) had shown the better gradient than CyberKnife plan (GI 3.74) although the maximum dose delivered by the CyberKnife was higher by 0.9 Gy. Although the CyberKnife can produce non-coplanar and non-isocentric beam arrangements coming from 1600 different directions, the beam entry is limited to the upper hemisphere above the couch and this may put some restriction on the overall plan quality.

A poor dose gradient with Tomotherapy as compared to other techniques could be because the smallest field size available from this MLC is 6.25 mm x 10 mm. This field size is relatively big for small targets such as spheres of diameter 6 mm. Finally, in the Tomotherapy the gantry rotates around the patient essentially in a coplanar arrangement and does not allow for non-coplanar beams. This would also help to explain the poorer dose gradient seen in the plans from the Tomotherapy.

Summary: This study showed that the Novalis cones and the CyberKnife were the best techniques for planning small spherical targets in SRS. Both techniques were able to achieve good dose gradients as well as clinically acceptable conformality. All the MLC based techniques showed poorer dose gradients. Similar results of better dose gradients by linac cones was also shown by Wolff et al.(2) by comparing them against the RapidArc technique. In a different study done by Cozzi et al.(3) static IMRT, helical tomotherapy and intensity modulated arc therapy techniques showed better improved target coverage but stereotactic arc therapy using cones and CyberKnife techniques showed most sparing of healthy normal brain tissue due to their sharp dose fall of outside the tumor boundaries.

4.2.2 IRREGULAR TARGETS

Table **4.2** summarizes the planning comparison results between DCA, NCP-IMRT, RapidArc, Cyberknife and Tomotherapy for the thirteen irregular targets.

	1	2	3	4	5	6	7	8	9	10	11	12	13	Mean ± σ
Volume (cm^3)	4.7	4.01	5.44	3.31	2.45	20.76	1.59	0.23	2.86	2.12	3.23	8.82	1.91	
SI	0.095	0.107	0.121	0.122	0.137	0.153	0.214	0.217	0.248	0.279	0.333	0.387	0.400	
PITV														
DCA	1.33	1.34	1.99	1.35	1.41	1.41	1.59	1.61	1.38	1.89	1.89	1.79	1.57	1.58±0.24
NCP-IMRT	1.23	1.28	1.67	1.33	1.32	1.29	1.28	1.57	1.33	1.59	1.51	1.63	1.17	1.4±0.17
RapidArc	1.25	1.09	1.77	1.20	1.10	1.28	1.56	1.26	1.14	1.54	1.29	1.26	1.23	1.3±0.2
CyberKnife	1.24	1.28	1.43	1.32	1.11	1.39	1.15	1.18	1.18	1.36	1.33	1.50	1.27	1.29±0.12
Tomotherapy	1.18	1.14	1.27	1.20	1.34	1.07	1.68	2.06	1.21	1.38	1.27	1.29	1.48	1.35±0.26
Paddick's CI														
DCA	0.75	0.74	0.50	0.74	0.71	0.71	0.63	0.62	0.72	0.53	0.52	0.56	0.63	0.64±0.09
NCP-IMRT	0.81	0.78	0.60	0.75	0.76	0.78	0.78	0.64	0.75	0.63	0.66	0.61	0.83	0.72±0.08
RapidArc	0.80	0.91	0.56	0.84	0.91	0.78	0.64	0.75	0.87	0.65	0.77	0.79	0.81	0.78±0.1
CyberKnife	0.80	0.78	0.70	0.76	0.88	0.72	0.86	0.85	0.85	0.73	0.75	0.67	0.79	0.78±0.07
Tomotherapy	0.83	0.86	0.77	0.82	0.74	0.91	0.59	0.49	0.82	0.72	0.77	0.77	0.68	0.75±0.12
Paddick's GI														
DCA	3.05	2.99	3.06	3.22	3.47	2.64	3.33	4.49	3.27	3.24	3.12	3.4	3.07	3.26±0.43
NCP-IMRT	3.18	3.16	3.22	3.19	3.60	2.62	4.25	6.08	3.44	3.72	3.74	3.17	4.06	3.65±0.85
RapidArc	3.14	3.93	5.18	3.89	3.32	2.89	4.48	5.62	4.07	3.82	4.12	3.85	3.8	4.01±0.75
CyberKnife	4.58	4.22	4.45	4.24	3.97	3.21	4.05	6.54	4.14	4.56	4.29	4.14	5.16	4.43±0.77
Tomotherapy	4.35	4.31	5.22	4.98	5.02	3.74	7.71	8.54	5.24	5.27	4.81	5.22	4.79	5.32±1.33
CGI														
DCA	76.9	78.2	59.2	77.8	76.3	64.1	75.6	81.6	77.4	67.9	65.4	53.7	76.6	71.59±8.6
NCP-IMRT	79.3	79	64	78.5	78.5	68.7	79.8	78.7	78.0	70.9	69.1	60.4	83.5	74.51±7.06
RapidArc	78.9	81.7	45.1	78.7	89.1	64.8	69.9	88.7	81.2	71.6	73.8	65.7	82.7	74.76±11.8
CyberKnife	67.7	70.7	59.6	70.8	84.0	55.2	75.8	97.4	78.7	71.8	70.3	52.8	73.2	71.37±11.8
Tomotherapy	72.8	76.6	61.3	72	69.8	63.9	53.5	66.5	72.0	68.7	70.5	53.0	69.2	66.9±7.2
MDPD														
DCA	1.23	1.28	1.34	1.24	1.22	1.25	1.36	1.4	1.35	1.37	1.31	1.31	1.45	1.32±0.07
NCP-IMRT	1.09	1.11	1.11	1.11	1.09	1.09	1.09	1.1	1.1	1.12	1.1	1.09	1.08	1.1±0.01
RapidArc	1.13	1.25	1.13	1.26	1.35	1.34	1.11	1.24	1.27	1.28	1.26	1.26	1.27	1.24±0.07
CyberKnife	1.28	1.28	1.35	1.35	1.39	1.39	1.12	1.22	1.19	1.25	1.37	1.32	1.25	1.29±0.08
Tomotherapy	1.15	1.21	1.21	1.14	1.15	1.13	1.05	1.26	1.13	1.21	1.2	1.27	1.21	1.18±0.06

Table 4.2 Summary of results for SRS planning of irregular targets. Paddick's CI is Conformity index, Paddick's GI is gradient index, CGI is conformity-gradient index, MDPD is the homogeneity index and SI is a symmetry index. The circled data indicates the best result for a particular criteria.

4.2.2.1 RESULTS FOR CONFORMALITY INDEX

The definition of conformity index is given in Chapter 3, section 3.3. Below is the bar chart representation of Paddick's conformity index for all thirteen irregular targets planned with all five techniques.

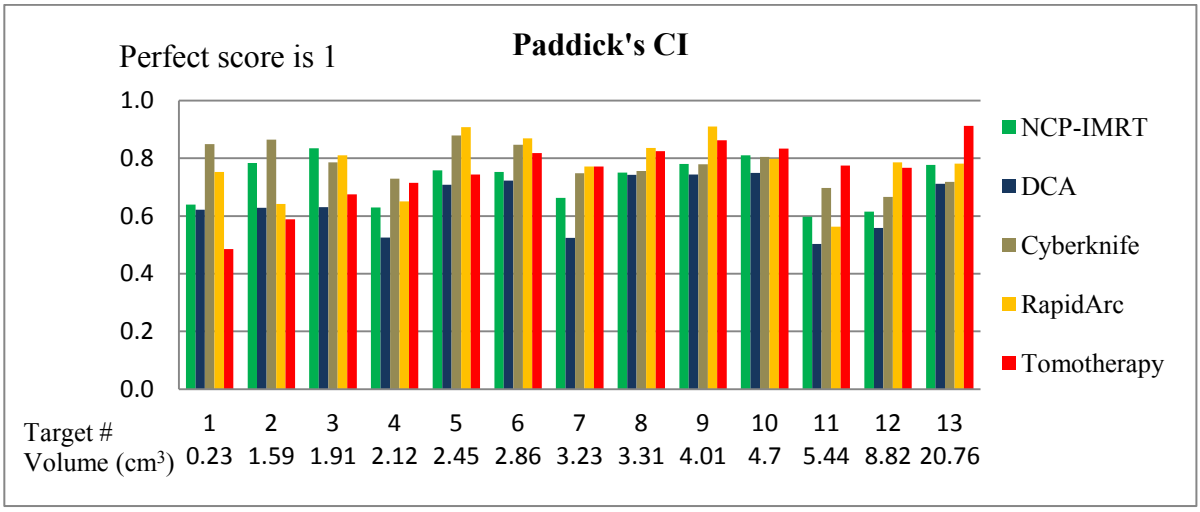

Figure 4.3 Paddick's conformity index for the thirteen irregular targets.

From Table 4.2 on average the Paddick's conformity index $CI_{Paddick}$ was 0.64±0.09, 0.72±0.08, 0.78±0.10, 0.78±0.07, and 0.75±0.12 for the DCA, NCP-IMRT, RapidArc, Cyberknife and Tomotherapy techniques respectively. All of the techniques produced plans with comparable conformality with the exception of dynamic conformal arcs (DCA).

For the DCA technique, shown by the blue bars in Figure 4.3, the conformality index improves with increasing target volume with the exception of the targets having volumes 3.23 cm^3, 5.44 cm^3 and 8.82 cm^3. The explanation for this might be because both the 3.23 cm^3 and 8.82 cm^3 targets were more irregular in shape with relatively larger SI of 0.333 and 0.387 respectively. The low conformality for the more symmetrical

target with volume 5.44 cm^3 could be because the plan was not fully optimized as DCA is a forward planning technique.

In the case of RapidArc and NCP-IMRT no such relation (between target volume and conformality) was observed except that for the smallest target 0.23 cm^3 both techniques showed poor conformality which may be problematic depending upon the dose prescribed to the target. In this study, plan conformality for both of these inversely planned techniques also appears to be independent from target symmetry. In both techniques the fluence of the beams is optimized to conform the dose to the shape of the target structure. As a result, the independence of conformality from target asymmetry may be expected except for small targets where the MLC leaf width becomes comparable to the target size. Overall, the NCP-IMRT and RapidArc techniques showed very similar plan characteristics, probably because we used the same beam arrangement (couch angles) and MLC for both techniques.

The CyberKnife plan also did not show any relation between conformality, symmetry or target volume. The capability of the CyberKnife to use inverse planning, one or more cones per treatment and a large number of beams coming from different directions using non-isocentric beam arrangements makes very conformal planning possible. In our study, the maximum number of cones used in a plan was 2, most plans were done with a single cone to improve treatment delivery time. At the time of planning, the center where the Cyberknife planning was done did not use the variable collimator called the IRIS. It is expected that conformality may be improved with planning using the IRIS(4). In addition, it may be possible to improve conformality further by allowing more than 150 beams, which was the limit we used in our study.

The Tomotherapy plans shows improvement in dose conformality with an increase in target volume. With the Tomotherapy, it is difficult to make conformal plans for small targets because of the relatively large minimum field size of 6.25 mm x 10 mm. This might explain the poorer conformality observed for the smaller targets with volumes 0.23 cm^3, 1.56 cm^3 and 1.91 cm^3. Overall, the conformality for larger sized target sizes was comparable with the other techniques. This was expected as the Tomotherapy uses a large number of beams (51 projections) in the IMRT optimization, expecting that it would be easier to conform the prescription dose to the target shape.

Table 4.3 show the number of cases in which each technique produced the best conformality. For one target, RapidArc and Tomotherapy had equivalent conformality indices so an equal score of 1 was given to both techniques.

	NCP-IMRT	DCA	RapidArc	CyberKnife	Tomotherapy
Number of cases where each technique showed best Paddick's CI	1	0	6	3	4

Table 4.3 Number of cases where each technique showed the best Paddick's CI.

Summary: In conclusion, all the techniques produced plans with comparable conformality but with the exception of DCA technique (using forward planning approach). The powerful optimization algorithms used in inverse planning allow for the calculation of beam fluence (MLC based plans) or beam directions (robotic planning) to generate a conformal plan. Schoonbeek et al. (5) compared dosimetric difference between DCA using Novalis, Gamma Knife, CyberKnife, Tomotherapy and conventional

3D conformal RT plans. They found that all these techniques have comparable plan conformality index for the target volume larger than 0.5 cm^3. Our study had similar results except that DCA had poorer plan conformality then the other techniques.

Figure 4.4 shows an example dose distribution through the central axial slice for a slightly irregular shaped target (volume = 2.9 cm^3) using all five techniques.

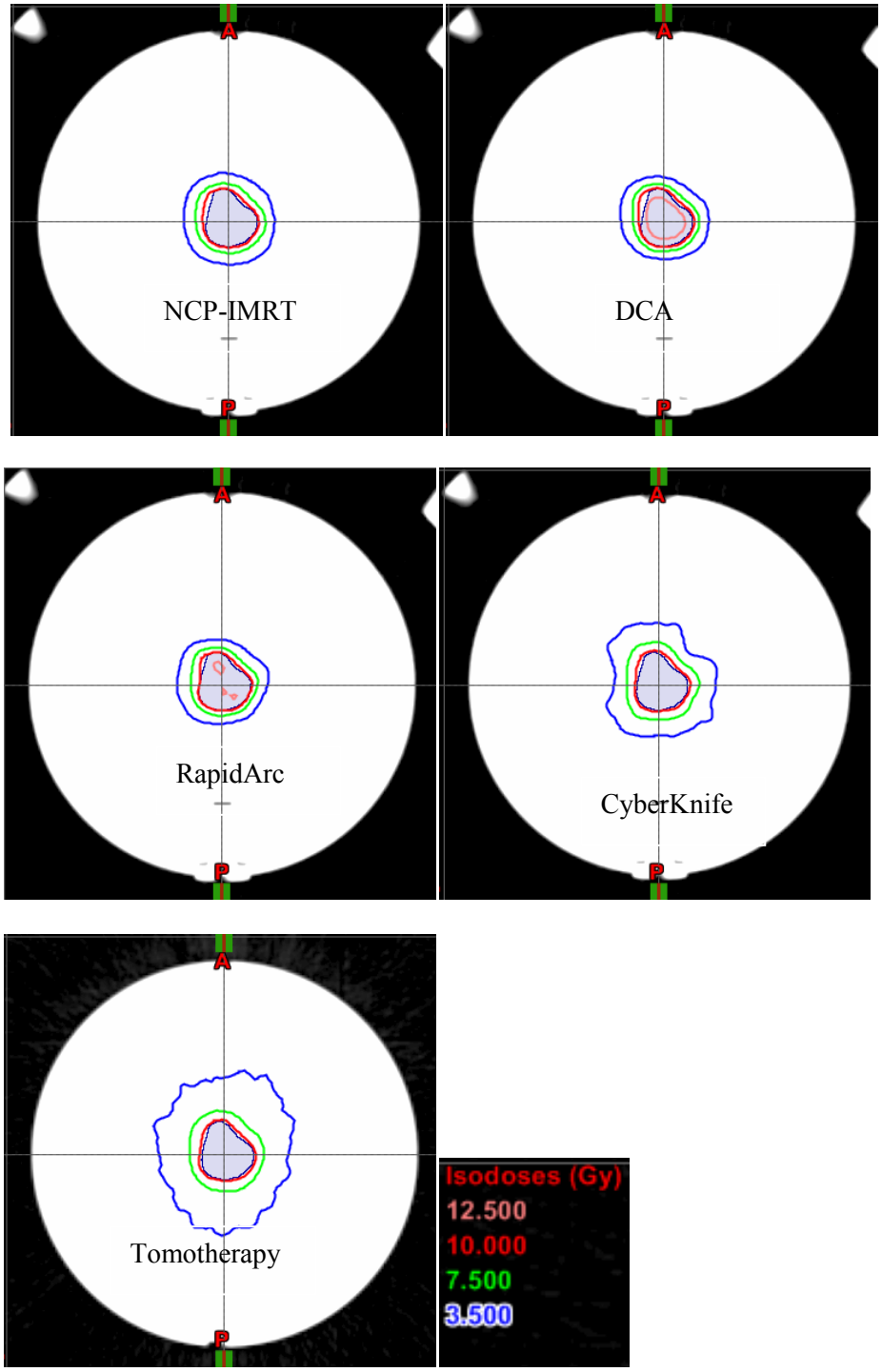

Figure 4.4 Axial isodose distribution for target with volume 2.9 cm^3 shown in the blue contour (Isodose lines: pink - 12.5 Gy, red - 10 Gy, green – 7.5 Gy, blue - 3.5 Gy).

4.2.2.2 RESULTS FOR GRADIENT INDEX

For the gradient comparison, Paddick's gradient index is calculated which is the ratio of the volume of the 50% isodose to the volume of the prescription isodose. The results of the gradient comparison are shown in Figure 4.5.

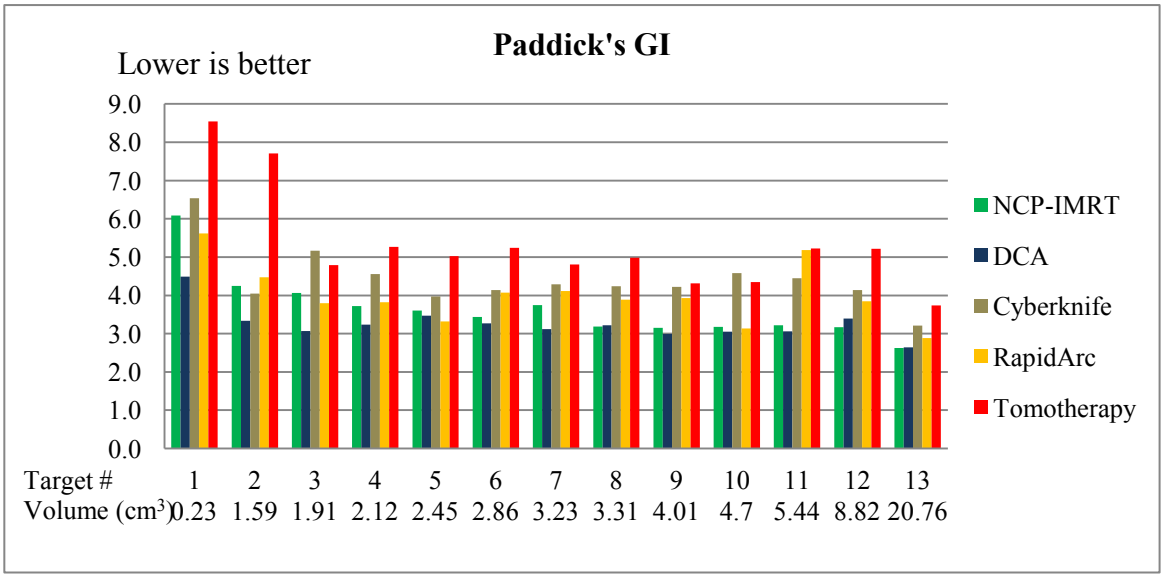

Figure 4.5 Gradient index for the thirteen irregular targets.

From Table 4.2, the average Paddick's gradient index $GI_{Paddick}$ was 3.26±0.43, 3.65±0.85, 4.01±0.75, 4.43±0.77, and 5.32±1.33 for the DCA, NCP-IMRT, RapidArc, Cyberknife and Tomotherapy techniques respectively.

Out of all the techniques included in this study, DCA had the lowest GI for most of the targets. It was also noticed in section 4.2.2.1, in general DCA is the technique that produced the least conformal plans and as such DCA follows a general trade off between plan conformality and the gradient index. The reason for this tradeoff is because DCA is a forward planning technique and does not use any intensity modulation, so achieving a sharp dose fall off (an essential requirement of SRS) results in higher dose at the center of

the tumor. As explained in section 3.3.3, a high dose in the center helps to improve the dose fall off. However, it also pushes outward the prescription isodose (10 Gy) that results into a larger volume of prescription isodose. A larger volume of prescription isodose results in poor conformality of the plan.

The next two techniques with the lowest gradient index were RapidArc and NCP-IMRT. A possible explanation for the sharper dose gradients seen could be because both of these techniques use the same non-coplanar beam geometry as DCA. The only difference being the beams are modulated with IMRT and RapidArc. It was found that the ratio of the averages for the conformity index and gradient index between DCA and NCP-IMRT were similar ($CI_{DCA}/CI_{NCP\text{-}IMRT}$ = 0.88 and $GI_{DCA}/GI_{NCP\text{-}IMRT}$ = 0.89). This means that as compared to DCA, a gain in conformality of NCP-IMRT was compensated by a corresponding loss in its gradient index. Similar behavior was observed when comparing RapidArc to DCA. Therefore, when comparing IMRT or RapidArc to DCA, a trade off between conformality and gradient index was also observed.

In contrast to DCA, for the CyberKnife a loss in dose gradient was not counterbalanced by an increase in conformality. In general, because the CyberKnife uses non coplanar beam arrangements coming from as many as 1600 different directions, it was expected to show better dose gradient. As explained earlier, a possible explanation could be the CyberKnife planner was not told about the gradient index achieved using the Novalis Tx based techniques. A prior knowledge of the gradient index could improve the CyberKnife planning because Multiplan is an inverse planning system that allows the planner to decide how much emphasis to place on dose gradient. In addition, to make the delivery time efficient a maximum number of beams per plans was restricted to 150.

Therefore, increases in total number of beams, a prior knowledge of gradient index and an iterative planning process could have helped to improve the gradient index with the CyberKnife.

On average and for almost every individual target, Tomotherapy produced the plans with the poorest dose fall off (or high GI). A possible explanation for the shallower dose fall off with Tomotherapy could be in the geometry of the dose delivery. In the Tomotherapy the gantry rotates around the couch on a circular slip ring and the couch moves during the gantry motion, despite the helical delivery the beam arrangement still resembles a coplanar beam arrangement. As explained in the section discussing the planning for spherical targets, coplanar beams tend to degrade the dose fall off because the exit of one beam overlaps the entrance of another.

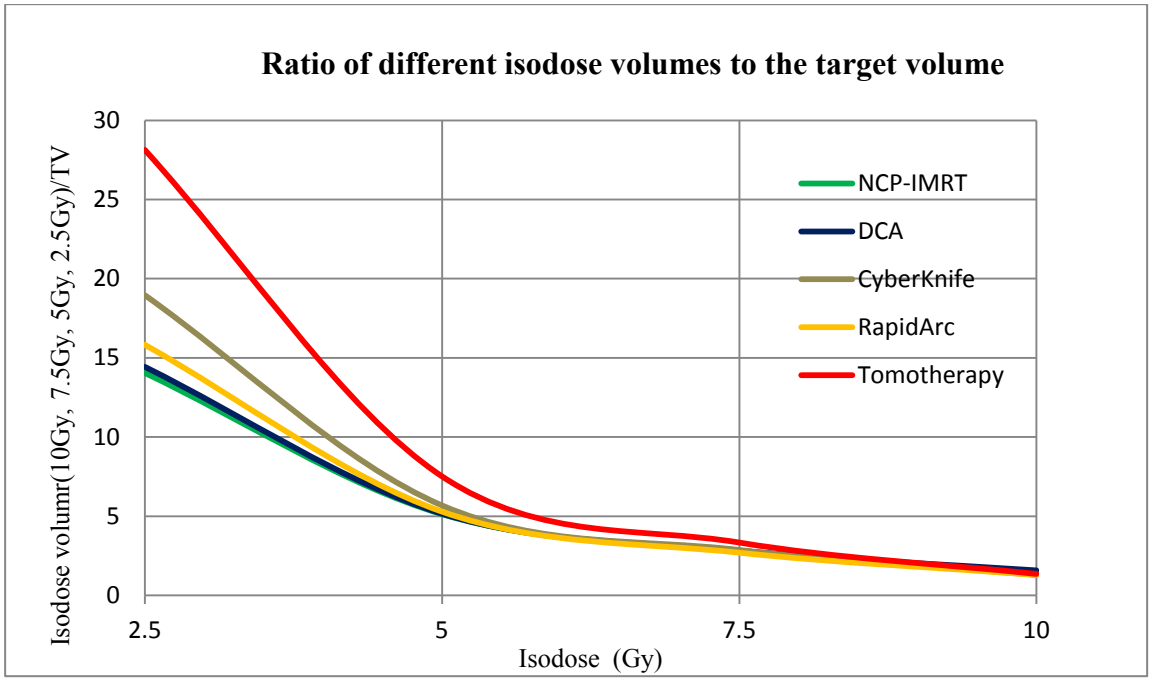

Figure 4.6 Ratio of different isodose volumes (10 Gy, 7.5 Gy, 5 Gy, and 2.5 Gy) to the target volume for each technique.

Figure 4.6 shows ratio of different isodose volumes (10 Gy, 7.5 Gy, 5 Gy, and 2.5 Gy) to the target volume for each technique. Here average of this ratio over all the thirteen irregular targets plotted for different isodose volumes. Graph shows that out of all the techniques included in this study, on average NCP-IMRT and DCA had the minimum volume receiving 5 Gy and 2.5 Gy of dose. However, the Tomotherapy had the largest volume receiving 2.5 Gy.

Table 4.4 shows number of cases where each technique produced the best gradient index.

	NCP-IMRT	DCA	RapidArc	CyberKnife	Tomotherapy
Number of cases where each technique showed best Paddick's GI	3	9	1	0	0

Table 4.4 Number of cases where each technique showed the best Paddick's GI.

Summary: For irregular targets, the DCA produced the plans with the highest fall off outside the target followed by NCP-IMRT, RapidArc and CyberKnife. Tomotherapy produced plans with the shallowest dose fall off. A study by Wiezorek et al.(6) compares different IMRT technique for 10 head and neck patients found although Tomotherapy has better sparing of organ at risks but delivers higher dose to the normal tissue. Although the targets and anatomy are different for head and neck patients compared to SRS, the idea that TomoTherapy is able to conform to complex shapes while increasing the volume of patient receiving low dose is important and may influence plan selection. The clinical relevance of the difference in conformality and dose gradient of the different techniques are discussed latter in the thesis.

Figure 4.7 shows an example of the axial distribution through the central slice of a target with volume 2.1 cm^3 for each technique.

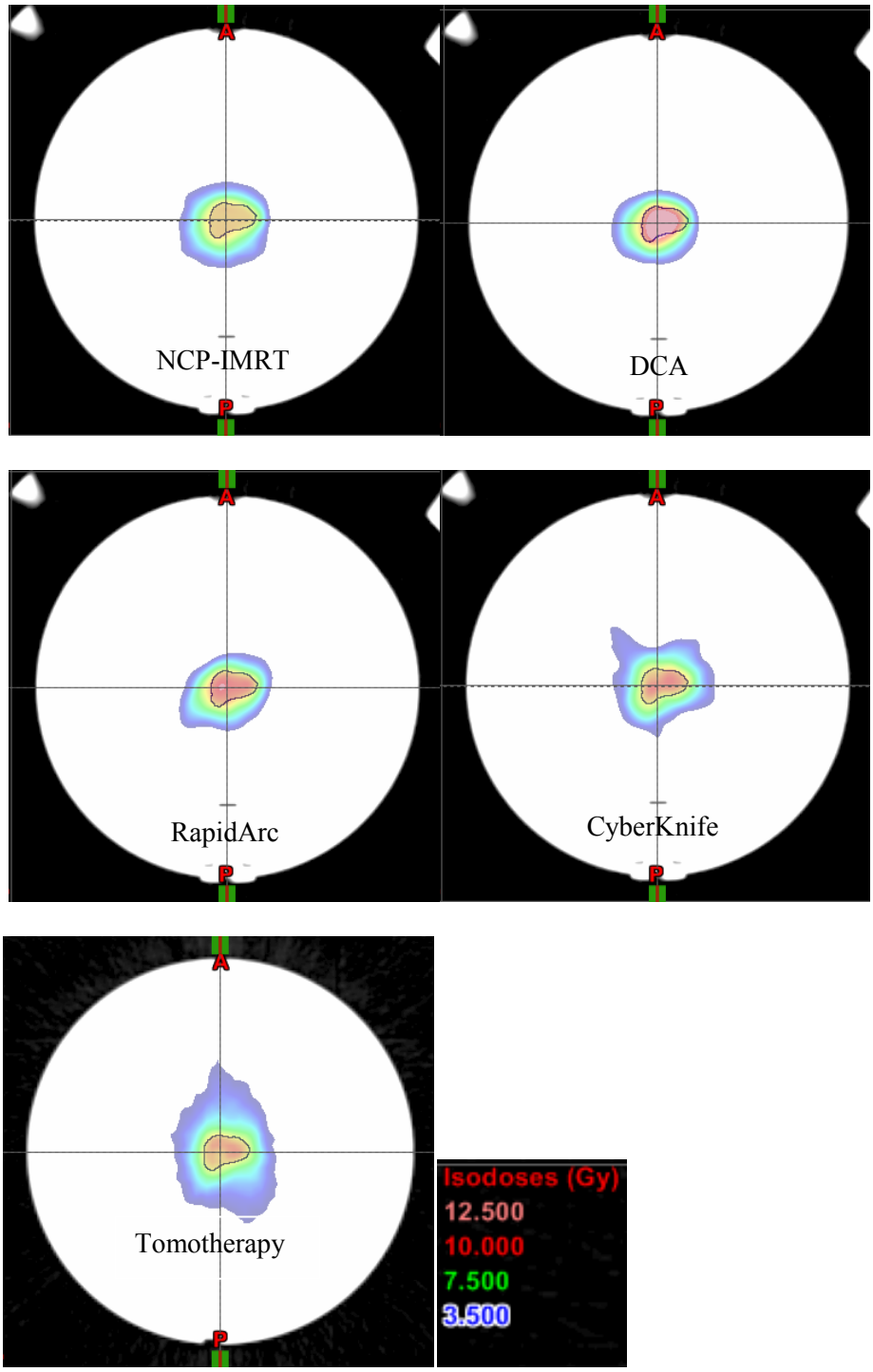

Figure 4.7 Axial dose wash distribution for target with volume 2.1 cm^3 shown in the blue contour (Isodose color wash: pink - 12.5 Gy, red - 10 Gy, green - 7.5 Gy, blue - 3.5 Gy).

4.2.2.3 RESULTS FOR CONFORMALITY/GRADIENT INDEX

The Wagner conformity/gradient index reflects both conformality (CGI_c) and dose-gradient (CGI_g) by weighting each metric equally and giving an average overall score. A perfect score for the CGI index is 100.

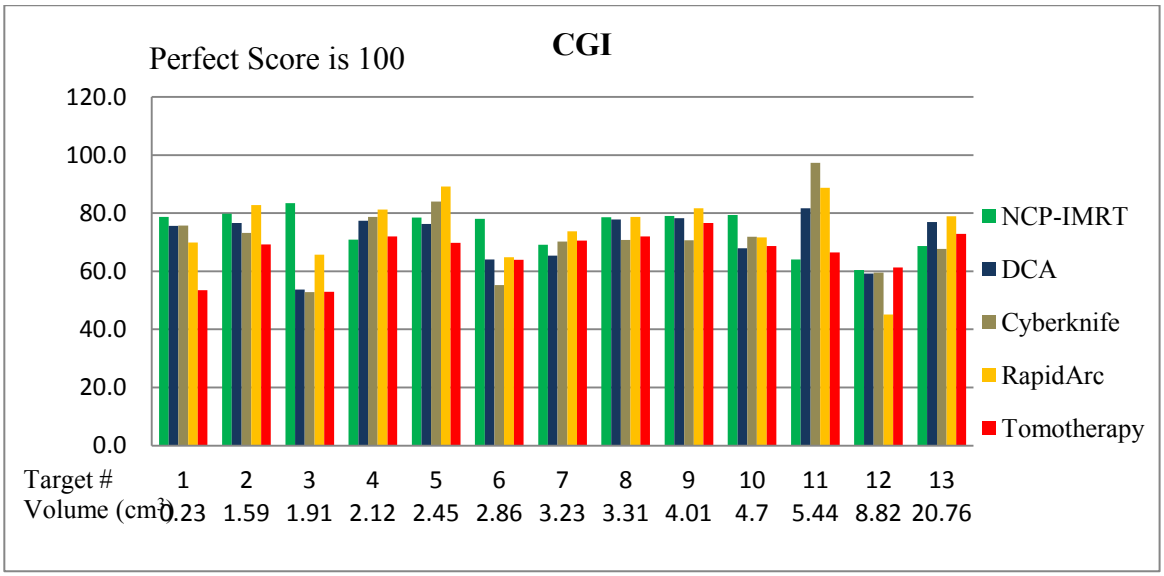

Figure 4.8 Conformity/gradient index for thirteen irregular targets.

	NCP-IMRT	DCA	RapidArc	CyberKnife	Tomotherapy
Number of cases where each technique showed best CGI	5	0	6	2	0

Table 4.5 Number of cases where each technique showed the best Wagner CGI.

From Table 4.2, the average CGI was 71.59±8.6, 74.51±7.06, 74.76±11.8, 71.37±11.8, and 66.9±7.2 for the DCA, NCP-IMRT, RapidArc, Cyberknife and Tomotherapy techniques respectively. All the techniques had shown comparable CGI values, with the exception of the Tomotherapy which had a relatively lower value. The

reason for the low CGI index in the case of the Tomotherapy is because this index gives equal importance to both conformality CGI_c and the gradient index CGI_g of the plan (Section 3.3.2.4). As shown in Table 4.6 the dose gradient calculated by CGI_g was relatively low with the Tomotherapy planning while conformality was comparable to the other techniques. Table 4.5 shows number of cases where each technique produced the best results.

	NCP-IMRT	DCA	RapidArc	CyberKnife	Tomotherapy
CGIg	76.64± 9.54	78.65±13.18	71.39±17	64.65±16.15	57.8±15.3
CGIc	72.37±8.37	64.53±9.13	78.13±10.49	78.1±9.12	76±12.03

Table 4.6 Average value of CGI_g and CGI_c for all techniques.

4.2.2.4 RESULTS FOR HOMOGENEITY INDEX

MDPD is the ratio of the maximum dose to the prescribed dose to the PTV. For a perfectly homogeneous dose distribution MDPD index should have a value of 1.

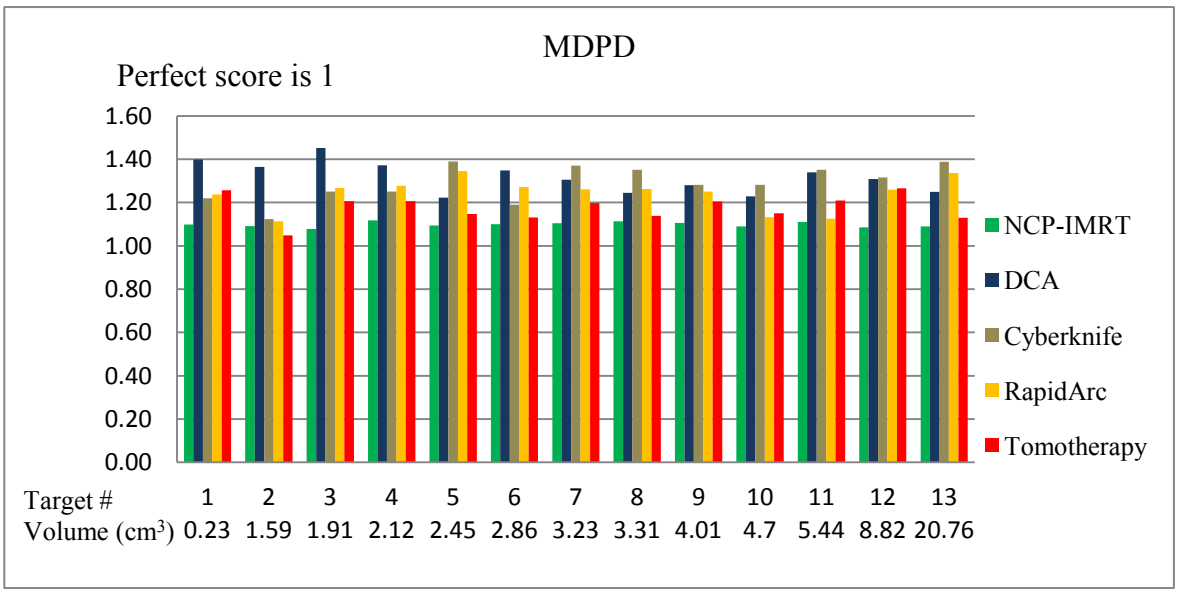

Figure 4.9 Homogeneity index for thirteen irregular targets.

	NCP-IMRT	DCA	RapidArc	CyberKnife	Tomotherapy
Number of cases where each technique showed best MDPD	12	0	0	0	1

Table 4.7 Number of cases where each technique showed the best MDPD.

From Table 4.2, techniques that produced the most homogeneous plans were NCP-IMRT and the Tomotherapy, followed by the RapidArc and the CyberKnife techniques. Table 4.7 show the number of cases in which each technique produced the best MDPD.

As expected DCA showed the highest MDPD index. For techniques such as DCA where no intensity modulation is used, typically a high dose is delivered at the center of the target. A high dose at the center helps to give a sharp dose fall off (lower GI index) outside the target boundaries. Targets with a relatively high MDPD index had correspondingly low GI index values, for example the targets with volumes 1.91 cm^3, 2.12 cm^3 and 5.44 cm^3 had higher than average MDPD values of 1.45, 1.37, 1.34 but corresponding lower than average GI values of 3.07, 3.24 and 3.06 respectively. In general, a higher MDPD index was seen for the more irregular shaped targets with volumes 2.86 cm^3 (SI 0.248, MDPD 1.35), 2.12 cm^3 (SI 0.279, MDPD 1.37) and 1.91 cm^3 (SI 0.4, MDPD 1.45). In addition, when comparing targets with comparable volumes such as the targets with volume 3.24 cm^3 (SI 0.122, MDPD 1.24) and 3.23 cm^3 (SI 0.333, MDPD 1.31), the more asymmetric target (larger SI index) had a higher MDPD index.

Of the NCP-IMRT and RapidArc techniques, NCP-IMRT had shown better MDPD index as well as better gradient index. Therefore, in general NCP-IMRT does not follow the standard relation between dose homogeneity and gradient index. For RapidArc planning, to achieve a better dose gradient the optimization algorithm was

forced to deliver a higher maximum dose to the PTV. On the contrary for the NCP-IMRT technique, in iPlan we chose to use consistently the "PTV only" option that favors a homogeneous dose distribution in the PTV. The results suggest that as compared to RapidArc, the NCP-IMRT technique, using a 16 beam non coplanar arrangement allows for steep dose gradient and homogeneous dose in the PTV with the "PTV only" option.

CyberKnife does not use beam modulation so it was expected to follow a similar relation between dose gradient and MDPD as shown by the DCA technique. Similarly, CyberKnife must deliver a higher dose at the center of the target to get a higher dose gradient. For example, the targets with volumes 8.82 cm^3, 3.23 cm^3 and 2.45 cm^3 had shown above average MDPD index values of 1.32, 1.37, 1.39 but also showed below average GI values of 4.14, 4.29 and 3.21 respectively.

It is well known that the Tomotherapy TPS uses an objective function that favors a homogeneous dose distribution in the target. So as expected, Tomotherapy produced plans with lower MDPD index values. For a few of the very symmetric targets, a previously published technique(1) was used to generate an inhomogeneous dose distribution in the target that would further help to generate a sharp dose gradient. In general, for most of the targets a standard clinical planning approach was used. As a result, it was expected that the Tomotherapy would generally result in plans that are more homogeneous. No general relationship is found for the Tomotherapy in terms of MDPD versus gradient index, volume or target asymmetry. However, when comparing the Tomotherapy to NCP-IMRT, the plans have similar homogeneity (MDPD) but very different dose gradient. The Tomotherapy dose gradient is more shallow than found with the NCP-IMRT technique.

In general, SRS allows a single large fraction of dose delivery to small size targets and to avoid toxicity in normal tissue a sharp dose gradient is preferred over dose homogeneity. In case of cone based planning on Linear accelerator, generally dose is prescribed to 50% isodose surface that could results into heterogeneous dose distribution due to the use of multiple isocenters that normally required to conform the dose to the irregular target shape. However, if a technique such as NCP-IMRT can produce homogeneous plans with a sharp dose gradient, then it would be very useful for special cases where dose homogeneity is also important.

Summary: NCP-IMRT and the Tomotherapy produced most homogeneous dose distribution followed by RapidArc and the CyberKnife. Similar results of comparable homogeneity index between NCP-IMRT, Tomotherapy and RapidArc were shown by Lu et al. (7) for twenty nasopharyngeal carcinoma patients. In another work from Ding et al. (8) that includes dosimetric comparison between DCA, NCP-IMRT and three dimensional conformal radiotherapy for fifteen brain tumor patients, also shows that plans produced by DCA were more inhomogeneous than NCP-IMRT technique. On the contrary, in a different study by Stecken et al. (9) that compare DCA and IMRT for six brain tumor patients, this study found DCA produce more homogeneous plans than the IMRT. It could be because lesser number of IMRT beams used in this study.

4.2.2.5 LIMITATIONS OF PLANNING STUDY

One possible limitation of this study could be that instead of real patient geometries we used a phantom geometry in this study and no organs at risk was included in the planning. The presence of patient geometry and OARs can change the planning parameters such as the optimized fluence and beam directions. In addition, the use of a

standard beam-planning template with fixed gantry and couch angles may not be practical for some cases. Secondly, in inverse planning different dose limits and priorities are used for different OARs. As we know different planning systems use different optimization functions for organ at risks and PTVs, so it could affect the dose distribution differently for different techniques. Therefore, results from this study cannot be generalized for all patients.

The standard dose prescription recommended by RTOG(10) for single brain metastasis were not followed in this study. Although the dose distributions could be scaled from the 10 Gy used in this study to the RTOG recommended dose prescription, this may not work for all cases. For example if a 20 Gy dose is prescribed to a target which is in the vicinity of OARs such as the brainstem (dose limit 12 Gy) or optic structure (dose limit 8 Gy) then the plan qualities for such a plan would be different from scaling a plan done with a 10 Gy prescription dose done without OARs.

In addition, the clinical relevance of the difference between the physical dose distribution (conformality, homogeneity and gradient index) also should be evaluated. Different studies(11-13) in the past had shown this by relating volume of the 12 Gy isodose to the risk of symptomatic brain necrosis. Therefore, it could be interesting to follow the prescription dose on the basis of target size (RTOG) and then, instead of comparing the dose gradient at the 50% isodose we could compare the volume receiving 12 Gy of dose. Also it would be worthwhile to investigate if the change in any physical parameters would reflect in the improvement in biological parameters (such as normal tissue complication probability, tissue control probability or integral biologically effective

dose). Previous studies(14, 15) had shown some correlations between NTCP with PITV and IBED with MDPD.

Lastly, this study was done for single intracranial targets only, the results could change significantly if multiple targets (such as multiple brain metastasis) were considered.

4.3 DELIVERY STUDY

Results to verify and compare the clinical deliverability of plans and the delivery accuracy of different techniques are shown ahead. A comparison between planned and delivered dose for the two spherical targets of diameter 6 mm and 10 mm and three irregular targets (a) Smallest target of volume 0.23 cm^3 (b) Medium sized irregular target of volume 8.82 cm^3 and (c) Biggest target of volume 20.76 cm^3 is reported.

4.3.1 SPHERICAL TARGETS

4.3.1.1 NOVALIS TX

For the spherical targets only the cone plans were delivered using the Novalis Tx. For small spherical targets where a sharp dose fall off is of primary interest only, the plans done with the cones was the method of preference as compared to the other MLC based techniques. As shown in section 4.2.1, of all the delivery techniques on the Novalis Tx, between the MLC based (DCA, IMRT-NCP and RapidArc) and cone based plans, the cones produced the plans with steepest dose gradient.

The results of the horizontal profile comparison and isodose distribution comparison between measured dose on EBT2 film and planned dose from TPS through

the central axial slice are shown in Figure 4.10 for the plans delivered on the Novalis. Table 4.8 gives the gamma index results for both plans delivered on the Novalis.

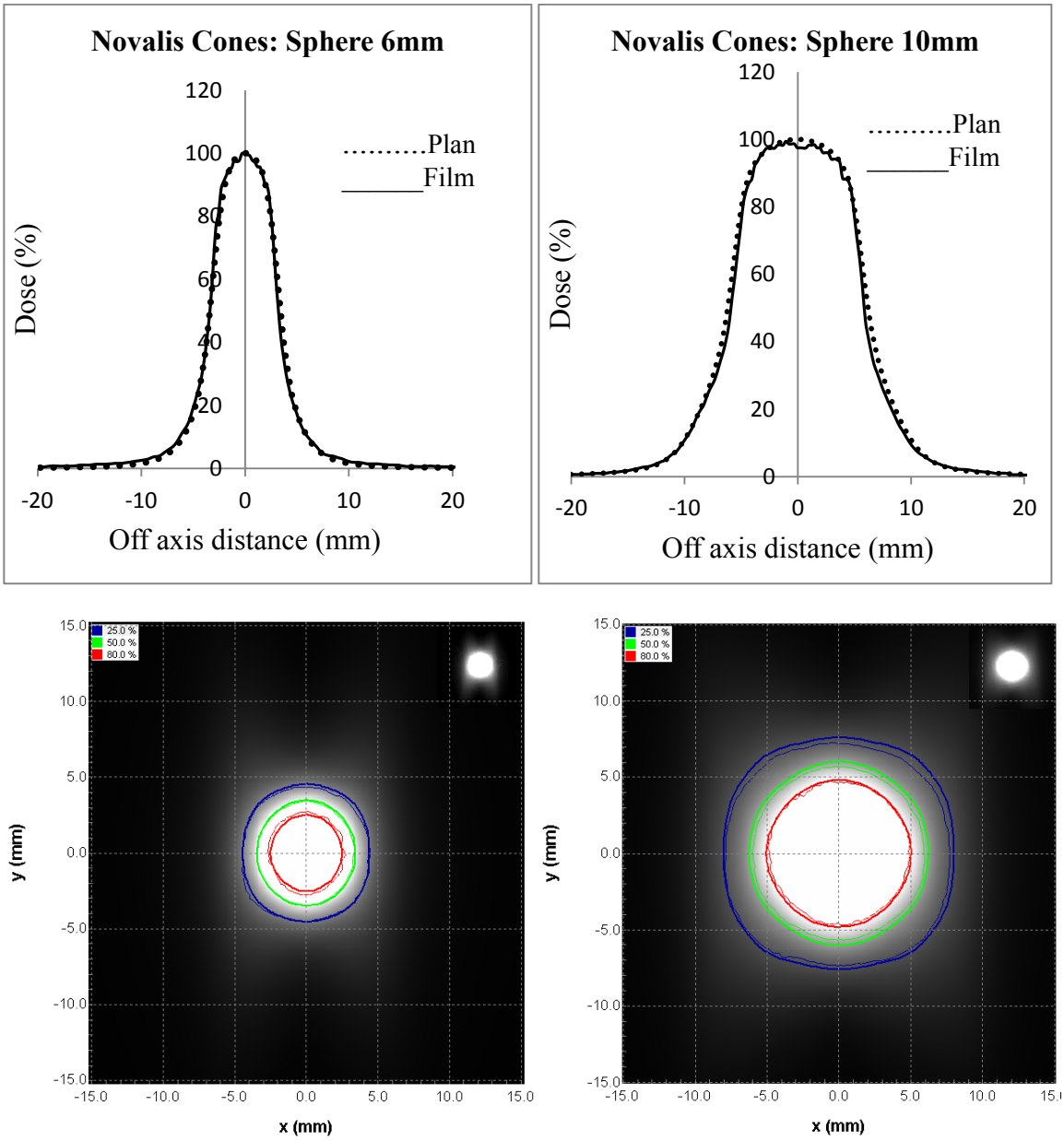

Figure 4.10 Delivery result of 6 mm and 10 mm spherical target delivered on the Novalis Tx. Horizontal dose profiles of axial slice are shown (black solid line represents measured profile on film and dotted line represents calculated profile by TPS). Isodose overlay for 25%-blue, 50%-green and 80%-red isodose line (normalized to 100% at origin).

Diameter	DD=3%, DTA=1mm	DD=3%, DTA=2mm	DD=5%, DTA=1mm
6mm	99.99	99.96	100
10mm	100	99.95	100

Table4.8 Number of pixels passing gamma criteria for different combinations of dose difference and distance to agreement – Novalis.

The delivered plans for the spherical targets on the Novalis showed good agreement between the measured dose on EBT2 film and the planned dose by the iPlan TPS. Dose profiles and isodose line superimpose on each other very well. For the profile comparison, a one-dimensional median filter of 3 pixels was used for noise reduction and to smooth the film profile. From Table 4.8, the gamma map has a very good passing rate of more than 99.95 percent for different combinations of DD and DTA.

The targeting accuracy of an SRS technique is normally done through a Winston-Lutz test. As a measure of the targeting accuracy of the delivery, Table 4.9 gives the profile shift in the x-direction (lateral) and y-direction (vertical) necessary for the film registration.

Diameter	ΔX	ΔY
6mm	-0.3 mm	0.4 mm
10mm	-0.2 mm	0.4 mm

Table4.9 Profile shift in x and y directions for film registration – Novalis.

A sub-millimeter level of profile shift was calculated in both the x (lateral) and y (vertical) directions. These results show a very good agreement between dose calculation by iPlan and overall targeting accuracy of the Novalis Tx unit.

4.3.1.2 CYBERKNIFE

The results of the horizontal profile comparison and isodose distribution comparison between measured dose on EBT2 film and planned dose from TPS through the central axial slice are shown in Figure 4.11 for the plans delivered on the Cyberknife.

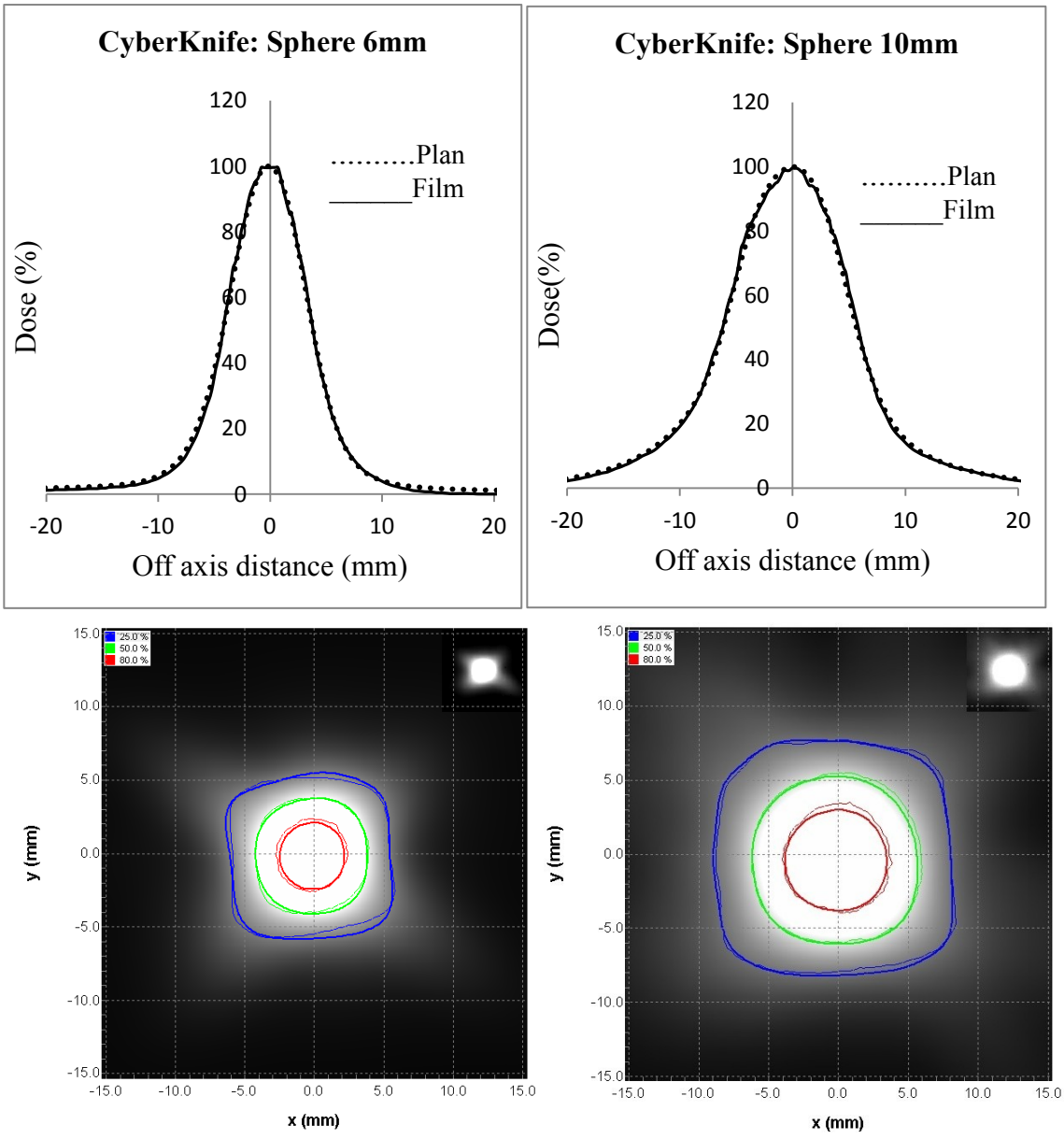

Figure 4.11 Delivery result of 6 mm and 10 mm spherical target delivered on the CyberKnife. Horizontal dose profiles of axial slice are shown (black solid line represents measured profile on film and dotted line represents calculated profile by TPS). Isodose overlay for 25%-blue, 50%-green and 80%-red isodose line (normalized to 100% at origin).

Table 4.10 gives the gamma index results for both plans delivered on the Cyberknife.

Diameter	DD=3%, DTA=1mm	DD=3%, DTA=2mm	DD=5%, DTA=1mm
6mm	99.95	99.99	100
10mm	99.27	99.86	100

Table 4.10 Number of pixels passing gamma criteria for different combinations of dose difference and distance to agreement - Cyberknife.

As found on the Novalis Tx, CyberKnife had also shown very good agreement between planned dose and measured dose. Dose profiles and isodose lines superimpose nicely. A similar one-dimensional median filter of 3 pixels was used to smooth the dose profile measured from the film. From Table 4.10, gamma passing was higher than 99.27 percent for different combinations of DD and DTA.

The profile shifts for the film registration between measured and calculated dose profiles in the x (lateral) and y (vertical) directions was less than 1 mm.

Diameter	ΔX	ΔY
6mm	0.4 mm	0.9 mm
10mm	0.3 mm	0.5 mm

Table 4.11 Profile shift in x and y directions for film registration – Cyberknife.

4.3.1.3 TOMOTHERAPY

In this study it was observed that for the Tomotherapy, the agreement between planned dose and measured dose largely depends upon the location of the target with respect to machine isocenter. Both spherical targets (6 mm and 10 mm diameter) were

planned and delivered in two different locations: (a) Targets placed 10 cm vertically higher than the machine isocenter and (b) Targets placed exactly at the machine isocenter.

Figure 4.12 shows the comparison results for two spherical (6 mm and 10 mm diameter) targets placed 10 cm up vertically (anterior) from the machine isocenter.

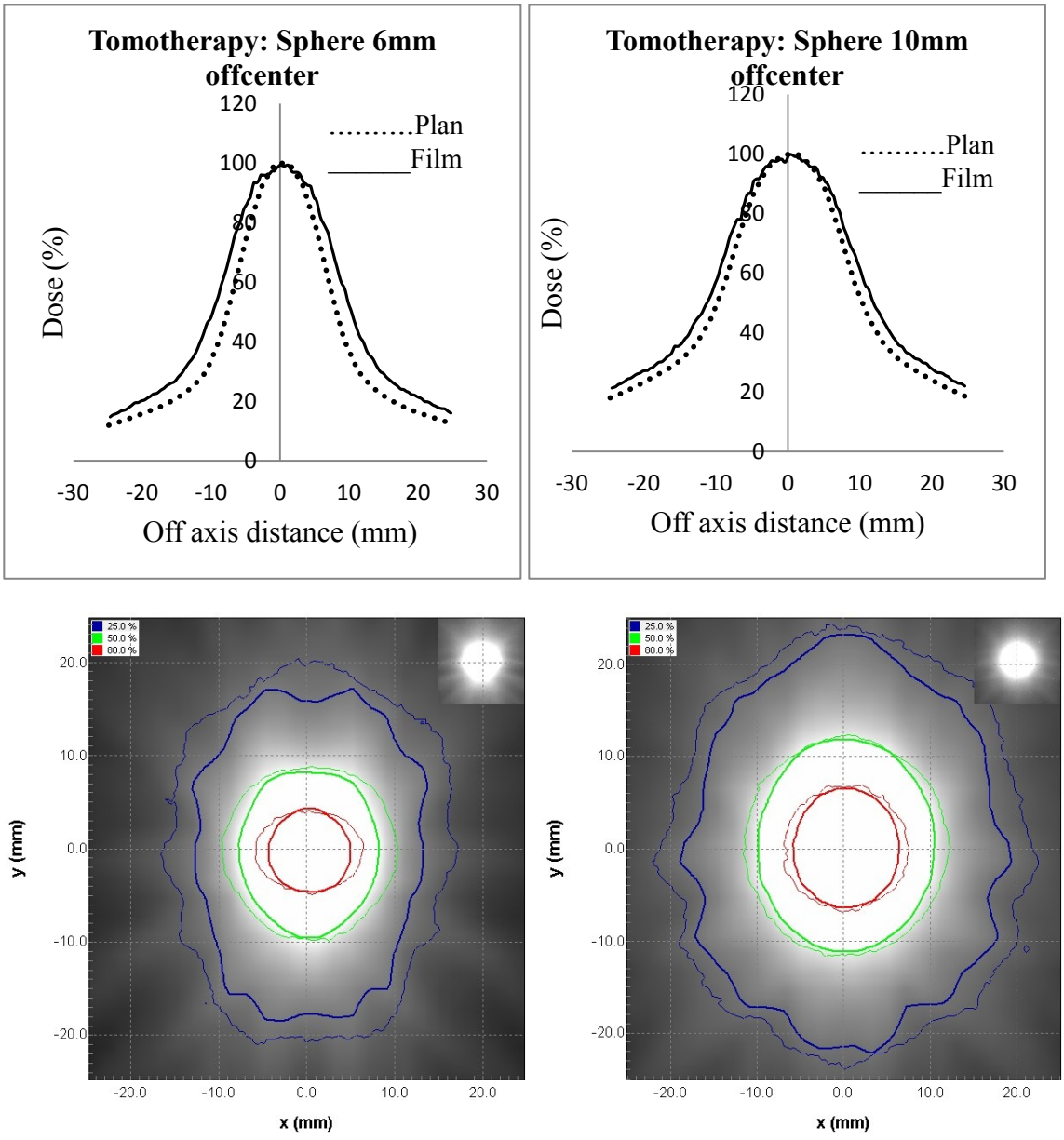

Figure 4.12 Delivery result of 6 mm and 10 mm spherical targets located 10 cm vertically up from the Tomotherapy machine isocenter. Horizontal dose profiles of axial slice are shown (black solid line represents measured profile on film and doted line represents calculated profile by TPS). Isodose overlap for 25%-blue, 50%-green and 80%-red isodose line (normalized to 100% at origin).

Table 4.11 gives the gamma index results for both plans.

Diameter	DD=3%, DTA=1mm	DD=3%, DTA=2mm	DD=5%, DTA=1mm
6mm	37.33	59.6	83.7
10mm	68.94	91.08	95.59

Table 4.12 Number of pixels passing gamma criteria for different combinations of dose difference and distance to agreement – Tomotherapy (off-centered targets).

Figure 4.13 shows the comparison results when the two spherical (6 mm and 10 mm diameter) targets were placed exactly at the machine isocenter. Table 4.12 gives the gamma index results for both plans.

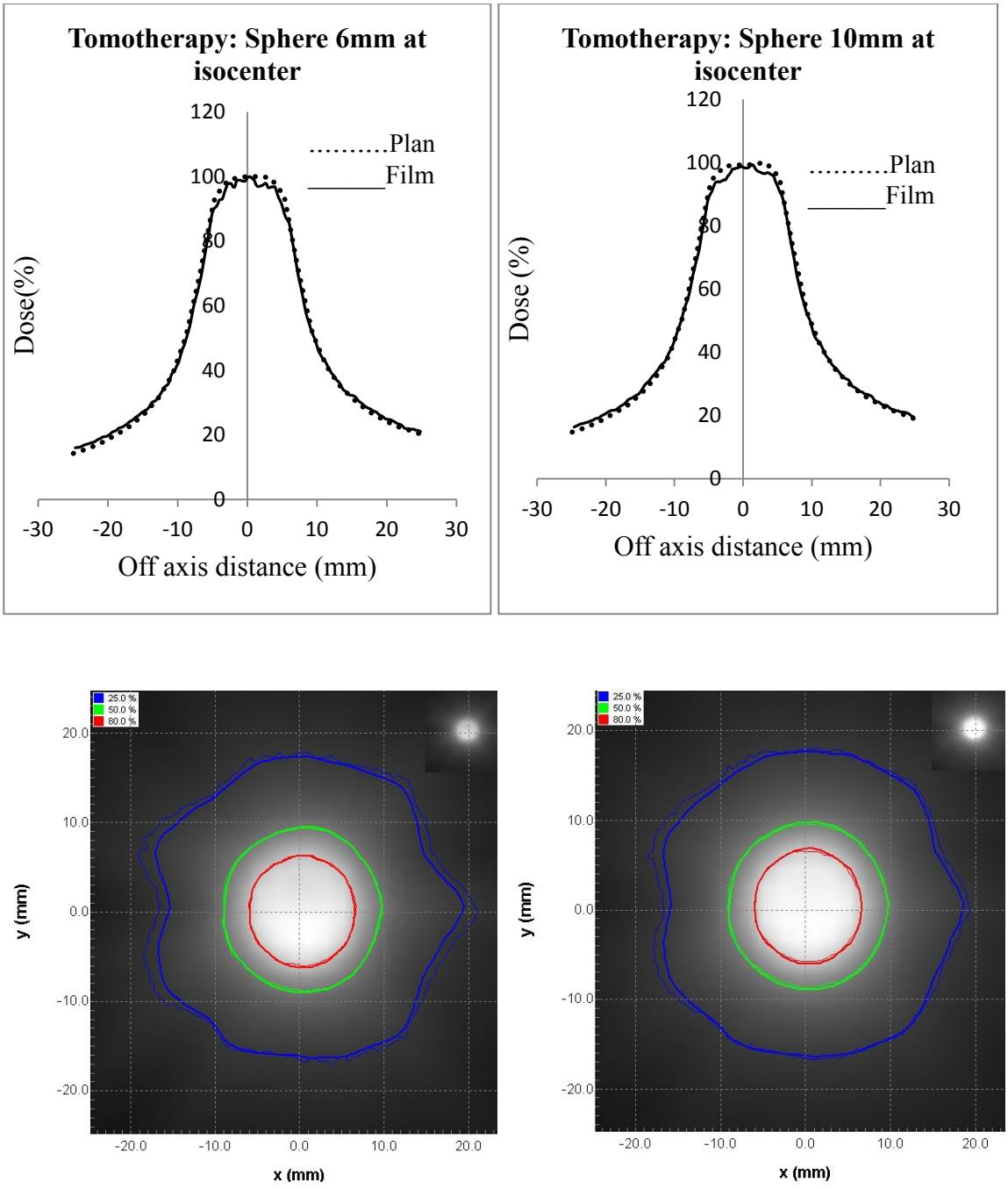

Figure 4.13 Delivery result of 6 mm and 10 mm spherical targets placed exactly at the Tomotherapy machine isocenter. Horizontal dose profiles of axial slice are shown (black solid line represents measured profile on film and doted line represents calculated profile by TPS). Isodose overlap for 25%-blue, 50%-green and 80%-red isodose line (normalized to 100% at origin).

Diameter	DD=3%, DTA=1mm	DD=3%, DTA=2mm	DD=5%, DTA=1mm
6mm	100	100	100
10mm	100	100	100

Table 4.13 Number of pixels passing gamma criteria for different combinations of dose difference and distance to agreement – Tomotherapy (targets at isocenter).

The profile shifts between measured and calculated dose profiles in x (lateral) and y (vertical) directions were less than 1 mm.

Diameter	ΔX	ΔY
6mm	-0.1mm	-0.7mm
10mm	-0.2 mm	-0.7 mm

Table 4.14 Profile shift in x and y directions.

Figure 4.12, Table 4.12, Figure 4.13 and Table 4.13 shows a profile comparison, isodose comparison and gamma passing rate between calculated and measured doses for both targets at two different locations. When the targets were placed at 10 cm vertically up from the isocenter, a poor agreement between measured and calculated dose was observed. The measured horizontal profiles and isodoses on the central axial slice were broader than the calculated profiles and calculated isodose lines. Resulting in a relatively low gamma passing rate had been seen for all dose difference and distance to agreement levels.

Where as in the second case when targets were placed exactly at the isocenter a very good match between profiles and isodose lines were noticed. In addition, the gamma-passing rate was 100% even for a dose difference of 3% and distance to

agreement of 1 mm. From Table 4.14 profile shifts for film registration for both targets was also less than 1 mm in both lateral and vertical directions.

From the results it was found that dose delivery accuracy depends upon the location of the target in the bore in the Tomotherapy. As mentioned in chapter 2, Tomotherapy may be more advantageous for radiosurgery when multiple targets are present. Under such situations where either there are multiple targets or it is hard to place the target at the machine isocenter, the delivered dose distribution could be different from the calculated dose distribution. Possible explanation for this discrepancy could be: for the optimizations and calculations, Tomotherapy TPS divides 360º full Linac rotation into 51 arcs of 7.06 º each. Planning system further assumes Linac is at static position at the center of each 7.06 º arc, whereas during the delivery Linac is moving. This effect even more pronounced when target is located off centered.

Summary: In conclusion, for small spherical targets, Novalis Tx cones and CyberKnife had shown very good agreement between measured dose on EBT2 film and calculated dose from TPS. It was observed that for both modalities, shifts between measured and calculated dose profiles in the x (lateral) and y (vertical) direction was less than 1 mm. The overall match and small shifts gives an indication of the overall accuracy of the on board imaging system of each modality and their targeting accuracy. For the Tomotherapy a good agreement between measured and calculated dose distribution was noticed only when targets were placed at machine isocenter. Based on this study, it is highly recommended that until there are some improvements on the Tomotherapy dose calculation algorithms, if possible place the target at the machine's isocenter.

4.3.2 IRREGULAR TARGETS

For the delivery study of three irregular targets, delivery from the five techniques were tested for first two targets (0.23 cm^3 and 8.82 cm^3) whereas only four techniques except CyberKnife were tested for third target (20.76 cm^3).

4.3.2.1 DCA

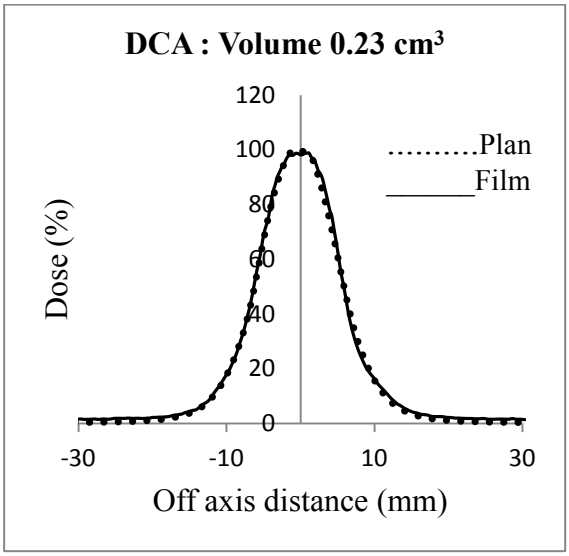
DCA : Volume 0.23 cm3
120
100
80
60
40
20
0
Dose (%)
.....Plan
_____Film
-30
-10
10
30
Off axis distance (mm)

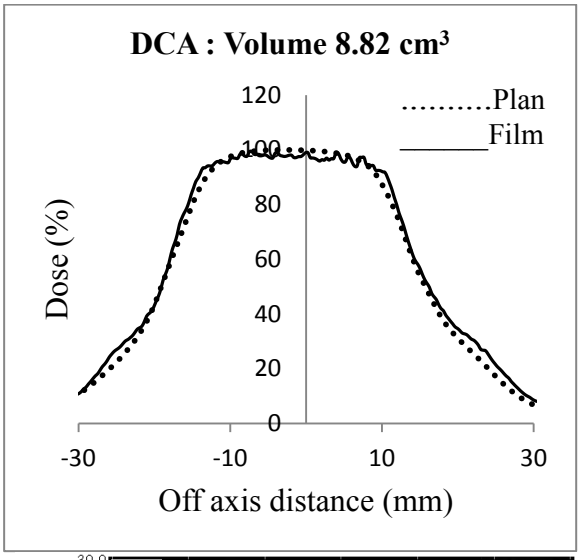
DCA : Volume 8.82 cm3
120
100
80
60
40
20
0
Dose (%)
.....Plan
_____Film
-30
-10
10
30
Off axis distance (mm)

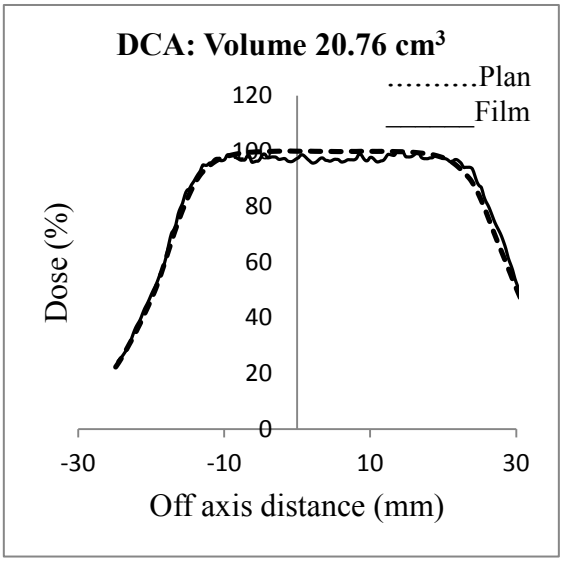
DCA: Volume 20.76 cm3
120
100
80
60
40
20
0
Dose (%)
.....Plan
_____Film
-30
-10
10
30
Off axis distance (mm)

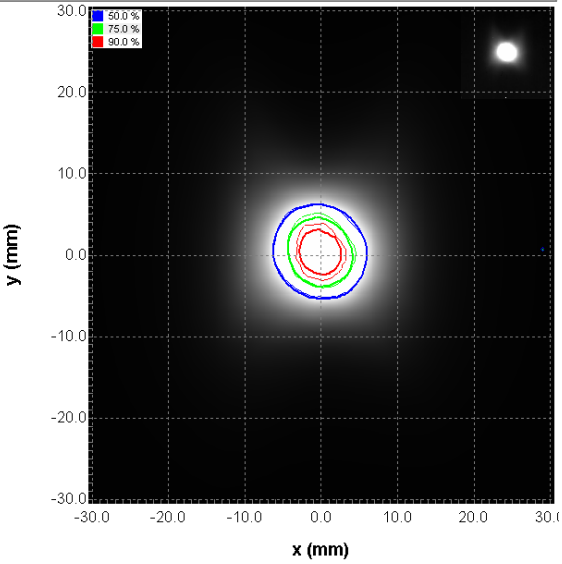
50.0 %
75.0 %
90.0 %
30.0
20.0
10.0
0.0
-10.0
-20.0
-30.0
y (mm)
-30.0
-20.0
-10.0
0.0
10.0
20.0
x (mm)

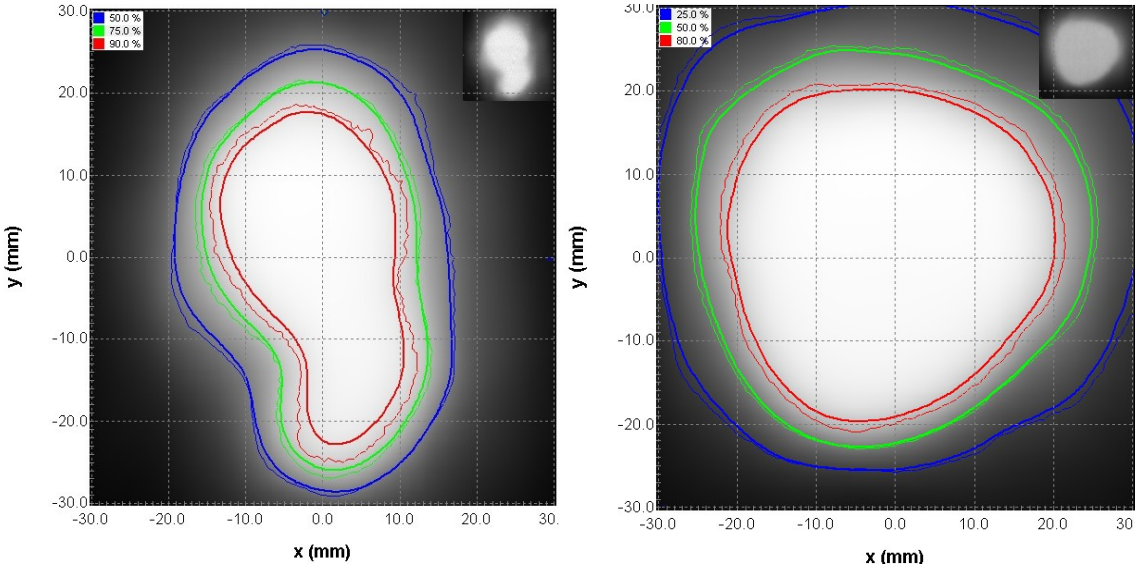

Figure 4.14 Delivery results of 0.23 cm^3, 8.82 cm^3 and 20.76 cm^3 irregular targets delivered using DCA technique. Horizontal dose profiles of axial slice are shown (black solid line represents measured profile on film and doted line represents calculated profile by TPS). Isodose overlap for 25%-blue, 50%-green and 80%-red isodose line (normalized to 100% at origin).

4.3.2.2 NCP-IMRT

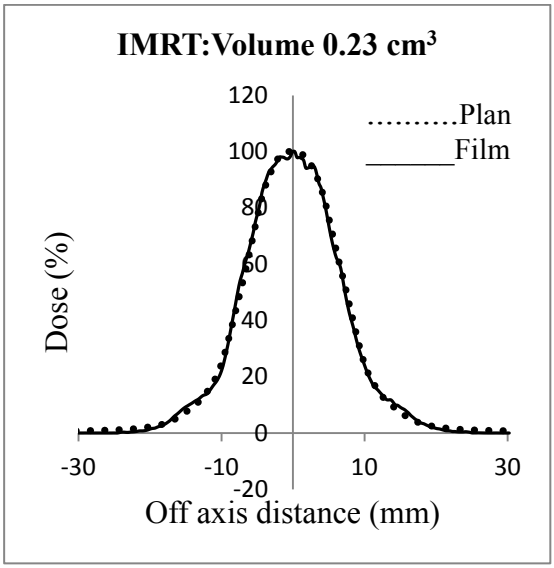

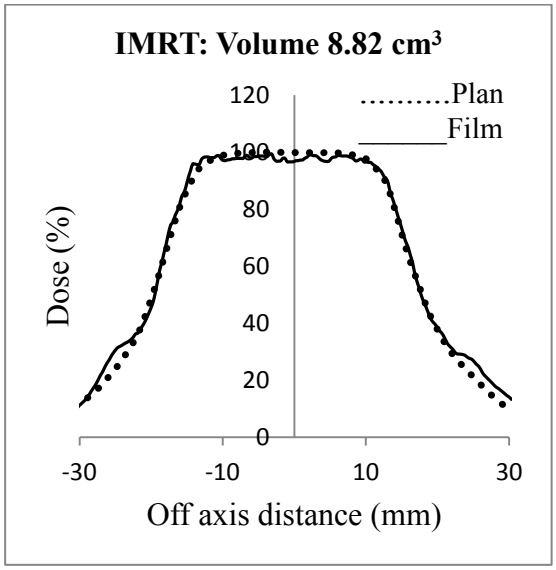

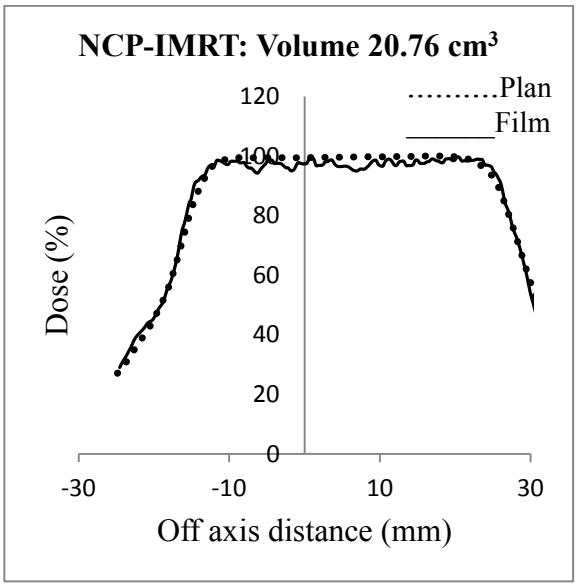

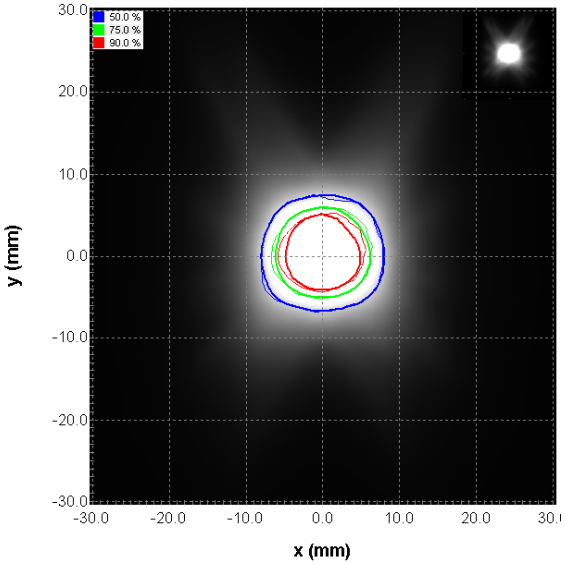

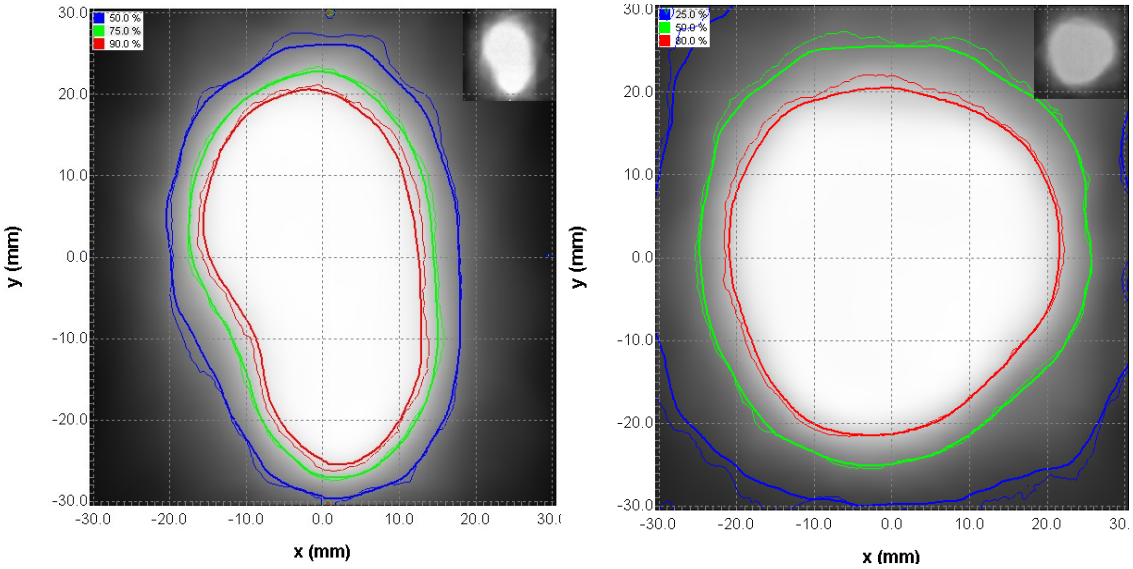

Figure 4.15 Delivery results of 0.23 cm^3, 8.82 cm^3 and 20.76 cm^3 irregular targets delivered using NCP-IMRT technique. Horizontal dose profiles of axial slice are shown (black solid line represents measured profile on film and doted line represents calculated profile by TPS). Isodose overlap for 25%-blue, 50%-green and 80%-red isodose line (normalized to 100% at origin).

4.3.2.3 RAPIDARC

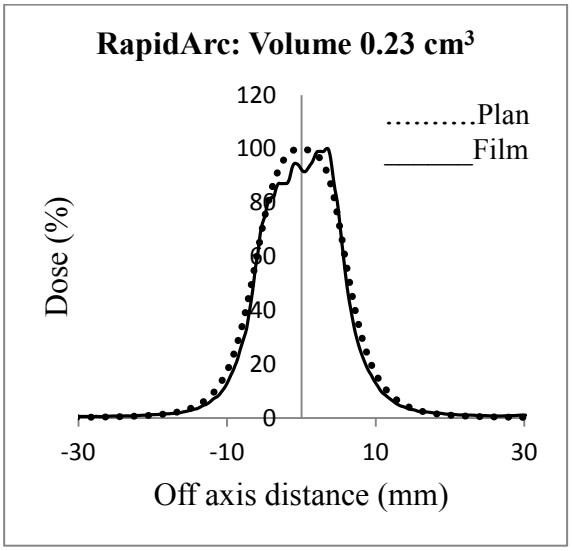

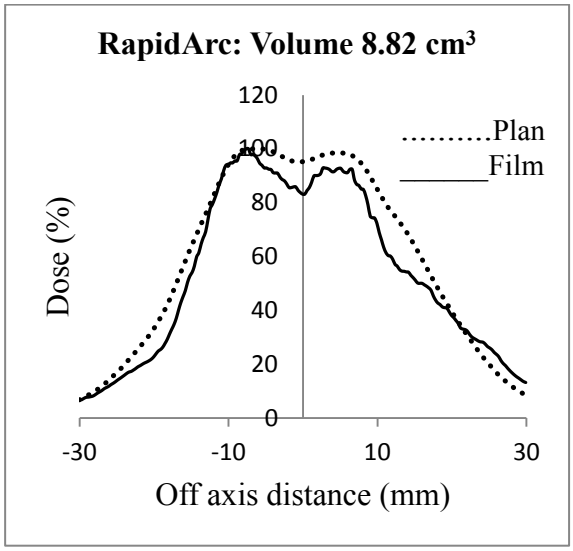

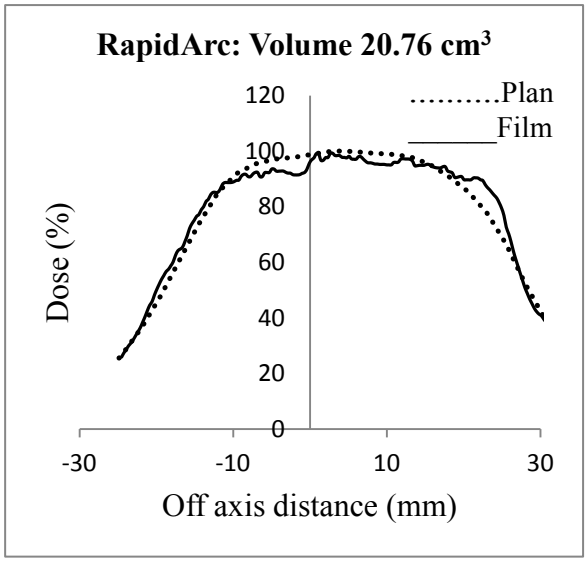

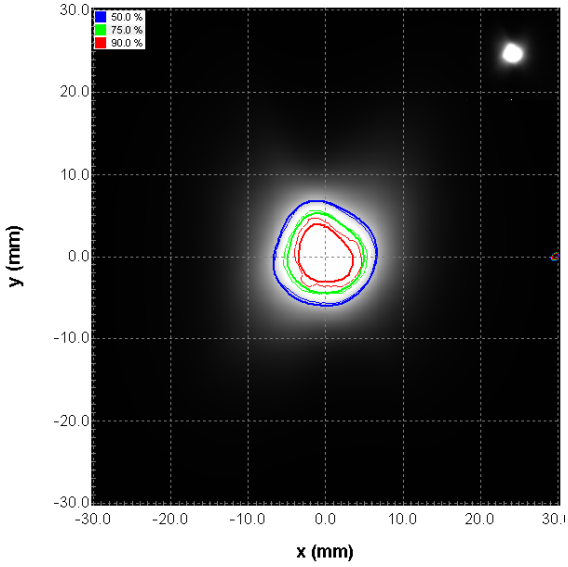

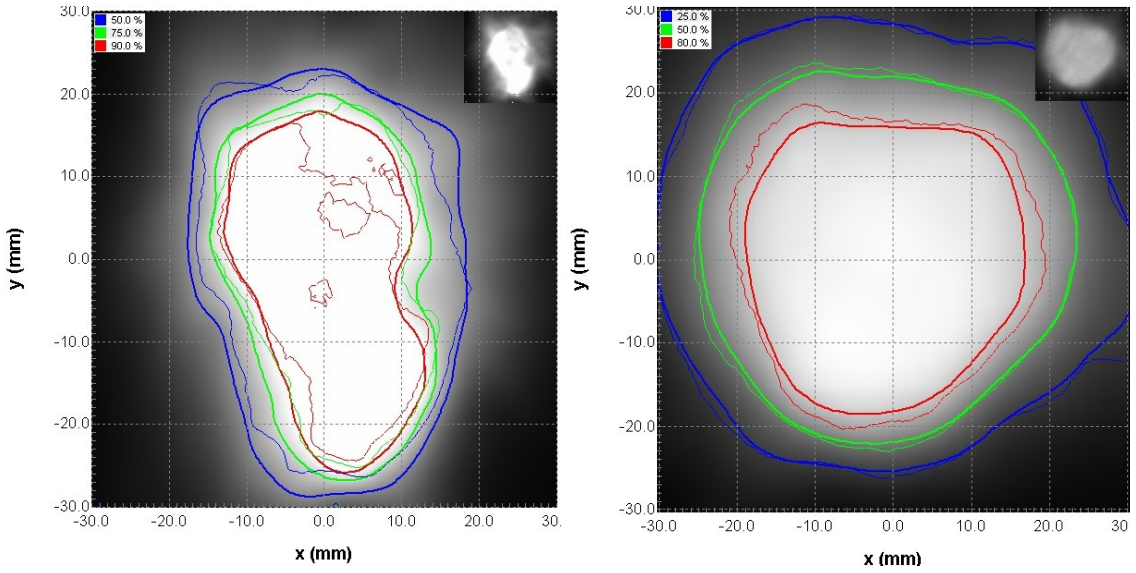

Figure 4.16 Delivery results of 0.23 cm^3, 8.82 cm^3 and 20.76 cm^3 irregular targets delivered using RapidArc technique. Horizontal dose profiles of axial slice are shown (black solid line represents measured profile on film and doted line represents calculated profile by TPS). Isodose overlap for 25%-blue, 50%-green and 80%-red isodose line (normalized to 100% at origin).

4.3.2.4 CYBERKNIFE

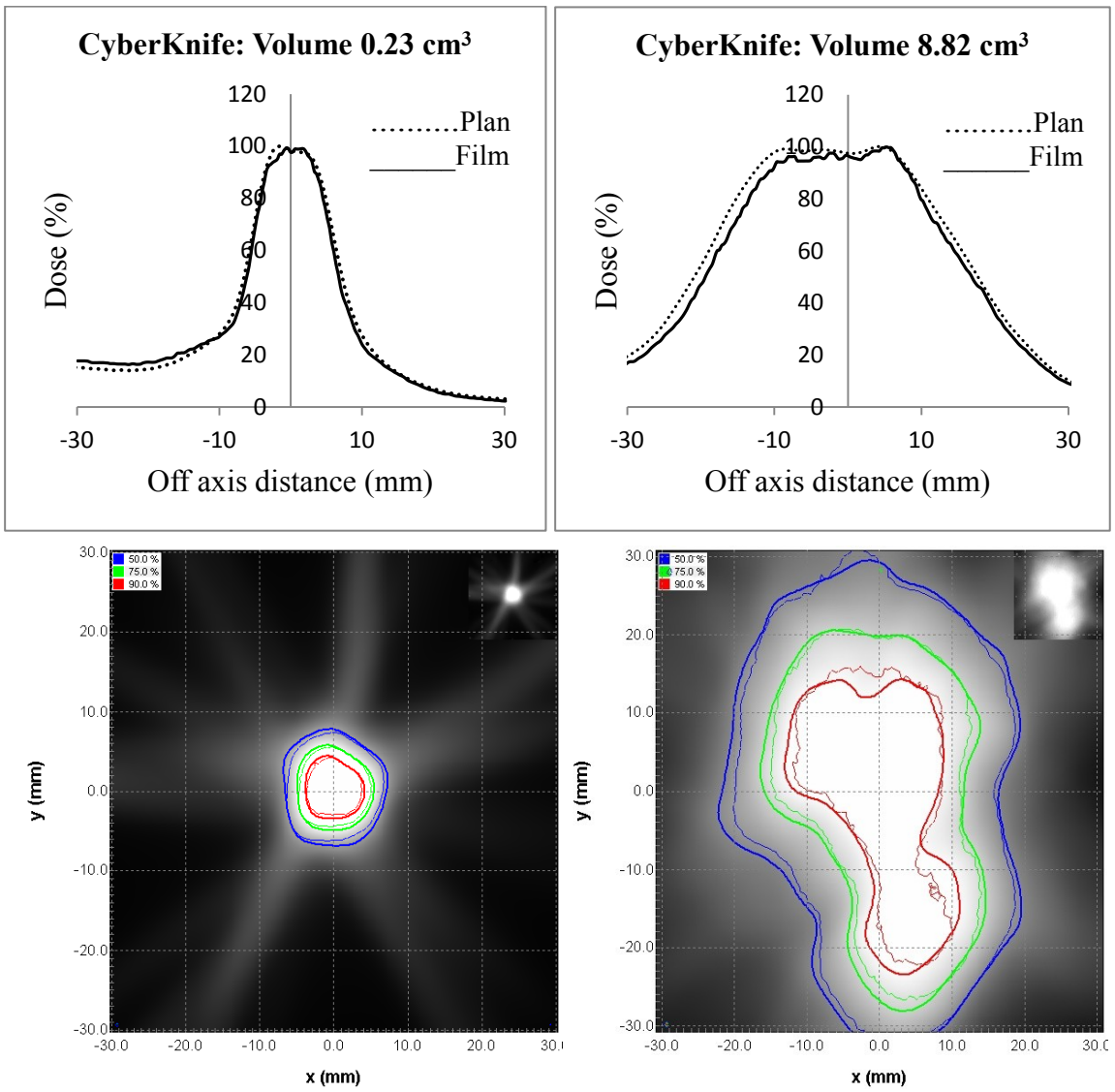

Figure 4.17 Delivery results of 0.23 cm^3, 8.82 cm^3 and 20.76 cm^3 irregular targets delivered on the CyberKnife. Horizontal dose profiles of axial slice are shown (black solid line represents measured profile on film and doted line represents calculated profile by TPS). Isodose overlap for 25%-blue, 50%-green and 80%-red isodose line (normalized to 100% at origin).

4.3.2.5 TOMOTHERAPY

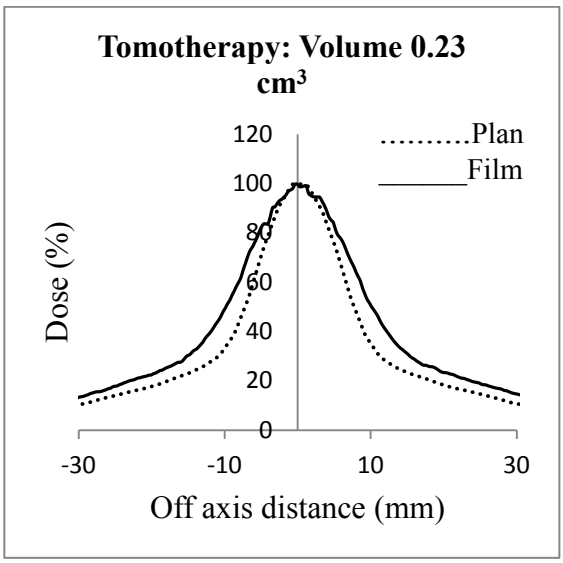

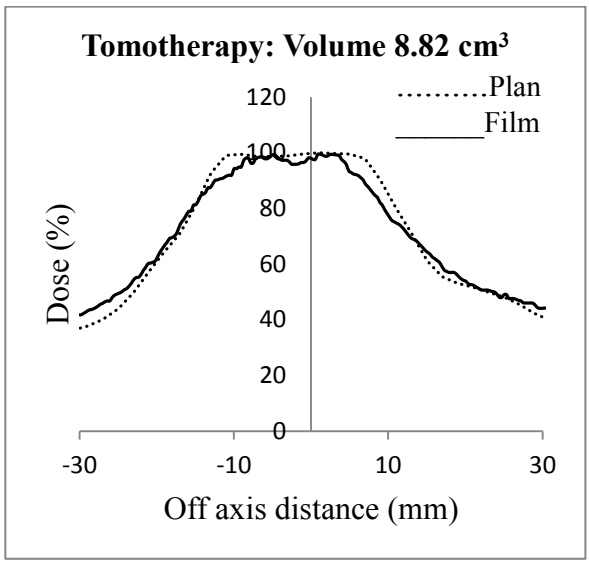

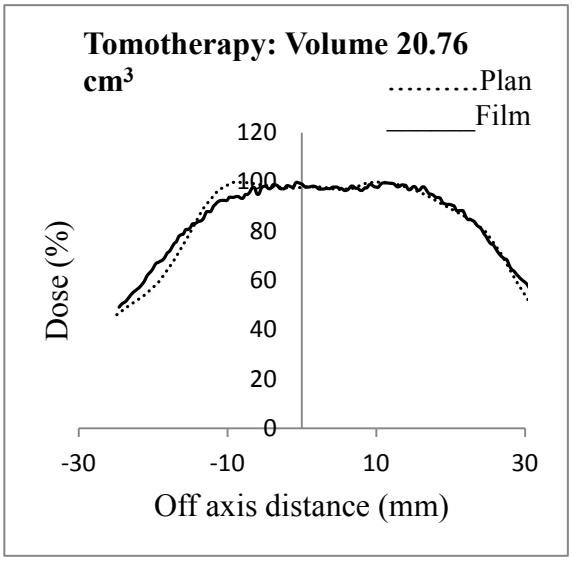

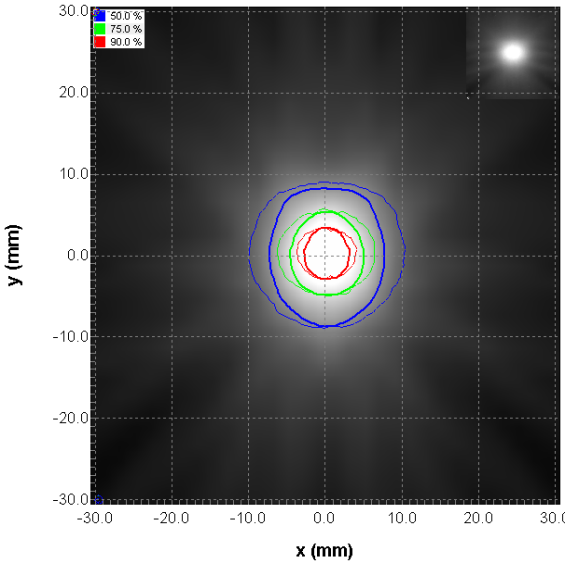

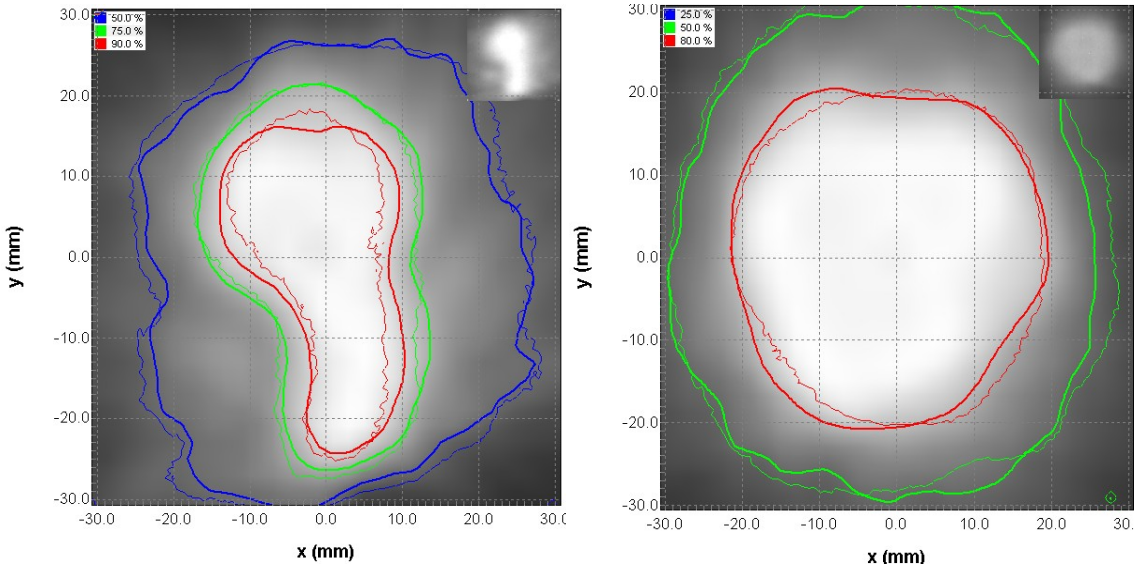

Figure 4.18 Delivery results of 0.23 cm^3, 8.82 cm^3 and 20.76 cm^3 irregular targets located 10 cm vertically up from the Tomotherapy machine isocenter. Horizontal dose profiles of axial slice are shown (black solid line represents measured profile on film and doted line represents calculated profile by TPS). Isodose overlap for 25%-blue, 50%-green and 80%-red isodose line (normalized to 100% at origin).

Table 4.15 gives the gamma index results for three targets on different techniques. Two gamma criteria values DD=3%, DTA=2 mm and DD=5%, DTA=1 mm are reported.

	Volume 0.23 cm^3	Volume 8.82 cm^3	Volume 20.76 cm^3
DCA			
DD=3%, DTA=2mm	99.97	94.36	93.7
DD=5%, DTA=1mm	100	96.53	90.76
NCP-IMRT			
DD=3%, DTA=2mm	99.99	81.24	96.27
DD=5%, DTA=1mm	99.84	79.58	96.53
RapidArc			
DD=3%, DTA=2mm	99.96	78.35	96.10
DD=5%, DTA=1mm	99.82	69.93	90.81
CyberKnife			
DD=3%, DTA=2mm	96.34	94.7	___
DD=5%, DTA=1mm	98.36	93.28	___
Tomotherapy			
DD=3%, DTA=2mm	50.39	89.21	85.13
DD=5%, DTA=1mm	81.98	89.78	86.97

Table 4.15 Number of pixels passing gamma criteria for different combinations of dose difference and distance to agreement.

Table 4.16 gives the profile shift in the x-direction (lateral) and y-direction (vertical) necessary for the film registration.

	Volume 0.23 cm^3	Volume 8.82 cm^3	Volume 20.76 cm^3
DCA			
ΔX	0.9	-0.2	-0.7
ΔY	-0.4	0.2	-0.4
NCP-IMRT			
ΔX	-0.5	-1	-0.8
ΔY	-0.4	-0.4	0
RapidArc			
ΔX	0.6	-1.3	0.7
ΔY	0.1	-0.7	-0.8
CyberKnife			
ΔX	0.2	0.3	—
ΔY	0.3	0.9	—
Tomotherapy			
ΔX	-0.9	0.5	2.1
ΔY	-0.6	0.4	-1.1

Table 4.16 Profile shift in x and y directions.

For all three irregular targets, a good agreement between calculated and measured dose was found. DCA, NCP-IMRT and Cyberknife had shown a good overlapping between calculated profile vs. measured profile and it was true for the isodose lines. A relatively poor matching was observed for target volume 8.82 cm^3 in case of RapidArc that could be due to poor alignment of the film for this particular case.

In case of Tomotherapy, a mismatching between calculated and measured dose was found for the smallest target (0.23 cm^3). As explained previously, it was again

because at the time of planning targets were placed 10 cm vertically up from the isocenter. Gamma passing rate for this particular target (50.39%) was lowest of all the other cases. Although, it was also observed that this issue has relatively small impact for the bigger targets.

Summary: In general, overlapping of profiles and isodose lines, acceptable gamma passing rate and less than 1mm of profile shift (in X and Y direction) for most of the cases confirms good delivery accuracy of all the techniques included in this study. Poor agreement between calculated and measured dose in case of Tomotherapy needs further investigation, delivery accuracy in lateral direction from the isocenter also needs to investigate.

4.4 REFERENCES

1. Soisson ET, Hoban PW, Kammeyer T, *et al.* A technique for stereotactic radiosurgery treatment planning with helical tomotherapy. *Medical dosimetry : official journal of the American Association of Medical Dosimetrists* 2011;36:46-56.
2. Wolff HA, Wagner DM, Christiansen H, *et al.* Single fraction radiosurgery using Rapid Arc for treatment of intracranial targets. *Radiation oncology* 2010;5:77.
3. Cozzi L, Clivio A, Bauman G, *et al.* Comparison of advanced irradiation techniques with photons for benign intracranial tumours. *Radiotherapy and oncology : journal of the European Society for Therapeutic Radiology and Oncology* 2006;80:268-273.
4. Echner GG, Kilby W, Lee M, *et al.* The design, physical properties and clinical utility of an iris collimator for robotic radiosurgery. *Physics in medicine and biology* 2009;54:5359-5380.
5. Schoonbeek A, Monshouwer R, Hanssens P, *et al.* Intracranial Radiosurgery in the Netherlands. A Planning Comparison of Available Systems with Regard to Physical Aspects and Workload. *Technology in Cancer Research & Treatment* 2010;9:279-289.
6. Wiezorek T, Brachwitz T, Georg D, *et al.* Rotational IMRT techniques compared to fixed gantry IMRT and tomotherapy: multi-institutional planning study for head-and-neck cases. *Radiation oncology* 2011;6:20.
7. Lu SH, Cheng JC, Kuo SH, *et al.* Volumetric modulated arc therapy for nasopharyngeal carcinoma: A dosimetric comparison with TomoTherapy and step-and-shoot IMRT. *Radiotherapy and oncology : journal of the European Society for Therapeutic Radiology and Oncology* 2012.
8. Ding M, Newman F, Kavanagh B, *et al.* Comparative dosimetric study of three-dimensional conformal, dynamic conformal arc, and intensity-modulated radiotherapy for

brain tumor treatment using Novalis system. *International Journal of Radiation OncologyBiologyPhysics* 2006;66:S82-S86.

9. Ernst-Stecken A, Lambrecht U, Ganslandt O*, et al.* Radiosurgery of small skull-base lesions. No advantage for intensity-modulated stereotactic radiosurgery versus conformal arc technique. *Strahlentherapie und Onkologie : Organ der Deutschen Rontgengesellschaft ... [et al]* 2005;181:336-344.
10. Shaw E, Scott C, Souhami L*, et al.* Single dose radiosurgical treatment of recurrent previously irradiated primary brain tumors and brain metastases: final report of RTOG protocol 90-05. *Int J Radiat Oncol Biol Phys* 2000;47:291-298.
11. Korytko T, Radivoyevitch T, Colussi V*, et al.* 12 Gy gamma knife radiosurgical volume is a predictor for radiation necrosis in non-AVM intracranial tumors. *International journal of radiation oncology, biology, physics* 2006;64:419-424.
12. Flickinger JC, Schell MC, Larson DA. Estimation of complications for linear accelerator radiosurgery with the integrated logistic formula. *International journal of radiation oncology, biology, physics* 1990;19:143-148.
13. Soisson ET, Mehta MP, Tome WA. A comparison of helical tomotherapy to circular collimator-based linear-accelerator radiosurgery for the treatment of brain metastases. *American journal of clinical oncology* 2011;34:388-394.
14. Oliveira SC. Comparison of three linac-based stereotactic radiosurgery techniques. *Medical Physics Unit McGill University, Montreal June 2003*.
15. Charpentier PE. Dosimetric evaluation of four techniques used in stereotactic radiosurgery. *Department of Medical Physics McGill University, Montreal December 2007*.

Chapter 5. CONCLUSIONS

5.1 SUMMARY OF WORK

This thesis work describes a comparative study between six stereotactic radiosurgery techniques: cones, dynamic conformal arcs (DCA), static non-coplanar intensity modulated radiotherapy (NCP-IMRT), volumetric modulated arc therapy (RapidArc), robotic radiosurgery using the CyberKnife system and helical Tomotherapy on the HI-ART Tomotherapy system. This work was divided into two sections. The first section described the planning study comparison between all the techniques used in our study. The second section discussed delivery verification by doing comparison between calculated and measured dose distributions for spherical and irregular targets.

The planning study was further divided into two sections: 1) Planning for very small spherical targets of diameters 6 mm and 10 mm and 2) Planning for thirteen irregularly shaped tumors. Plans were compared against each other using different quantitative indices (1) prescription isodose volume to tumor volume (PITV), Paddick's conformity index $CI_{Paddick}$ (2) Paddick's gradient index ($GI_{Paddick}$) (3) Wagner's conformality-gradient index (CGI) (4) maximum dose to prescription does (MDPD).

Similar to planning study, delivery study was performed for both spherical and irregular targets. To verify the comparison between planned and delivered dose a comparison between dose delivered to the film and the corresponding dose plane from the TPS was performed. To quantify the comparison between two dose distributions a

gamma map for different combinations of dose difference and distance to agreement was calculated, a further comparison between dose profiles and isodose line was also performed.

Results of the planning study comparison for spherical targets showed that Novalis Cones and CyberKnife plans had the sharpest dose fall off while they also maintained good conformality whereas Tomotherapy plans were least conformal. For cases where a large fraction of dose is to be delivered to a small spherical target, Novalis cones or CyberKnife are both suitable techniques.

The results of the planning comparison of thirteen irregular targets revealed the DCA technique produced plans with the sharpest dose gradient but with poor conformality. NCP-IMRT technique was surprising in that it delivered quite homogenous plans yet also had steep dose gradients comparable to the DCA technique. Moreover, the conformality produced by NCP-IMRT was quite favorable. Similarly, the RapidArc technique also produced acceptable SRS plans however in contrast to NCP-IMRT, the RapidArc technique was intentionally planned with a large inhomogeneity to attempt to increase the dose fall-off. One potential drawback of the techniques studied here is the large number of static beams (16) used for NCP-IMRT and arcs (4) used for RapidArc that could results into long delivery time however with high dose rate delivery and fast IGRT positioning on modern dedicated SRS linacs, the treatment time should be clinically acceptable. The Cyberknife plans had a high degree of conformality yet shallower dose fall-off. Theoretically, one would expect superior dose gradient from robotic radiosurgery.

It was noted that Tomotherapy was capable of producing acceptable SRS plans for some but not all of the cases tested. Plans produced by Tomotherapy had comparable conformality to other techniques but they had shown poor a gradient index. In addition, the large computing time required to produce a distribution when using 1 cm field width and fine dose resolution grid could also be a concern.

Results of the delivery verification had shown that for small spherical targets (diameter 6 mm and 10 mm), Novalis Tx cones and CyberKnife had shown very good agreement between measured dose and calculated dose from TPS. However, for Tomotherapy this agreement largely depends upon the position of the tumor with respect to machine isocenter.

Finally, the process and results of this study revealed some problems when carrying out a comprehensive SRS planning comparison. It was found that specifying a minimum dose was not reasonable as the planner may require renormalizing the plan simply to cover a small portion of the target resulting in degraded conformality. Clinically this would not be done and could have been left out as a constraint in our planning goals. Specifying dose coverage at the prescription dose level would be sufficient. Finally, with inverse planned comparisons, one must not only specify the prescription and conformality desired but also a desired dose fall-off (gradient index) prior to optimization.

In conclusion, six SRS delivery modalities available on linac based SRS systems were studied and evaluated. All methods were able to produce comparable plans for most of the targets tested. More importantly, it is suggested that for future planning studies the plan criteria must be explicit in their goals. In particular, the gradient index should be

specified along with the desired dose prescription and conformality when comparing inverse optimized SRS planning systems. Finally, for small spherical targets, Novalis cones and CyberKnife had shown a good agreement between measured and calculated dose but for Tomotherapy this agreement depends upon the position of tumor with respect to machine isocenter. Therefore, for Tomotherapy under the situations where either there are multiple targets or it is hard to place the target at the machine isocenter, the delivered dose distribution could be different from the calculated dose distribution.

5.2 FUTURE WORK

The clinical importance of difference between physical dose distributions needs further investigation. This can be achieved by evaluating relationship between physical dose distribution and biological parameters. Secondly, this study uses single brain lesions for planning comparison, any change in plan qualities for multiple targets (multiple brain metastasis) could be incorporated in the study. This work includes all the Linac based SRS techniques available at present; conventional Gamma Knife planning could also be included in the planning comparison. Finally, in case of Tomotherapy dosimetric accuracy of targets treated away from the isocenter and effect of different grid size on dosimetric precision needs to be investigated further.

Appendix

Figure A Target volumes and shape of their central transversal slice (left) and reconstructed coronal slices (right):

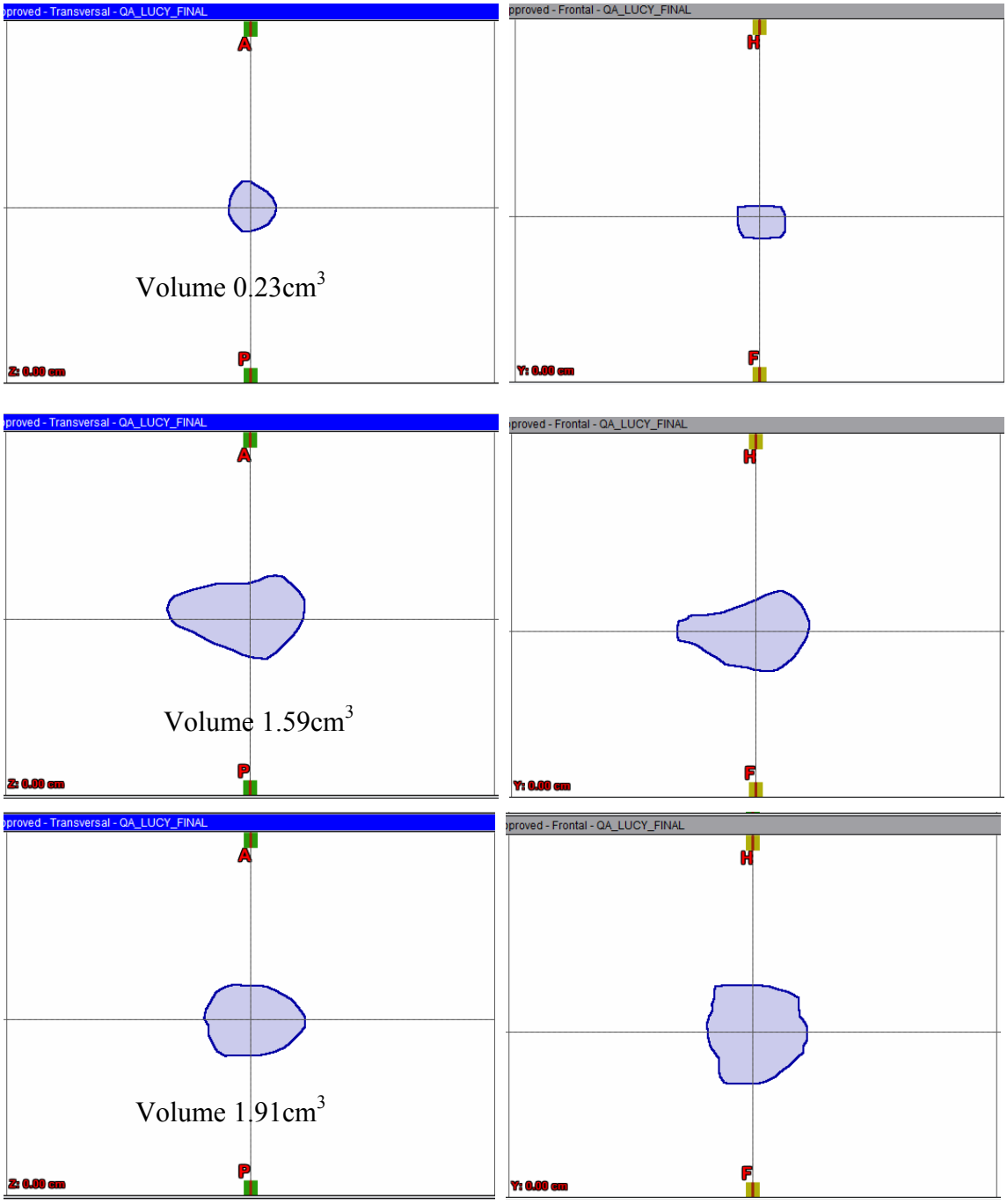

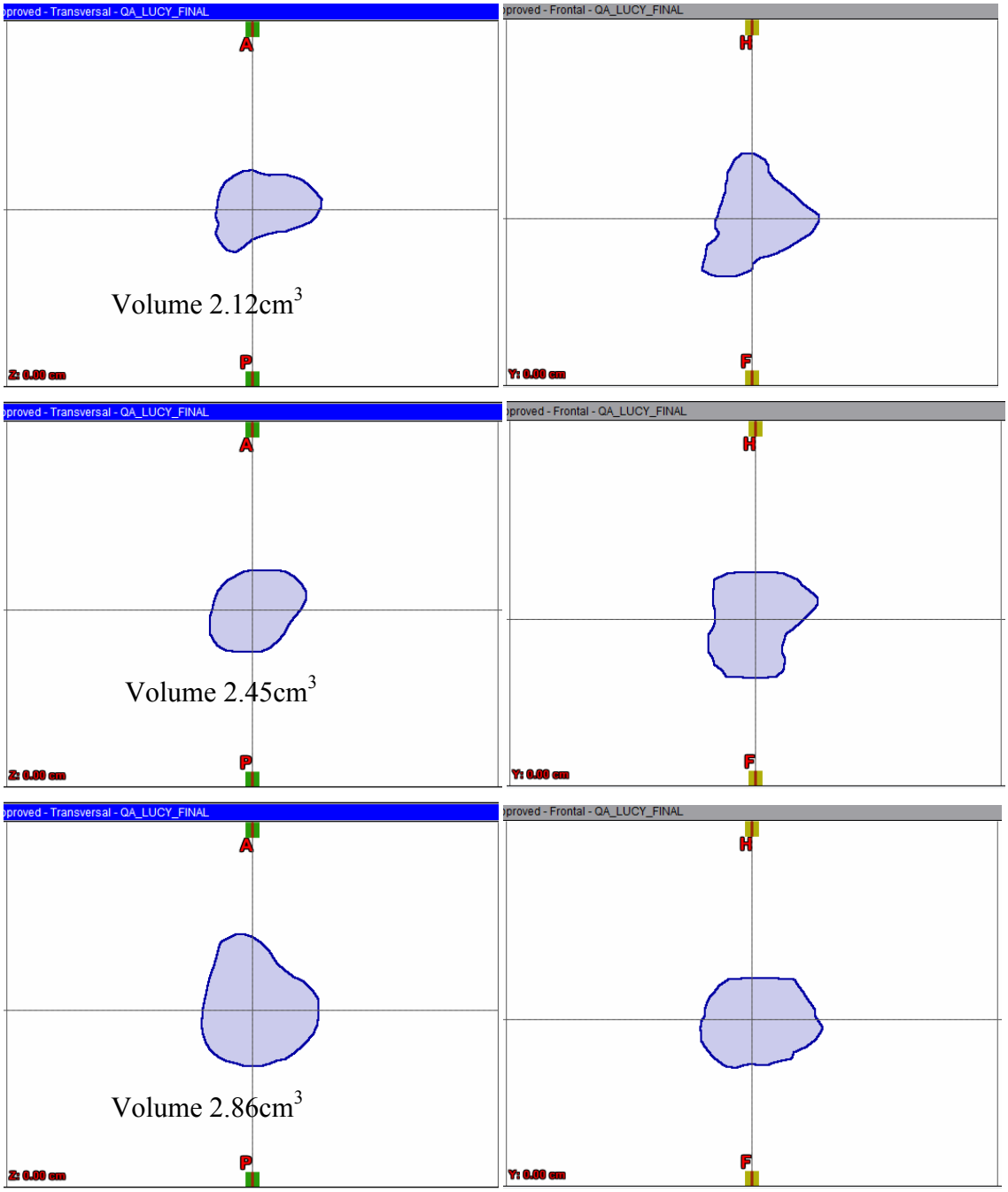
proved - Transversal - QA_LUCY_FINAL
A
P
Volume 2.12cm3
proved - Frontal - QA_LUCY_FINAL
H
F
proved - Transversal - QA_LUCY_FINAL
A
P
Volume 2.45cm3
proved - Frontal - QA_LUCY_FINAL
H
F
proved - Transversal - QA_LUCY_FINAL
A
P
Volume 2.86cm3
proved - Frontal - QA_LUCY_FINAL
H
F

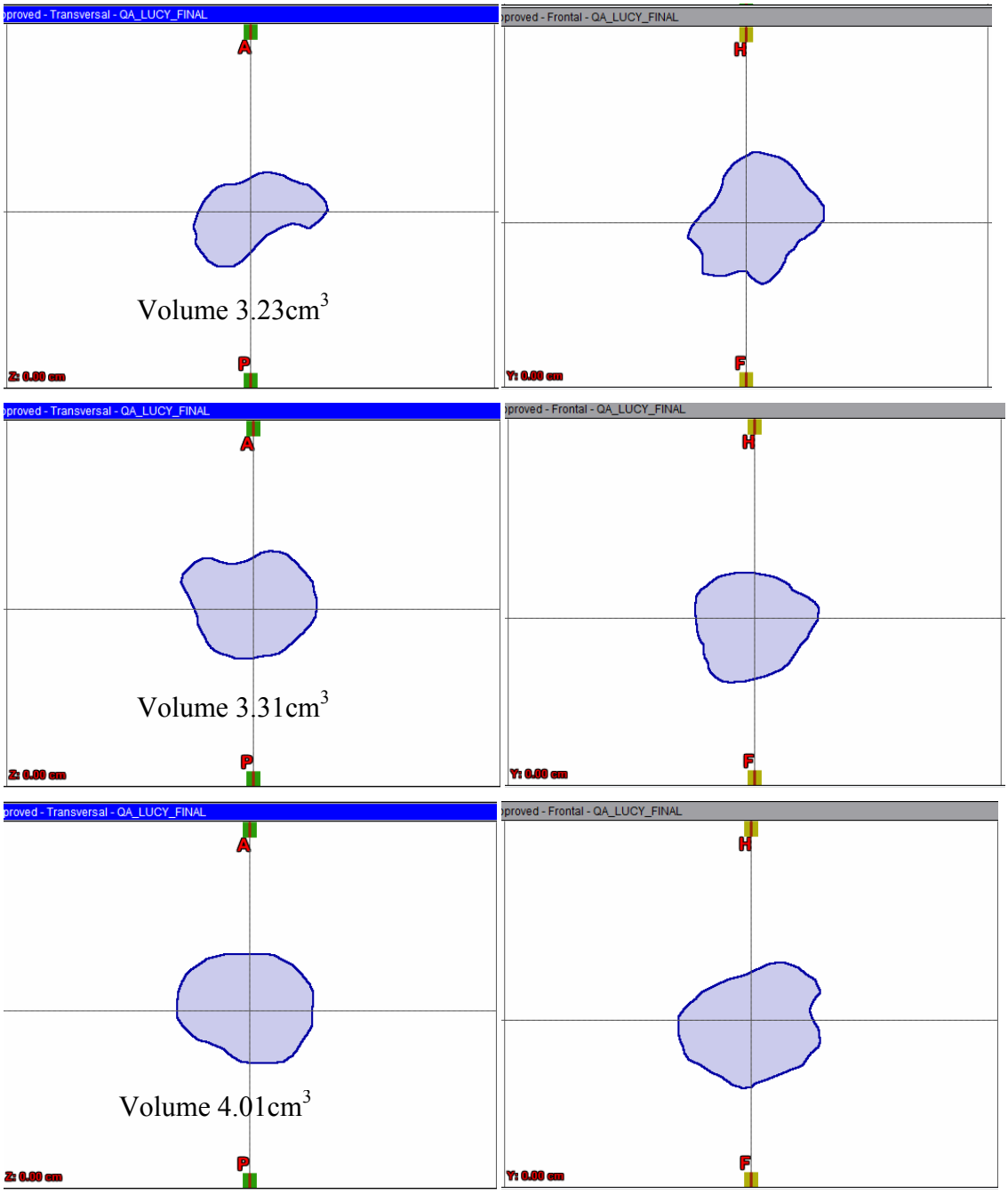
proved - Transversal - QA_LUCY_FINAL
A
P
Volume 3.23cm3
Z: 0.00 cm
proved - Frontal - QA_LUCY_FINAL
H
F
Y: 0.00 cm
proved - Transversal - QA_LUCY_FINAL
A
P
Volume 3.31cm3
Z: 0.00 cm
proved - Frontal - QA_LUCY_FINAL
H
F
Y: 0.00 cm
proved - Transversal - QA_LUCY_FINAL
A
P
Volume 4.01cm3
Z: 0.00 cm
proved - Frontal - QA_LUCY_FINAL
H
F
Y: 0.00 cm

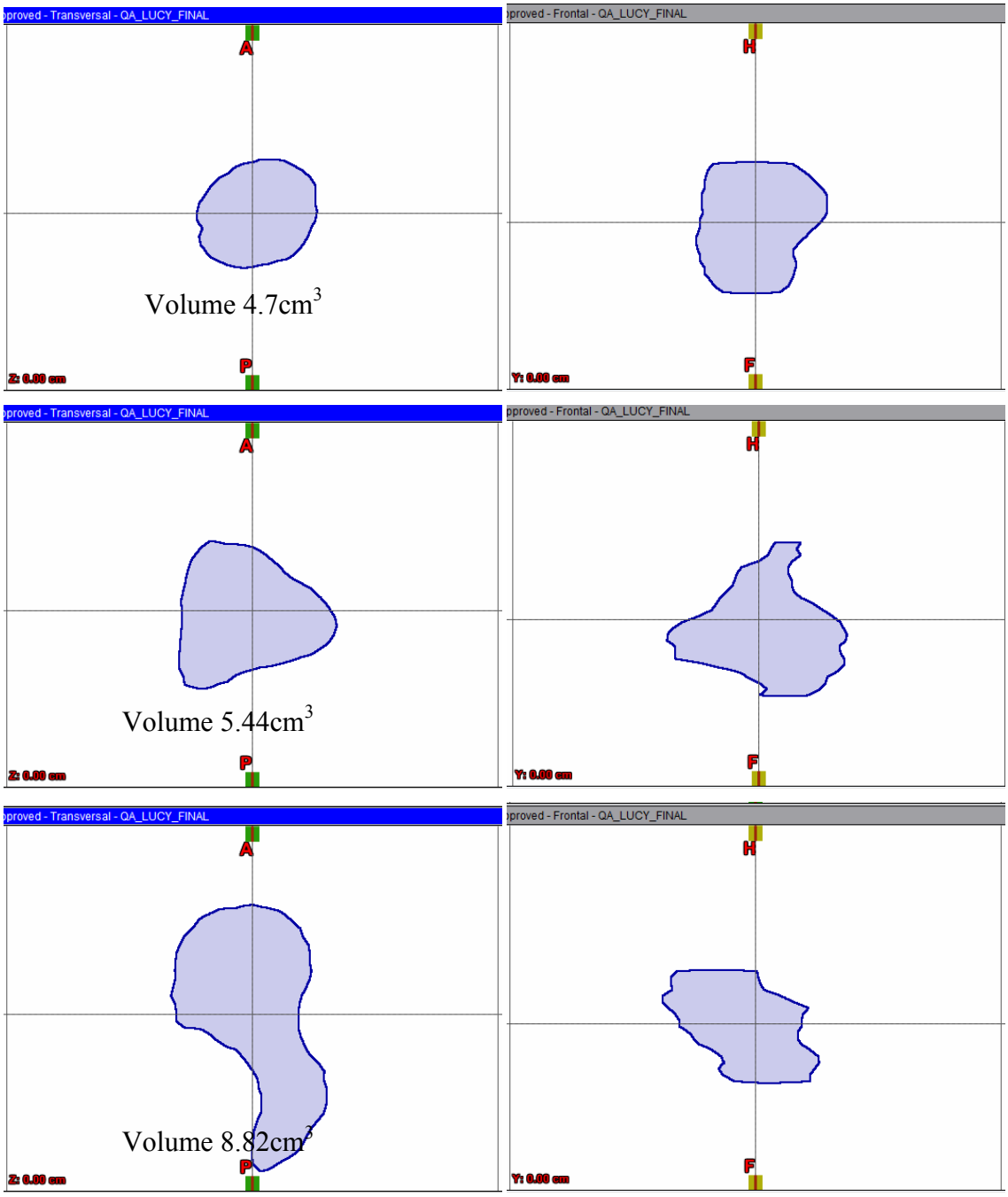
Volume 4.7cm3
Volume 5.44cm3
Volume 8.82cm3

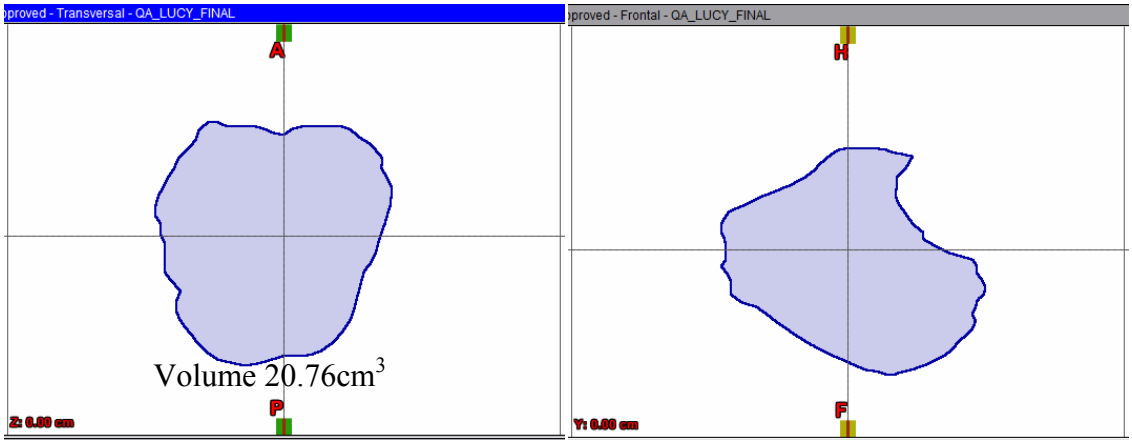
proved - Transversal - QA_LUCY_FINAL
A
P
Z: 0.00 cm
Volume 20.76cm3
proved - Frontal - QA_LUCY_FINAL
H
F
Y: 0.00 cm

Bibliography

Accuray. Physics Essentials Guide, 2007. (39,41)

Adler, J. R., Jr., Chang, S. D., Murphy, M. J., Doty, J., Geis, P., & Hancock, S. L. (1997). The Cyberknife: a frameless robotic system for radiosurgery. *Stereotact Funct Neurosurg, 69*(1-4 Pt 2), 124-128. (5,25)

BarinLAB, G. (2008). Technical Reference Guide, Revision 1.0, BrainLAB Physics. (27,33)

Battista, J. J., Rider, W. D., & Van Dyk, J. (1980). Computed tomography for radiotherapy planning. *International journal of radiation oncology, biology, physics, 6*(1), 99-107. (8)

Baumert, B. G., Norton, I. A., & Davis, J. B. (2003). Intensity-modulated stereotactic radiotherapy vs. stereotactic conformal radiotherapy for the treatment of meningioma located predominantly in the skull base. [Comparative Study Evaluation Study Research Support, Non-U.S. Gov't]. *International journal of radiation oncology, biology, physics, 57*(2), 580-592. (14)

Betti O, D. V. (1984). Hyperselective encephalic irradiation with a linear accelerator. . *Acta Neurochir*. (4)

Boswell, S., Tome, W., Jeraj, R., Jaradat, H., & Mackie, T. R. (2006). Automatic registration of megavoltage to kilovoltage CT images in helical tomotherapy: an evaluation of the setup verification process for the special case of a rigid head phantom. [Evaluation Studies Research Support, N.I.H., Extramural Research Support, Non-U.S. Gov't Validation Studies]. *Medical Physics, 33*(11), 4395-4404. (59)

Breneman, J. C., Steinmetz, R., Smith, A., Lamba, M., & Warnick, R. E. (2009). Frameless image-guided intracranial stereotactic radiosurgery: clinical outcomes for brain metastases. *Int J Radiat Oncol Biol Phys, 74*(3), 702-706. (8)

Cardinale, R. M., Benedict, S. H., Wu, Q., Zwicker, R. D., Gaballa, H. E., & Mohan, R. (1998). A comparison of three stereotactic radiotherapy techniques; ARCS vs. noncoplanar fixed fields vs. intensity modulation. [Comparative Study]. *International journal of radiation oncology, biology, physics, 42*(2), 431-436. (14)

Carol, M. P. (1995). PeacockTM: A System for Planning and Rotational Delivery of Intensity-Modulated Fields. *International Journal of Imaging Systems and Technology, 6, 56-61*. (4)

Chang, S. D., Main, W., Martin, D. P., Gibbs, I. C., & Heilbrun, M. P. (2003). An analysis of the accuracy of the CyberKnife: a robotic frameless stereotactic radiosurgical system. *Neurosurgery, 52*(1), 140-146; discussion 146-147. (8,26,59)

Chang, S. D., Murphy, M., Geis, P., Martin, D. P., Hancock, S. L., Doty, J. R., et al. (1998). Clinical experience with image-guided robotic radiosurgery (the Cyberknife) in the treatment of brain and spinal cord tumors. *Neurol Med Chir (Tokyo), 38*(11), 780-783. (5)

Charpentier, P. E. Dosimetric evaluation of four techniques used in stereotactic radiosurgery. *Department of Medical Physics McGill University, Montreal December 2007*. (14,88)

Cheung, T., Butson, M. J., & Yu, P. K. (2005). Post-irradiation colouration of Gafchromic EBT radiochromic film. *Phys Med Biol, 50*(20), N281-285. (60)

Clark, B. G., Robar, J. L., & Nichol, A. M. (2001). Analysis of treatment parameters for conformal shaped field stereotactic irradiation: comparison with non-coplanar arcs. [Comparative Study]. *Physics in medicine and biology, 46*(12), 3089-3103. (14)

Clivio, A., Fogliata, A., Franzetti-Pellanda, A., Nicolini, G., Vanetti, E., Wyttenbach, R., et al. (2009). Volumetric-modulated arc radiotherapy for carcinomas of the anal canal: A treatment planning comparison with fixed field IMRT. *Radiother Oncol, 92*(1), 118-124. (36)

Cozzi, L., Clivio, A., Bauman, G., Cora, S., Nicolini, G., Pellegrini, R., et al. (2006). Comparison of advanced irradiation techniques with photons for benign intracranial tumours. *Radiotherapy and oncology : journal of the European Society for Therapeutic Radiology and Oncology, 80*(2), 268-273. (71,113)

CyberKnife, A. Equipment specification, 2009. (40,41)

Ding, M., Newman, F., Kavanagh, B., Stuhr, K., Johnson, T., & Gaspar, L. (2006). Comparative dosimetric study of three-dimensional conformal, dynamic conformal arc, and intensity-modulated radiotherapy for brain tumor treatment using Novalis system. *International Journal of Radiation OncologyBiologyPhysics, 66*(4), S82-S86. (87,113)

Drzymala, R. E., Mohan, R., Brewster, L., Chu, J., Goitein, M., Harms, W., et al. (1991). Dose-volume histograms. *International journal of radiation oncology, biology, physics, 21*(1), 71-78. (13,50)

Echner, G. G., Kilby, W., Lee, M., Earnst, E., Sayeh, S., Schlaefer, A., et al. (2009). The design, physical properties and clinical utility of an iris collimator for robotic radiosurgery. [Evaluation Studies Research Support, Non-U.S. Gov't]. *Physics in medicine and biology, 54*(18), 5359-5380. (75)

Ernst-Stecken, A., Lambrecht, U., Ganslandt, O., Mueller, R., Fahlbusch, R., Sauer, R., et al. (2005). Radiosurgery of small skull-base lesions. No advantage for intensity-modulated stereotactic radiosurgery versus conformal arc technique. *Strahlentherapie und Onkologie : Organ der Deutschen Rontgengesellschaft ... [et al], 181*(5), 336-344. (87)

Flickinger, J. C., Schell, M. C., & Larson, D. A. (1990). Estimation of complications for linear accelerator radiosurgery with the integrated logistic formula. [Research Support, Non-U.S. Gov't]. *International journal of radiation oncology, biology, physics, 19*(1), 143-148. (88)

Forrest, L. J., Mackie, T. R., Ruchala, K., Turek, M., Kapatoes, J., Jaradat, H., et al. (2004). The utility of megavoltage computed tomography images from a helical tomotherapy system for setup verification purposes. [Evaluation Studies Research Support, Non-U.S. Gov't

Research Support, U.S. Gov't, P.H.S.]. *International journal of radiation oncology, biology, physics, 60*(5), 1639-1644. (24,59)

Gevaert, T., Verellen, D., Tournel, K., Linthout, N., Bral, S., Engels, B., et al. (2011). Setup Accuracy of the Novalis ExacTrac 6DOF System for Frameless Radiosurgery. *International journal of radiation oncology, biology, physics*. (59)

Hamilton, R. J., Kuchnir, F. T., Sweeney, P., Rubin, S. J., Dujovny, M., Pelizzari, C. A., et al. (1995). Comparison of static conformal field with multiple noncoplanar arc techniques for stereotactic radiosurgery or stereotactic radiotherapy. [Comparative Study]. *International journal of radiation oncology, biology, physics, 33*(5), 1221-1228. (14)

Heifetz, M. D., Wexler, M., & Thompson, R. (1984). Single-beam radiotherapy knife. A practical theoretical model. *Journal of neurosurgery, 60*(4), 814-818. (3)

Hong, L. X., Garg, M., Lasala, P., Kim, M., Mah, D., Chen, C. C., et al. (2011). Experience of micromultileaf collimator linear accelerator based single fraction stereotactic radiosurgery: tumor dose inhomogeneity, conformity, and dose fall off. *Medical Physics, 38*(3), 1239-1247. (55)

Ishihara, H., Saito, K., Nishizaki, T., Kajiwara, K., Nomura, S., Yoshikawa, K., et al. (2004). CyberKnife radiosurgery for vestibular schwannoma. *Minim Invasive Neurosurg, 47*(5), 290-293. (5)

Janne Sievinen, W. U., Wolfgang Kaissl. AAA Photon Dose Calculation Model in Eclipse™. (34)

Jin, J. Y., Yin, F. F., Tenn, S. E., Medin, P. M., & Solberg, T. D. (2008). Use of the BrainLAB ExacTrac X-Ray 6D system in image-guided radiotherapy. *Med Dosim, 33*(2), 124-134. (21)

Khan, F. M. (2009). The Physics of Radiation Therapy. *Lippincott Williams & Wilkins*. (5)

Khoo, V. S., Oldham, M., Adams, E. J., Bedford, J. L., Webb, S., & Brada, M. (1999). Comparison of intensity-modulated tomotherapy with stereotactically guided conformal radiotherapy for brain tumors. [Comparative Study Research Support, Non-U.S. Gov't]. *International journal of radiation oncology, biology, physics, 45*(2), 415-425. (14)

Kim, J., Jin, J. Y., Walls, N., Nurushev, T., Movsas, B., Chetty, I. J., et al. (2011). Image-guided localization accuracy of stereoscopic planar and volumetric imaging methods for stereotactic radiation surgery and stereotactic body radiation therapy: a phantom study. [Comparative Study Evaluation Studies]. *International journal of radiation oncology, biology, physics, 79*(5), 1588-1596. (59)

Korytko, T., Radivoyevitch, T., Colussi, V., Wessels, B. W., Pillai, K., Maciunas, R. J., et al. (2006). 12 Gy gamma knife radiosurgical volume is a predictor for radiation necrosis in non-AVM intracranial tumors. *International journal of radiation oncology, biology, physics, 64*(2), 419-424. (88)

Larsson, B., Liden, K., & Sarby, B. (1974). Irradiation of small structures through the intact skull. *Acta Radiol Ther Phys Biol, 13*(6), 512-534. (2)

Lawrence S. Chin, W. F. R. (c2008). *Principles and practice of stereotactic radiosurgery*: New

York : Springer,. (9,11)

Lee, T. F., Fang, F. M., Chao, P. J., Su, T. J., Wang, L. K., & Leung, S. W. (2008). Dosimetric comparisons of helical tomotherapy and step-and-shoot intensity-modulated radiotherapy in nasopharyngeal carcinoma. [Comparative Study]. *Radiotherapy and oncology : journal of the European Society for Therapeutic Radiology and Oncology, 89*(1), 89-96. (113)

Leksell, L. (1951). The stereotaxic method and radiosurgery of the brain. *Acta Chir Scand, 102*(4), 316-319. (2,11)

Leksell, L. (1968). Cerebral radiosurgery. I. Gammathalanotomy in two cases of intractable pain. *Acta chirurgica Scandinavica, 134*(8), 585-595. (3)

Leksell, L. (1983). Stereotactic radiosurgery. *J Neurol Neurosurg Psychiatry, 46*(9), 797-803. (11)

Levy, R. P., Schulte, R. W., Slater, J. D., Miller, D. W., & Slater, J. M. (1999). Stereotactic radiosurgery--the role of charged particles. *Acta oncologica, 38*(2), 165-169. (2)

Lu, S. H., Cheng, J. C., Kuo, S. H., Lee, J. J., Chen, L. H., Wu, J. K., et al. (2012). Volumetric modulated arc therapy for nasopharyngeal carcinoma: A dosimetric comparison with TomoTherapy and step-and-shoot IMRT. *Radiotherapy and oncology : journal of the European Society for Therapeutic Radiology and Oncology*. (87,113)

Ma, J., Chang, Z., Wang, Z., Jackie Wu, Q., Kirkpatrick, J. P., & Yin, F. F. (2009). ExacTrac X-ray 6 degree-of-freedom image-guidance for intracranial non-invasive stereotactic radiotherapy: comparison with kilo-voltage cone-beam CT. [Comparative Study]. *Radiotherapy and oncology : journal of the European Society for Therapeutic Radiology and Oncology, 93*(3), 602-608. (59)

Mackie, T. R., P. J. Reckwerdt, J. Purdy, W. Grant III, J. Palta, B. Butler and C. Perez. Madison, WI,. (2001). The convolution algorithm in IMRT. 3-D Conformal and Intensity Modulated Radiation Therapy. *Advanced Medical Publishing Inc.: 179-90.* (37)

Mackie, T. R., Bielajew, A. F., Rogers, D. W., & Battista, J. J. (1988). Generation of photon energy deposition kernels using the EGS Monte Carlo code. *Phys Med Biol, 33*(1), 1-20. (37)

Mackie, T. R., Holmes, T., Swerdloff, S., Reckwerdt, P., Deasy, J. O., Yang, J., et al. (1993). Tomotherapy: a new concept for the delivery of dynamic conformal radiotherapy. *Medical Physics, 20*(6), 1709-1719. (4,16)

Mackie, T. R., Scrimger, J. W., & Battista, J. J. (1985). A convolution method of calculating dose for 15-MV x rays. *Med Phys, 12*(2), 188-196. (37)

Mackie, T. R. a. R. P. J. O. G. H., and Shepard D M. (2000). Convolution/superposition photon dose algorithm. *General Practice of Radiation Oncology Physics in the 21st Century A. S. a. D. Mellenberg. College Park, MD, American Association of Physicists in Medicine: 39-56.* (37)

Meeks, S. L., Harmon, J. F., Jr., Langen, K. M., Willoughby, T. R., Wagner, T. H., & Kupelian,

P. A. (2005). Performance characterization of megavoltage computed tomography imaging on a helical tomotherapy unit. [Evaluation Studies]. *Medical Physics, 32*(8), 2673-2681. (24)

Mehta, V. K., Lee, Q. T., Chang, S. D., Cherney, S., & Adler, J. R., Jr. (2002). Image guided stereotactic radiosurgery for lesions in proximity to the anterior visual pathways: a preliminary report. *Technology in cancer research & treatment, 1*(3), 173-180. (5)

Mohan, R., Chui, C., & Lidofsky, L. (1985). Energy and angular distributions of photons from medical linear accelerators. *Med Phys, 12*(5), 592-597. (27)

Mohan, R., Chui, C., & Lidofsky, L. (1986). Differential pencil beam dose computation model for photons. *Med Phys, 13*(1), 64-73. (27)

Oliveira, S. C. Comparison of three linac-based stereotactic radiosurgery techniques. *Medical Physics Unit McGill University, Montreal June 2003*. (14,88)

Otto, K. (2008). Volumetric modulated arc therapy: IMRT in a single gantry arc. [Research Support, Non-U.S. Gov't]. *Medical Physics, 35*(1), 310-317. (4,35)

Paddick, I. (2000). A simple scoring ratio to index the conformity of radiosurgical treatment plans. Technical note. *J Neurosurg, 93 Suppl 3*, 219-222. (13,53)

Paddick, I., & Lippitz, B. (2006). A simple dose gradient measurement tool to complement the conformity index. *J Neurosurg, 105 Suppl*, 194-201. (13)

Papanikolaou, N., Mackie, T. R., Meger-Wells, C., Gehring, M., & Reckwerdt, P. (1993). Investigation of the convolution method for polyenergetic spectra. *Med Phys, 20*(5), 1327-1336. (37)

Podgorsak, E. B., Olivier, A., Pla, M., Lefebvre, P. Y., & Hazel, J. (1988). Dynamic stereotactic radiosurgery. *International journal of radiation oncology, biology, physics, 14*(1), 115-126. (4)

Podgorsak, E. B., Pike, G. B., Olivier, A., Pla, M., & Souhami, L. (1989). Radiosurgery with high energy photon beams: a comparison among techniques. *Int J Radiat Oncol Biol Phys, 16*(3), 857-865. (3,14)

Schell MC, B. F., Larson DA, Leavitt, DD, Lutz WR, Podgorsak EB, Wu A. . (1995). Stereotactic Radiosurgery. . *The American Institute of Physics*. (1,2)

Schoonbeek, A., Monshouwer, R., Hanssens, P., Raaijmakers, E., Nowak, P., Marijnissen, J. P., et al. (2010). Intracranial radiosurgery in the Netherlands. A planning comparison of available systems with regard to physical aspects and workload. [Comparative Study]. *Technology in cancer research & treatment, 9*(3), 279-290. (76)

Schoonbeek, A., Monshouwer, R., Hanssens, P., Raaijmakers, E., Nowak, P., Marijnissen, J. P. A., et al. (2010). Intracranial Radiosurgery in the Netherlands. A Planning Comparison of Available Systems with Regard to Physical Aspects and Workload. *Technology in cancer research & treatment, 9*(3), 279-289. (14)

Shaw, E., Kline, R., Gillin, M., Souhami, L., Hirschfeld, A., Dinapoli, R., et al. (1993). Radiation

Therapy Oncology Group: radiosurgery quality assurance guidelines. [Guideline Multicenter Study Practice Guideline]. *International journal of radiation oncology, biology, physics, 27*(5), 1231-1239. (1,51,54)

Shaw, E., Scott, C., Souhami, L., Dinapoli, R., Kline, R., Loeffler, J., et al. (2000). Single dose radiosurgical treatment of recurrent previously irradiated primary brain tumors and brain metastases: final report of RTOG protocol 90-05. *International journal of radiation oncology, biology, physics, 47*(2), 291-298. (12,88)

Soisson, E. T., Hoban, P. W., Kammeyer, T., Kapatoes, J. M., Westerly, D. C., Basavatia, A., et al. (2011). A technique for stereotactic radiosurgery treatment planning with helical tomotherapy. [Research Support, N.I.H., Extramural]. *Medical dosimetry : official journal of the American Association of Medical Dosimetrists, 36*(1), 46-56. (4,39,48,69,86)

Soisson, E. T., Mehta, M. P., & Tome, W. A. (2011). A comparison of helical tomotherapy to circular collimator-based linear-accelerator radiosurgery for the treatment of brain metastases. [Comparative Study Research Support, N.I.H., Extramural]. *American journal of clinical oncology, 34*(4), 388-394. (14,88)

Solberg, T. D., Boedeker, K. L., Fogg, R., Selch, M. T., & DeSalles, A. A. (2001). Dynamic arc radiosurgery field shaping: a comparison with static field conformal and noncoplanar circular arcs. [Comparative Study]. *International journal of radiation oncology, biology, physics, 49*(5), 1481-1491. (14)

Steiner, L., Leksell, L., Greitz, T., Forster, D. M., & Backlund, E. O. (1972). Stereotaxic radiosurgery for cerebral arteriovenous malformations. Report of a case. *Acta chirurgica Scandinavica, 138*(5), 459-464. (3)

Takakura, T., Mizowaki, T., Nakata, M., Yano, S., Fujimoto, T., Miyabe, Y., et al. (2010). The geometric accuracy of frameless stereotactic radiosurgery using a 6D robotic couch system. *Physics in medicine and biology, 55*(1), 1-10. (8)

TomoTherapy Planning Guide *Inc. Madison, WI* 2007. (39)

Tsai, J. T., Lin, J. W., Chiu, W. T., & Chu, W. C. (2009). Assessment of image-guided CyberKnife radiosurgery for metastatic spine tumors. [Clinical Trial]. *Journal of neuro-oncology, 94*(1), 119-127. (59)

Ulmer W, H. D. Corrected Tables of the Area Integral I(z) for the Triple Gaussian Pencil Beam Model. *Z. Med. Phys., 7 (1997) 192-193*. (34)

Ulmer W, H. D. A Triple Gaussian Pencil Beam Model for Photon Beam Treatment Planning. *2. Med. Phys, 5 (1995) 25-30*. (34)

van't Riet, A., Mak, A. C., Moerland, M. A., Elders, L. H., & van der Zee, W. (1997). A conformation number to quantify the degree of conformality in brachytherapy and external beam irradiation: application to the prostate. *Int J Radiat Oncol Biol Phys, 37*(3), 731-736. (52)

Verbakel, W. F., Cuijpers, J. P., Hoffmans, D., Bieker, M., Slotman, B. J., & Senan, S. (2009).

Volumetric intensity-modulated arc therapy vs. conventional IMRT in head-and-neck cancer: a comparative planning and dosimetric study. *Int J Radiat Oncol Biol Phys, 74*(1), 252-259. (36)

Verhey, L. J., Smith, V., & Serago, C. F. (1998). Comparison of radiosurgery treatment modalities based on physical dose distributions. [Comparative Study]. *International journal of radiation oncology, biology, physics, 40*(2), 497-505. (14)

Wagner, T. H., Bova, F. J., Friedman, W. A., Buatti, J. M., Bouchet, L. G., & Meeks, S. L. (2003). A simple and reliable index for scoring rival stereotactic radiosurgery plans. *International journal of radiation oncology, biology, physics, 57*(4), 1141-1149. (13,53)

Wang, L. T., Solberg, T. D., Medin, P. M., & Boone, R. (2001). Infrared patient positioning for stereotactic radiosurgery of extracranial tumors. *Comput Biol Med, 31*(2), 101-111. (21)

Webb, S. (1994). Optimizing the planning of intensity-modulated radiotherapy. [Research Support, Non-U.S. Gov't]. *Physics in medicine and biology, 39*(12), 2229-2246. (4)

Webb, S. (2003). The physical basis of IMRT and inverse planning. *Br J Radiol, 76*(910), 678-689. (32)

Welsh, J. S., Bradley, K., Ruchala, K. J., Mackie, T. R., Manon, R., Patel, R., et al. (2004). Megavoltage computed tomography imaging: a potential tool to guide and improve the delivery of thoracic radiation therapy. [Clinical Trial]. *Clinical lung cancer, 5*(5), 303-306. (24,59)

Wiezorek, T., Brachwitz, T., Georg, D., Blank, E., Fotina, I., Habl, G., et al. (2011). Rotational IMRT techniques compared to fixed gantry IMRT and tomotherapy: multi-institutional planning study for head-and-neck cases. [Comparative Study Evaluation Studies Multicenter Study]. *Radiation oncology, 6*, 20. (81)

Wolff, H. A., Wagner, D. M., Christiansen, H., Hess, C. F., & Vorwerk, H. (2010). Single fraction radiosurgery using Rapid Arc for treatment of intracranial targets. [Clinical Trial]. *Radiation oncology, 5*, 77. (71,113)

Woo, S. Y., Grant, W. H., 3rd, Bellezza, D., Grossman, R., Gildenberg, P., Carpentar, L. S., et al. (1996). A comparison of intensity modulated conformal therapy with a conventional external beam stereotactic radiosurgery system for the treatment of single and multiple intracranial lesions. [Comparative Study]. *International journal of radiation oncology, biology, physics, 35*(3), 593-597. (14)

Woodford, C., Yartsev, S., & Van Dyk, J. (2007). Optimization of megavoltage CT scan registration settings for thoracic cases on helical tomotherapy. [Evaluation Studies Research Support, Non-U.S. Gov't]. *Physics in medicine and biology, 52*(15), N345-354. (59)

Woodruff, K. H., Lyman, J. T., Lawrence, J. H., Tobias, C. A., Born, J. L., & Fabrikant, J. I. (1984). Delayed sequelae of pituitary irradiation. *Hum Pathol, 15*(1), 48-54. (2)

Yu, C., Jozsef, G., Apuzzo, M. L., & Petrovich, Z. (2003). Dosimetric comparison of CyberKnife with other radiosurgical modalities for an ellipsoidal target. [Comparative Study Evaluation Studies]. *Neurosurgery, 53*(5), 1155-1162; discussion 1162-1153. (14,113)